Design, development and validation of iron-based composites for biodegradable implant applications

Thèse en cotutelle
Doctorat en génie des matériaux et de la métallurgie

Malgorzata Sikora-Jasinska

Université Laval
Québec, Canada
Philosophiæ doctor (Ph. D.)

et

Politecnico di Milano
Milano, Italie

Design, development and validation of iron-based composites for biodegradable implant applications

Thèse en cotutelle
Doctorat en génie des matériaux et de la métallurgie

Malgorzata Sikora-Jasinska

Sous la direction de:

Diego Mantovani, directeur de recherche
Maurizio Vedani, directeur de cotutelle

Résumé

Récemment, le Fe et ses alliages ont montré leur potentiel en tant que matériaux dégradables pour des applications biomédicales. Néanmoins, la vitesse de corrosion lente limite leurs performances dans certaines situations. Les matériaux composites à matrice de fer représentent une approche possible, non seulement pour améliorer leurs propriétés mécaniques, mais aussi pour accélérer et ajuster la vitesse de corrosion dans un environnement physiologique.

Dans ce travail, des composites à base de Fe renforcés par des particules Mg_2Si ont été proposés. Les poudres initiales ont été préparées par différentes combinaisons de procédés de mélange et de broyage, et finalement consolidées par laminage à chaud. L'influence de la microstructure sur les propriétés mécaniques et le comportement à la corrosion de Fe/Mg_2Si a été étudiée. Les échantillons contenant des particules Mg_2Si plus petites présentaient une distribution plus homogène du renforcement. Le rendement et l'état limite ultime à la traction ont augmenté par rapport à ceux du Fe pur. La présence des particules de renforcement a joué un rôle crucial dans la susceptibilité à l'attaque de corrosion localisée dans les composites à base de Fe. L'initiation de la corrosion et son développement ont été systématiquement suivis pour étudier le mécanisme de corrosion. L'importance des particules de Mg_2Si dans le déclenchement des processus de corrosion a été expliquée. Des mesures électrochimiques et des tests d'immersion statique ont indiqué que l'ajout de Mg_2Si pourrait augmenter le taux de corrosion du Fe. Il a été constaté que la taille et la distribution des particules de renfort jouaient un rôle crucial à l'uniformité de l'attaque de corrosion. Après, une série de tests d'immersion à différents intervalles d'exposition (20, 50 et 100 jours) à la solution modifiée de Hanks a été réalisée à fin d'évaluer le comportement de dégradation des composites Fe/Mg_2Si et Fe pur préparés par différentes techniques de métallurgie des poudres. Les résultats ont révélé l'importance du Mg_2Si dans la composition et la stabilité des films protecteurs formés lors des expériences de corrosion statique. Les composites Fe/Mg_2Si présentaient des taux de dégradation plus élevés que le Fe pur à toutes les étapes du test d'immersion. Les taux de dégradation à des intervalles d'exposition distincts dépendaient fortement de la composition et de la stabilité des films protecteurs d'oxyde, d'hydroxyde, de carbonate et de phosphate formés sur les surfaces dégradées. La libération d'ions Fe dans la solution aux stades ultérieurs de l'expérience était limitée en raison de l'effet de barrière dû au dépôt insoluble. Cette étude fondamentale a servi de base aux processus de formation de film protecteur dans la solution de Hanks modifiée, permettant une identification détaillée de leurs caractéristiques.

Abstract

Fe-based alloys have shown a potential as a degradable material for biomedical applications. Nevertheless, the slow corrosion rate limits their performance as a biodegradable implant. One approach to control and modify their corrosion properties is the reinforcement addition, to create metal matrix composites in which the second phase is aimed at tuning not only the mechanical properties but also the corrosion mode and rate in a physiological environment.

This thesis presents an original and thorough contribution on a very pertinent topic, the design, development, and validation of a new Fe/Mg_2Si composites prepared powder metallurgy. The initial powders were prepared by different combinations of mixing and high energy ball milling processes and finally consolidated by hot rolling. Mechanical properties, microstructural features, as well as the corrosion performance, were extensively investigated in relation to the reinforcement size and distribution. The composites made of small size reinforcement particles showed a general increase in tensile strength. For instance, high energy ball milled samples exhibited better tensile performances (YS = 523 MPa, UTS = 630 MPa) while having the lower ductility (around 4%). A fundamental understanding of corrosion initiation, protective film formation, and growth on Fe-based materials and leads to a design of smarter and surface responsive biomaterials with modulable degradation rates, at distinct stages of the corrosion process. Here, the corrosion performance of Fe/Mg_2Si composites varied with the reinforcement size and distribution. The predominant localized pitting corrosion in Fe/Mg_2Si prepared by mixing was replaced by a more uniform pattern found in samples produced by mechanical milling. Further, it was found that Mg_2Si plays a significant role in the composition and stability of the protective films formed during the static corrosion experiments. Fe/Mg_2Si showed a higher corrosion rate compared to that of pure Fe at all stages of the corrosion experiment (1, 10, 20, 50 and 100 days). Moreover, the final degradation products varied with the substrate chemical composition and microstructure. In case of pure Fe, low solubility ($Fe_3(PO_4)_2$) covered the entire surface, while Fe/Mg_2Si exhibited the presence of carbonates at the latest stages of the test. The details about the degradation behaviour during long-term exposure times to the physiological environment highlighted in this work add a new knowledge on corrosion mechanism of degradable implant materials. In particular, the ability to tune mechanical and corrosion behavior of the composites as a function of reinforcement properties and manufacturing method was experimentally verified, highlighting the microstructure-corrosion property relationship.

Sommario

I biomateriali in ferro puro e in leghe a base di ferro presentano una combinazione interessante di proprietà meccaniche, elettrochimiche e biologiche; per questo motivo, questa classe di materiali metallici possono trovare utilizzo in applicazioni di tipo impiantistico biomedicale. Malgrado ciò, nonostante le sue soddisfacenti proprietà meccaniche, questo elemento impiegato allo stato puro mostra un inconveniente rilevante - un basso tasso di degradazione.

L'oggetto di questa tesi è lo studio di un nuovo gruppo di materiali biodegradabili compositi a matrice ferrosa (Fe/Mg_2Si), in cui il Fe costituisce la matrice e il Mg_2Si è impiegato come rinforzo; questi materiali sono stati sviluppati con tecniche di metallurgia delle polveri, e presentano un, alta resistenza meccanica come caratteristica principale. Le polveri che costituiscono i materiali di partenza sono stati preparati con diverse combinazioni di procedure oltre al semplice mescolamento e/o high energy ball milling (macinatura in mulino a sfere a alta energia). Tutte le formulazioni preparate sono state compattate attraverso laminazione a caldo. Le proprietà meccaniche, le caratteristiche microstrutturali, la composizione delle fasi e le prestazioni in termini di corrosione sono state studiate dettagliatamente, in relazione alla dimensione delle particelle di rinforzo e della loro distribuzione. Lavori precedenti hanno confermato l'efficacia dell'aggiunta di una seconda fase, soprattutto se finemente dispersa, per aumentare il tasso di degradazione di materiali metallici per applicazioni biomedicali a base Fe: gli esperimenti condotti in questo lavoro hanno confermato che i compositi Fe/Mg_2Si hanno mostrato, rispetto al Fe puro che compone la matrice, non solo una resistenza meccanica più elevata, ma anche un tasso di degradazione più alto negli esperimenti di laboratorio in vitro. Infine, i materiali ottenuti tramite high energy ball milling, presentano una resistenza alla trazione migliore (carico di snervamento= 523 MPa, resistenza alla trazione = 630 MPa), ma contemporaneamente una ridotta duttilità (circa 4%). Una attenzione particolare è stata posta nello studio degli effetti della presenza di Mg_2Si sui meccanismi di corrosione.Tutti i compositi studiati hanno mostrato un tasso di degradazione più elevato rispetto alla matrice fabbricata con la stessa procedura; inoltre, la formazione del film di prodotti di degradazione sulla superficie del materiale cambiava in maniera rilevante in funzione della composizione chimica del substrato e della sua microstruttura. Nel caso del Fe puro, cristalli isolati di vivianite ($Fe_3(PO_4)_2$) erano presenti su tutta la superficie, mentre carbonati di Fe si formavano principalmente sulla superficie dei compositi, specialmente negli ultimi stadi del processo di degradazione.

Table of contents

List of Figures

List of Tables

List of symbols and abbreviations

α: Body Centered Cubic Phase of Fe
ρ: Density [$g \cdot cm^{-3}$]
A: Area [cm^2]
ASTM: American Society for Testing Materials
BM/ BMs: Biodegradable Metal / Biodegradable Metals
BSE: Back Scattered Electron
CR_P: Corrosion Rate calculated on the base of potentiodynamic measurements [$mm \cdot year^{-1}$]
CR_S: Corrosion Rate calculated on the base of static immersion test [$mm \cdot year^{-1}$]
CTE: Coefficient of Thermal Expansion
DMEM: Dulbecco's Modified Eagle's Medium
EBSD: Electron Backscatter Diffraction
ECAP: Equal-Channel Angular Pressing
EDS: Energy Dispersive Spectroscopy
EW: Equivalent Weight [-]
HEBM: High Energy Ball Milling
HA: Hydroxyapatite
FTIR: Fourier Transform Infrared Spectroscopy
FBS: Fetal Bovine Serum
FDA: Food and Drug Administration
GND: Geometrically Necessary Dislocations
i_{corr}: Corrosion Current Density [$A \cdot cm^{-2}$]
ICP–ES: Inductively–Coupled Plasma Emission Spectroscopy
ISO: International Organization for Standardization
JCPDS: Joint Committee on Powder Diffraction Standards
MA: Mechanical Alloying
MM: Mechanical Milling
MMCs: Metal Matrix-Composites
MRI: Magnetic Resonance Imaging
MX: Mixing
PM: Powder Metallurgy
RE: Rare Earth Elements
SPD: Severe Plastic Deformation
SCE: Saturated Calomel Electrode
SEM: Scanning Electron Microscope
SS316L: Stainless Steel Type 316L
t: Time of Exposure [h]
UTS: Ultimate Tensile Strength (MPa)
W: Weight Loss [mg]
XPS: X-ray Photoelectron Spectroscopy
XRD: X–ray Diffraction
YS: Yield Strength (MPa)

Dedicated to the memory of my grandmother Adelka who always believed in my ability to be successful in the academic arena. You are gone but your belief in me has made this journey possible

Acknowledgments

I would like to express my deepest gratitude to my supervisors Prof. Diego Mantovani and Prof. Maurizio Vedani. Thanks for your ideas, suggestions, and supports. Thanks for giving me the opportunity for this doctoral experience in a dynamic and multicultural environment. I would like to thank you for encouraging my research and for allowing me to grow as a research scientist. Your advice on my research and career have been invaluable.

I would also like to thank my committee members, professor Carla Martini, professor Francesco Migliavacca, professor Hendra Hermawan for serving as my committee members. I also want to thank them for letting my defense be an enjoyable moment, and for your brilliant comments and suggestions.

I would like to acknowledge all my colleagues from Laval University, Laboratory of Biomaterials and Bioengineering and Mechanical Engineering Department at Politecnico di Milano who have been involved in my project.

Special thanks go to technicians Vicky Dodier, Nathalie Moisan, Jean Frenette, Luca Signorelli, Maurizio Pardi from Laval University and Politecnico di Milano for their highly professional help in offering me the resources in running my project. They made a significant contribution to my research. I wish to thank you for your patient teachings and for the skills and competences you shared with me every day, with generosity and professionalism, and for the enthusiasm and energy that you put every day in your work.

I would like to thank the administrative staff: Karine Fortin, Andree Lord, and Cinzia Farina for their sincere helps in the department.

I would like to acknowledge the kind financial support from the Italian Ministry of Education, Universities and Research (Ministero dell'Istruzione, dell'Università e della Ricerca, MIUR) and the Natural Science and Engineering Research Council (NSERC) of Canada.

Foreword

The present thesis has been developed in the framework of a double PhD degree program between *Laval University* (Quebec, Canada) and *Politecnico di Milano* (Milan, Italy). The project was focused on the design, development, and validation of novel Fe/Mg_2Si composites for biodegradable biomaterials applications. The materials manufacturing route and mechanical testing are as important as the corrosion testing and characterization methods used to validate the newly developed composites. The techniques and materials selected were directly related to the expertise of the two laboratories involved in this research project:

The **Laboratory for Biomaterials and Bioengineering** (LBB) at Laval University has developed several kinds of Fe-based biodegradable implant materials (Fe-Mn, Fe-P, Fe-Co, Fe-Mn-C) prepared by different techniques (electroforming, powder metallurgy, casting, etc.). Besides, LBB has developed several strategies and established some internal protocols for the static immersion tests and electrochemical properties assessment of biodegradable metals. The biocorrosion behavior was investigated and characterized by employing several techniques such as by X-ray diffractometry (XRD), scanning electron microscopy (SEM) equipped with an electron dispersive X-ray spectrometry (EDS), X-Ray Photoelectron Spectroscopy (XPS) and Fourier transform infrared spectroscopy (ATR-FTIR).

The activities of the **Advanced Materials Research group** at Politecnico di Milano are centered on manufacturing technologies and the thermo-mechanical processing of advanced and non-conventional metallic alloys such as nanostructured and ultrafine-grained metals, magnesium-, zinc- and iron-based alloys and their composites for biodegradable implant applications. Various facilities for production and processing of metals such as furnaces, high energy ball milling, extrusion, rolling and equal-channel angular pressing (ECAP) were employed to fabricate different kinds of biodegradable biomaterials. The microstructure, chemical composition and mechanical performance of newly manufactured materials can be investigated by scanning electron microscopy (SEM) equipped with electron backscatter diffraction (EBSD) detector, compression and tensile tests at room or elevated temperatures, fatigue tests, and micro- and macro-hardness.

Hence, the ensemble of expertise of these two groups allowed this project to have complementary investigations for the application searched.

Prof. Diego Mantovani and Prof. Maurizio Vedani are my supervisors. This thesis was prepared as an article insertion thesis. It includes three papers in which I have taken the role as the principal investigator as well as the first author.

Chapter 1 presents a literature review of the status of biodegradable metals. It starts with a brief review on magnesium and zinc biodegradable metals. Subsequently, a detailed review on Fe-based biomaterials is presented.

Chapter 2 introduces the problem statement, the definition of the objectives and strategies to realize the project.

Chapters 3, 4 and **5** present the obtained results.

Chapter 3: *Synthesis, mechanical properties and corrosion behavior of powder metallurgy processed Fe/Mg_2Si composites for biodegradable implant applications.*

The first article's objective was to explore the effect of the addition of the reinforcement on microstructure, mechanical properties and corrosion behavior of Fe/Mg_2Si composites. Moreover, the effect of initial powder preparation on the properties of the investigated materials was studied and the effect of other parameters as well.

Authors: M. Sikora-Jasinska, C. Paternoster, E. Mostaed, R. Tolouei, R. Casati, M. Vedani, D. Mantovani

Article history:
Journal: *Materials Science and Engineering C*
Submitted: 20th July 2016
Accepted: 20th October 2016
Published: 29th June 2017

Malgorzata Sikora-Jasinska carried out personally all the experiments and characterizations. She performed a first analysis of the results, which were later discussed with the rest of the

authors. She also wrote a full first draft of the paper which was corrected and modified by the other authors. She oversaw the final form of the paper including figures and tables.

Chapter 4: *Understanding the effect of the reinforcement addition on corrosion behavior of Fe/Mg_2Si composites for biodegradable implant applications*

The details of localized corrosion of Fe matrix were studied in the present work. Techniques such scanning electron microscopy, X-ray diffraction, atomic emission spectroscopy and Fourier transform infrared spectroscopy were used to investigate the mechanisms of localized corrosion attack and the first phases of degradation in modified Hanks' solution. The importance of addition Mg_2Si reinforcement in the initiation of corrosion processes is demonstrated in the paper.

Authors: M. Sikora-Jasinska, P Chevallier, S Turgeon, E Mostaed, C Paternoster, M Vedani, D Mantovani

Article history:

Journal: *Materials Chemistry and Physics, Elsevier*

Submitted: 19th January 2018

Accepted with minor revision: 28th Mai 2018

The experiments were designed by Malgorzata Sikora-Jasinska. The analysis of results was performed in collaboration with all the authors. Malgorzata Sikora-Jasinska wrote a full first draft of the paper which was corrected and modified by the rest of the authors. She was also in charge of the redaction of final form of the paper including figures and tables.

Chapter 5: *Long-term in vitro degradation behaviour of Fe and Fe/Mg_2Si composites for biodegradable implant applications*

This paper reports the effect of long-term static immersion tests of Fe and Fe/Mg_2Si composites prepared by powder metallurgy techniques. Predicting *in vitro* degradation behavior of biodegradable metals is crucial for the clinical success of these medical devices. Thus far, this is the only research work that systematically investigates their long-term *in vitro* corrosion behavior and explores their corrosion mechanism. These are fundamental and vital to develop novel Fe-based materials with improved corrosion characteristics.

Authors: M. Sikora-Jasinska, P Chevallier, S Turgeon, E Mostaed, C Paternoster, M Vedani, D Mantovani

Article history:
Journal: *RSC Advances*
Submitted: 14th January 2018
Accepted: 26th February 2018
Published: 6th March 2018

The experiments were designed by Malgorzata Sikora-Jasinska. The analysis of results was performed in collaboration with all the authors. Malgorzata Sikora-Jasinska wrote a full first draft of the paper which was corrected and modified by the rest of the authors. She was also in charge of the final form of the paper including figures and tables.

After the results presented in Chapters **3**, **4** and **5**, a link between the problems and their solutions is made and presented in **Chapter 6**. A detailed analysis of the limitations of the research project including the materials and the corrosion testing methodology for biodegradable metallic biomaterials are also exposed. Finally, some perspectives are presented in this chapter.

Chapter 7 presents the general conclusion of the studies on Fe-based biodegradable composites and their further perspectives as well.

1. Introduction

****

The following aspects are addressed in the introduction: (i) permanent implant materials available on the market, (ii) concepts of biodegradable metals, (iii) and their recent developments with a focus on biodegradable Fe-based alloys

****

1.1. Permanent implant materials

During the last five decades, tremendous advances in the biomaterials field have been made. Nowadays, biomaterials have been used in a wide range of applications such as a cardiovascular stent, dental implant, hip prosthesis, heart valve, skin repair etc. Implant material candidate should have the ability to comport with an appropriate host response. Moreover, the definition of mechanical properties of a biomaterial is crucial. For example, the design of cardiovascular stent material pertains balancing opposed mechanical requirements. The prospective characteristics are contradictory: high elastic modulus (prevents recoil), low yield strength (allowing the stent expansion), high ultimate tensile strength after expansion (allowing achievement of high radial strength and permitting the use of thinner struts) and high ductility (withstanding the plastic deformation during expansion). In case of bone fixation/replacement applications, characteristics such as high wear and fatigue strength, low elastic modulus and low friction are desired to provide a long service life of these biomaterials. It is very difficult to combine aforementioned features into only one material. Table 1.1. presents the mechanical properties of commercially available metallic implant materials.

Table 1.1. *Mechanical properties of different permanent biomaterials [1–3]*

Material	Young's modulus (GPa)	Yield Strength (MPa)	Ultimate Tensile strength (MPa)	Elongation %
SS316L (ASTM F138 annealed)	190	250	580	55
Ti-6Al-4V (annealed)	185	138	207	14
Nitinol (annealed)	83	195-690	895	10
Cobalt-chromium (ASTM F90)	210	379	896	30
L605 (Co-Cr)	243	629	1147	46

The corrosion resistance is one of the most prominent features of permanent metallic biomaterials. Most metals can only be tolerated by the human body in low amounts even in the form of metallic ions. Further, the progressing corrosion leads to the deterioration of mechanical properties, the disintegration of the implant and the loss of mechanical integrity, which might weaken the implant and cause its failure. The main categories of the permanent metallic biomaterials are as follows: stainless steel, titanium, and cobalt based alloys. Table 1.2. lists the most common metallic biomaterials and their main applications.

Table 1.2. *Biomaterials used for permanent implants [1–3]*

Metals and alloys	Advantages	Disadvantages	Principal applications
316L stainless steel	High wear resistance, superior corrosion resistance, high strength, and ductility, easy to be machined	Potential allergic reactions because of the Cr, Ni and Mo release.	Stents, Fracture fixation surgical instruments,
Co-Cr alloys such as Co-Cr-Mo, Cr-Ni-Cr-Mo	High wear resistance and corrosion resistant, excellent fatigue and wear resistance, Biocompatibility	Allergic reaction with Ni, Cr and Co much, high modulus and related with stress shielding effect, expensive and difficult to be machined	Permanent implants such stents, bone and joint replacement, dental implants and restorations heart valves
Ni-Ti	Shape form memory. Good visibility by fluoroscopy.	Ni cause allergy	Self-expanding stents, bo plates, orthodontic wire
Ti-based alloys such as: CP-Ti, Ti-Mo-Zr-Fe, Ti-Al-V, Ti-Al-Nb, Ti-13Nb-13Zr	High biocompatibility, the highest corrosion resistance among metallic biomaterials, low density, good weldability, relatively low Young's modulus.	Poor tribological properties, Toxic effect of certain alloying elements such as Al and V, lower shear strength, low tensile ductility, low wear resistance	Dental screws, Bone fixation/replacement implants, femoral hip ste
Platinum and Pt-Ir	High corrosion resistant under high voltage potential and charge transfer conditions	Low mechanical strength and ductility	Stents, Electrodes

316L stainless steel (ASTM F 138/139), despite its susceptibility to crevice corrosion, has been used widely over decades for cardiovascular and fracture repair devices [8]. Co-based alloys feature a very high strength and are frequently used in dental, orthopedic and cardiovascular applications, demonstrating excellent biocompatibility with a blood and soft tissues. Titanium alloys, because of their light weight, good mechanical properties, and outstanding biological performance are finding increasing interest in biomedical devices field. Ti is now the metal of choice for internal fixation, prosthetics, and instrumentation. Ti alloys are the only permanent metallic biomaterials with capacity for joining with bone and other tissue (osseointegrate). In addition, the formation of an adherent, thin protective titanium oxide film in the passivation process is the main reason for their high corrosion resistance [9–11].

1.2. A new emerging class of biomaterials: Biodegradable metals

Conventional metallic biomaterials for medical applications are made of corrosion resistant materials and are designed to remain intact in a human body for a long time. They are characterized by appropriate mechanical properties (for searched applications) and excellent corrosion resistance. Although over the last decades permanent materials have been largely used, they have certain disadvantages.

Implant for bone fracture fixation should be removed after one or two years after implantation. From an economic point of view, noticeable cost for healthcare systems and implant removal constitute 30% of orthopedic procedures [5,12,13]. Biodegradable metals (BMs) could adapt the human body and eventually dissolve when their presence is no longer required. Such materials would help patients suffering from fractures of long bones or limb length discrepancies. Further, the expenses of multiple procedures including implantation, removal, and re-implantation of the permanent implant could be avoided. Another example is a metallic stent used to treat blockages in the coronary arteries. This small implant can cause an immune response that leads to the formation of blood clots or restenosis. The use of bioabsorbable stents drastically reduces, if not annihilate, some potentially long-term clinical problems related to permanent stents including chronic inflammation, late stent thrombosis, in-stent restenosis and stent strut fracture which can damage the local vasculature. The concept of an absorbable stent is to keep the occluded arteries open during the remodeling period and degrade harmlessly afterward when its mechanical scaffolding effect is no longer needed. The stent material and its corrosion product must be non-toxic and compatible with the vascular environment [14–17]. BM stents, as well as bone fixation implants, have other advantages in pediatric applications showing the ability to adjust to the tissue growth.

The biodegradable implant should be able to compromise its degradation and mechanical integrity after implantation and during tissue healing period. The BM should start its dissolution just after the implantation, which results from low corrosion resistance comparing to inert material. The modulable corrosion rate is needed to retain the optimal mechanical integrity of the implant until the tissue remodeling is achieved.

Fig. 1.1a schematically describes an ideal biodegradable stent as a device which should be able to compromise its mechanical integrity and its corrosion rate during healing process.

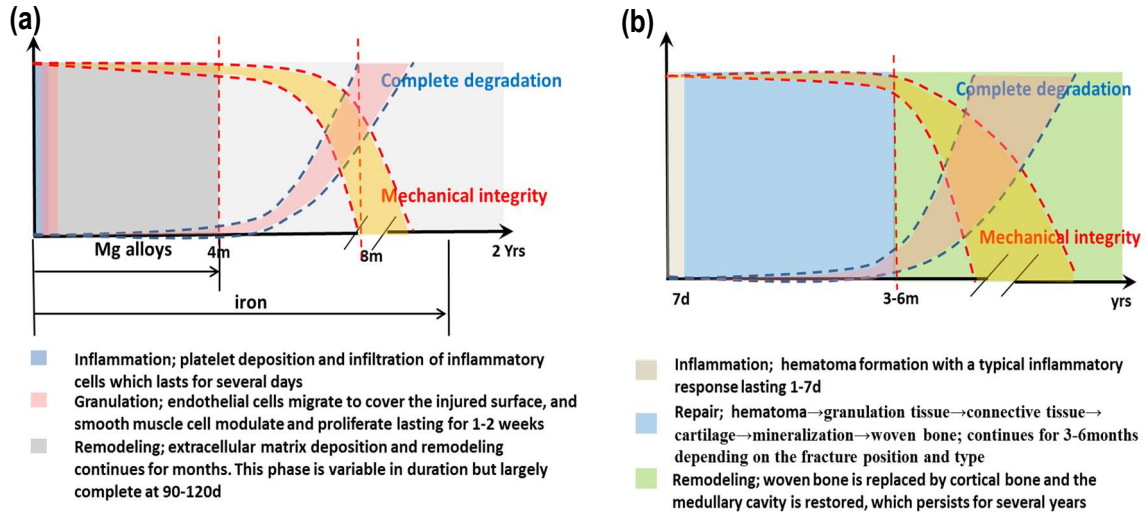

Figure 1.1. *The schematic diagram of corrosion behavior and the change of mechanical integrity of* ***(a)*** *BM stent during the vascular healing process,* ***(b)*** *BM implant during the bone healing process, adapted from Witte et al.* [4]

Gradual corrosion rate is initially required to preserve the optimal mechanical integrity of the implant until the arterial vessel remodeling and healing process is completed. Afterward, the stent is supposed to disappear and leave behind a natural functioning artery. An ideal period of 6-12 months is foreseen for the artery tissue remodeling [37, 38]. In case of bone fracture, as seen in Fig. 1.1b healing occurs in three stages: inflammation, repair and remodeling phases. The time to reach the hard bone merger depends on the fracture type and its location, the state of the surrounding soft tissues, as well as patient characteristics (age, health, other injuries/diseases) [18,19].

Over the last two decades, polymeric and metallic materials have been rigorously studied to use as degradable vascular stents. Polymeric stents, despite their predictable degradation products, identical degradation mechanisms *in vitro* and *in vivo* and acceptable biocompatibility, require a greater strut thickness than most metal stents due to their low radial strength. Thicker polymeric stents thus require larger catheters for delivery, which makes their use challenging in pediatric interventions. Polymers also exhibit poor visibility characteristics thereby leading to lack of radiopacity for *in vivo* imaging. Moreover, the

inability to attain an acceptable permanent expansion along with restenosis susceptibility are further concerns when using polymeric stent materials. To date, in the field of degradable metals, numerous studies on iron (Fe), magnesium (Mg) and zinc (Zn)-based alloys have been reported with efforts on tailoring mechanical and corrosion behavior to address the requirements of degradable load and non-load bearing bone implants, cardiovascular stents, and other implantable medical devices such as biodegradable sutures and clips.

Table 1.3. *Main classes of biodegradable biomaterials [4–6]*

Material	Characteristics	Disadvantages
Fe	-high elastic modulus -reduction of proliferation of smooth muscle cells in *in vivo* conditions in rabbits -endothelialization observed in animal -thrombogenicity and neointimal proliferation were reduced	- the long-term impact of elevated local concentration of this element is unknown -the degradation rate is too slow, corrosion properties do not suit the requirements for stent material -ferromagnetism of iron
Mg	-certain Mg alloys as AE21 contains aluminum (2%) and rare earth metals (1%) -MRI compatible - reduced smooth muscle cell growth and enhanced endothelialization were observed in porcine models	-the long-term impact of elevated local concentration of this element is unknown -poor radial strength because of its low elastic modulus -stents may fracture because of its low ductility -cannot be imaged by X-ray -the mechanical and corrosion properties do not match the requirements for stent material
Zn	-essential element for human beings, second most abundant transition metal in human body -zinc has been already used as an alloying element in Mg alloys -steady state corrosion rate in *in vivo* condictions	-the long-term impact of elevated local concentration of this element is unknown -poor radial force because of its low elastic modulus -low ductility –stent may fracture -the mechanical properties do not match the requirements for stent material.
Polymers	-low mechanical performance -successful material for cardiovascular grafts	-body inflammatory reaction -an intense proliferative neointimal response that resulted in the complete occlusion of the vessel

From the mechanical point of view, Fe and its related alloys possess high strength and high ductility. On the other side, it is found that there are two main concerns regarding using Fe as a degradable material; first, it cannot be fully degraded over its service period, leaving a large portion of the stent intact even one year after implantation.

More importantly, upon degradation, it produces a relatively large volume of potentially hazardous iron oxide products which might not be comfortably metabolized in the body. Mg has received a lot of attention as an attractive BM due to its excellent biocompatibility and low thrombogenicity. However, its rapid degradation in physiological environments leads to early undermining the mechanical integrity of the implant. During the last few years, Zn has been introduced to the biomedical community as a potential biodegradable implant material due to its prominent corrosion rate. However, its mechanical properties still need to be significantly improved for load-bearing implants applications.

1.3. Mg-based biodegradable metals

Mg is an essential element to human metabolism with a normal blood serum level of 0.73– 1.06 mmol/L, and the fourth most abundant element in the human body [20]. Its recommended intake for adults lies between 375-500 mg/day, and it is not a source of concern for stents. However, its rapid degradation in physiological environments leads to early undermining the stent's mechanical integrity and the neointimal formation due to the accumulation of the degradation products at the implantation site.

During the past years, so much effort has been made to tailor the properties of Mg through alloying, advanced processing and surface modification techniques. However, still there is evidence that the aforementioned treatments do not fully meet all the expected requirements for an ideal stent [20–22].

1.3.1. Development of Mg-based biodegradable materials

Pure Mg cannot be used for load-bearing implant applications due to the insufficient mechanical properties such as low strength and ductility. Alloying can directly improve its mechanical performance by the contribution of strengthening mechanism such as solid solution strengthening and particle dispersion strengthening [23,24]. Mostly investigated degradable Mg alloys are Mg-Al, Mg-Zn and Mg–rare earth (RE)-based alloys. All these alloy systems show distinct precipitation hardening due to the high solubility of the secondary element in Mg. By now, Al-bearing (e.g. AZ31, AZ61, AZ91and AM80), Zn bearing (ZK30 and ZK60) and RE-bearing (WE43) alloys have been largely investigated [25–28]. Novel Mg-based alloys with as low toxicity level as possible must be formulated for biomedical applications [25,29–32]. Fig. 1.2 shows the typical tensile yield stress versus fracture

elongation of the recently developed Mg-based alloys. As seen, Mg–RE-based alloys show the highest tensile strength while having appropriate elongation.

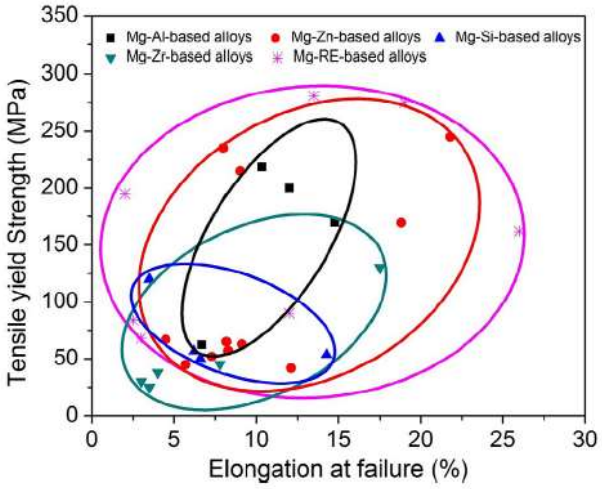

Figure 1.2. *Typical yield strength and fracture elongation of representative biodegradable Mg–X-based alloys [25]*

Mg–Zn-based alloys seem to be promising materials due to the relatively high strength and ductility. In contrast, in this compilation, Mg–Zr-based alloys represent the lowest mechanical properties.

1.3.2. *In vitro* corrosion mechanism

In the nearly neutral physiological environment (pH: 7.4–7.6; Cl^-: 104–150 mmol/L) Mg degrades through the following corrosion process. The corrosion of Mg in aqueous solution comprises three reactions involving the following anodic dissolution of the metal and the cathodic reduction reaction:

$$Mg \rightarrow Mg^{2+} + 2e^- \qquad \text{(Eq. 1.1.)}$$

$$H_2O + 2e^- \rightarrow H2 + 2OH^- \qquad \text{(Eq. 1.2.)}$$

$$Mg^{2+} + 2OH^- \rightarrow Mg(OH)_2 \qquad \text{(Eq. 1.3.)}$$

$$Mg + H_2O \rightarrow Mg(OH)_2 + H_2 \qquad \text{(Eq. 1.4.)}$$

As illustrated in Fig. 1.3., these reactions occur on the implant surface. Different potentials between the metal matrix and second phases cause a micro-galvanic corrosion. $Mg(OH)_2$ precipitates on the Mg surface, forming a protective film with ongoing corrosion. However, in the body fluid with high chloride concentration $Mg(OH)_2$ is not stable and can be further transformed into $MgCl_2$. It results in breaking down the $Mg(OH)_2$ protective layer, leading to the pitting corrosion [4]. Current Mg alloys corrode too fast in the human body resulting in a reduction of mechanical properties of the implants before the host tissue is sufficiently healed [33].

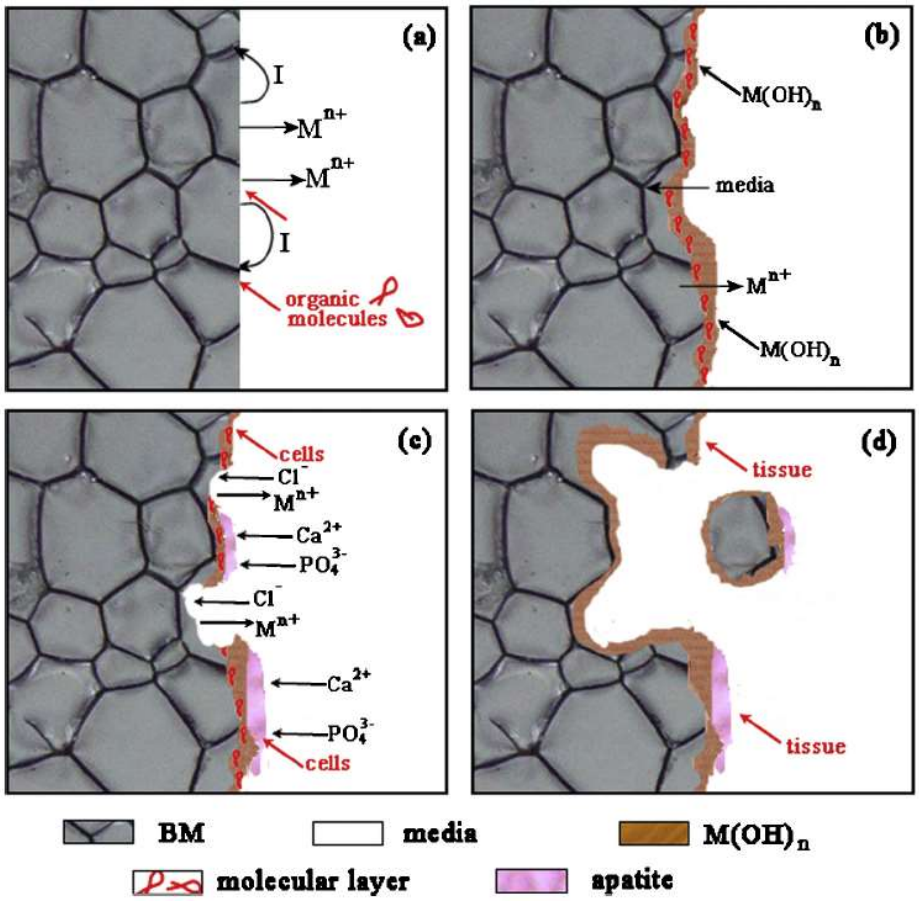

Figure 1.3. *Schematic illustration of a metal degradation in the physiological environment [4]*

During the rapid degradation of Mg-based alloys in the physiological environment a considerable amount of hydrogen gas is released. It affects surrounding tissues, delaying a healing process [34] by forming distinct tissues callus and causing a gas embolism [35,36].

A fast-degrading Mg alloy (ZX50) implanted in the femur of rats filled up the medullary cavity with hydrogen gas bubbles 8 weeks post-operation, resulting in an irregular bone shape even after complete degradation [34]. The hydrogen gas release and rapid corrosion result in a local alkalization and even poisoning if the local pH exceeds 7.8 [36]. Further, the precipitates formed with progressing degradation have a low solubility in body fluids and they cannot be easily eliminated. $Mg(OH)_2$ has an intermediate solubility and during *in vivo* dissolution it reacts with Cl ions, forming soluble $MgCl_2$ [37]. Other degradation products of Mg-based BMs (such as $MgCO_3$, $Zn(OH)_2$, $Mg_3(PO_4)_2$, $Zn_3(PO_4)_2$ and $Ca_3(PO_4)_2$) feature very low solubility [38].

1.3.3. *In vivo* and *clinical* performance

Thus far, several Mg-based alloy implants for orthopedic and cardiovascular applications have been largely investigated *in vivo* [39–41]. Because of their outstanding biocompatibility several clinical trials have been performed on Mg-based BMs. It is worth to mention that among the three BM systems, only for Mg-based BMs number of successful clinical trials was reported in the literature. The results of these trials can be summarized as follows:

- Mg-based alloys have been tested for fracture fixation implants in China, Germany and Korea.
- The clinical trial results of Mg-based screws in hallux valgus surgery was reported by German scientists. MgYReZr screw was approved by official body and got an access to the medical device market for its intended use. In 2015, MgYReZr screws were used in Ireland and Iran [42].
- Mg-Ca-Zn screws for clinic use by the Korea Food and Drug Administration in April 2015. This Mg-based implant is the second approved by an official body in the world [42].
- In 2013, clinical trials of a Mg-based stent were performed. Despite of their success the development of biodegradable metallic stents this potentially still requires more research on the dynamic interaction between the degrading metal surface and the surrounding tissues [43].

1.4. Zn-based biodegradable metals

In recent years, research works have been undertaken to introduce Zn among the potential biodegradable materials due to its excellent biodegradability and adaptability to tissue regeneration. Furthermore, it is an essential element in human nutrition and is the second most abundant transition metal element in the human body, playing a crucial role in cell proliferation as well as in the immune and nervous systems [44,45].

In 2013, a landmark report was published by Bowen et al. [46] introducing Zn as an outstanding BM candidate. They implanted pure Zn wires into the abdominal aorta of adult male Sprague-Dawley rats for up to 6 months. They found that in the first 3 months Zn exhibited a uniform corrosion mode, while after 4.5 and 6 months *in vivo*, a relatively severe and localized attack was observed. As seen in Fig. 1.4, it was reported that Zn exhibits an excellent degradation rate of ~ 0.01-0.02 mm/year in the first three months of degradation in rat arteries, which is a promising value i.e. for biodegradable stent applications. Alongside its good biocompatibility and the appropriate degradation rate, Zn has a low melting point (420°C) and low reactivity in the molten state (unlike Mg), permitting melting and hot processing in the air.

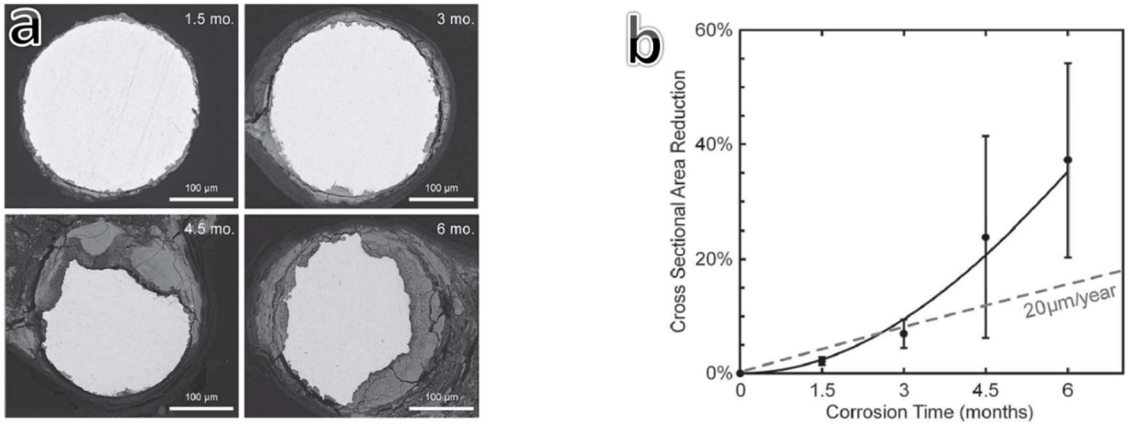

Figure 1.4. *(a) Backscattered electron images of Zn explant cross sections (b) Measured cross-sectional area reduction of Zn wire explants after 1.5, 3, 4.5, and 6 months in vivo [46]*

Nevertheless, the major concern of using pure Zn is its poor mechanical properties with a markedly low ultimate tensile strength (UTS) of about 20 MPa and 120 MPa in cast and wrought conditions, respectively [47,48]. However, compared to Mg, Zn intrinsic lower

corrosion rate provides larger freedom for metallurgical manipulation such as designing alloys with a wide range of non-toxic elements and in a wide range of amounts. In addition to alloying, grain refinement induced by thermomechanical treatments could further improve the mechanical properties of cast Zn alloys.

1.4.1. Development of Zn-based biodegradable materials

The first consideration for alloying element selection to develop biodegradable Zn alloys is elemental toxicity. Elements with potential toxicological problems must preferably be avoided in the initial design stage for biodegradable alloys. The degradation products of the alloys should be non-toxic and readily absorbable by the surrounding tissues. Only limited types of Zn alloy systems have been investigated as potential biodegradable materials thus far [48–58]. Various alloying elements such as Mg, Ag, Sr, Ca, Li, Mn and Cu have been added to Zn to improve its mechanical performance.

In Fig. 1.5. the mechanical properties of investigated Zn-based alloys in the cast and wrought conditions are collected. As seen, cast alloys display a wide range of tensile strength, ranging between 70 MPa and 250 MPa, but very poor ductility (below 4%). The highest tensile strength can be found in Zn-1.5Mg-Ca/Sr alloys due to the combined strengthening contributions of brittle Zn + Mg_2Zn_{11} eutectic constituents, $CaZn_{13}$ and $SrZn_{13}$ intermetallic phases. However, the general mechanical performance, considered as the combination of strength and ductility, for all the reported cast Zn alloys listed in Fig. 1.5a is far below the requirements for the implant materials. Additional improvement in properties could be achieved by post thermomechanical treatments through tailoring the microstructural features such as grain size, secondary phase size/distribution and crystallographic texture. Fig. 1.5b summarizes the tensile strength and fracture elongation of several wrought Zn-based alloys explored to use in the biomedical application during the last two years [47,48,50–55,57–63]. However, by now, no Zn-based alloys have been introduced fulfilling the benchmark values required for an ideal absorbable stent/bone implant material. For Zn-Mg based alloys, which are the most investigated alloys, a parabolic trend can be seen, so that with increasing Mg concentration UTS increases, while the elongation to failure decreases concurrently. However, it is apparent that any percentage of Mg higher than 0.5 wt% results in a drastic drop in fracture elongation. This trend is attributed to the increasing volume fraction of the

brittle $MgZn_{11}$ intermetallic phase. Conversely, in case of Zn-Ag alloys, with increasing Ag content from 2.5 wt.% to 7.0 wt.%, despite a meaningful improvement of tensile strength, fracture elongation remains in the range 32-36%.

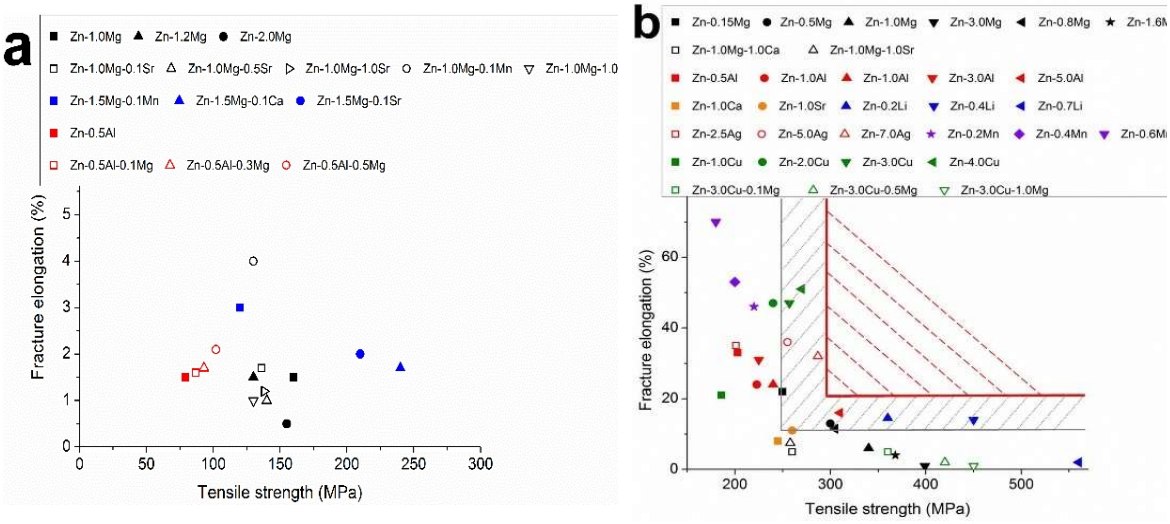

Figure. 1.5. *Fracture elongation versus ultimate tensile strength of (a) as-cast and (b) wrought Zn-based alloys [47,48,50–55,57–63]*

It should be noted that relative to the all binary and ternary Zn alloys, Zn-7.0Ag exhibits the best mechanical properties with UTS and fracture elongation of 287 MPa and 32 %, respectively. Such an excellent combination of high strength and ductility relies on the small grains, very fine and uniformly distributed precipitates and indeed favorable texture orientation. Although among all the reported wrought alloys no materials seem to fully satisfy the mechanical benchmarks required for implant materials, some alloys distributing in the grey hachured region are believed to be promising potential candidates after further development (Zn-0.15Mg, Zn-0.5Mg, Zn-3.0Cu, Zn-4.0Cu, Zn-5.0Ag, Zn-7.0Ag, Zn-5Al, Zn-0.4Li and Zn-0.7Li). It is expected that the mechanical properties of the mentioned alloys could be improved through composition modulation, microstructural optimization (e.g. thermal treatments), further grain/second phase refinement down to submicron regime and texture modification. The latter two issues might be obtained through advanced metal forming processes such as severe plastic deformation techniques by which Mg alloys have been already successfully processed, achieving superior mechanical properties owing to the large strain-induced ultrafine-grained structure and to the texture modification [64,65].

1.4.2. *In vitro* corrosion mechanism

Research on the corrosion of Zn and Zn-based alloys for BMs applications have been carried out over the last few years. Zinc, with a standard potential of -0.8 V, between those of Mg (-2.4 V) and Fe (-0.4 V), seems to satisfy the prerequisites to meet clinical requirements for a potential biodegradable implant material. To date, studies have been focused on the alloying and processing of Zn-based biodegradable materials [48,50–53]. A detailed investigation on the corrosion mechanism and the formation of *in vitro* corrosion products for this biodegradable metal candidate remains largely unexplored. Commercial Hanks' [50,52,58], modified Hanks' balanced salts [48,53], simulated body fluids [55,66], Dulbecco's phosphate buffered saline [67] solutions are among the most common solutions adopted to conduct *in vitro* tests on recently elaborated Zn based alloys. The Pourbaix diagram for Zn shows that in acidic environment (i.e. urine), no surface oxides of Zn are stable, while under neutral or slightly alkaline conditions (i.e. blood plasma) zinc has the tendency to be passivated. Pure Zn is a chemically reactive metal which dissolves in aqueous solutions through the following electrochemical reactions [68]:

$$Zn + OH^- = Zn(OH)_{ads.} + e \qquad \text{(Eq. 1.5.)}$$

$$Zn(OH)_{ads.} + 2OH^- = Zn(OH)_3^- + e\ (rds) \qquad \text{(Eq. 1.6.)}$$

In near neutral environment, predominant Zn species have been identified to be tetrahedral $Zn(OH)_4^{2-}$.

$$Zn(OH)_3^- + OH^- = Zn(OH)_4^{2-} \qquad \text{(Eq. 1.7.)}$$

$$Zn(OH)_4^{2-} = Zn(OH)_2 + 2OH^- \qquad \text{(Eq. 1.8.)}$$

$$Zn + 2OH^- = Zn(OH)_2 + 2e \qquad \text{(Eq. 1.9.)}$$

$$Zn + 2OH^- = ZnO + H_2O + 2e \qquad \text{(Eq. 1.10.)}$$

According to the above-mentioned reactions, solid $Zn(OH)_2$ and ZnO are formed, with no gas evolution during the Zn corrosion. H_2 release during Zn corrosion is expected to be negligible contrarily to the case of Mg. The presence of $Zn(OH)_4^{2-}$ ions in an aqueous

solution generally results in a decrease of H_2 reduction rate. The stability of both $Zn(OH)_2$ and ZnO is limited by environmental parameters. Furthermore, depending on the mentioned environmental parameters other Zn compounds can be formed. Recent studies on Zn and its alloys revealed the presence of several elements such as Zn, P, O, C, Cl, Ca among the corrosion products after the *in vitro* degradation tests. It can be assumed that they are mainly based on calcium phosphates and carbonates [47,48,69]. The oxygen content may imply the precipitation of oxides and insoluble hydroxides. This is probably a result of the ionic interaction between Zn corrosion products and a series of acid radicals such as: $Cl^-, HCO_3^-, HPO_4^{2-}$ [70]. The stability of Zn compounds has been found to affect the corrosion resistance of zinc in many environments. The dissolution of zinc may be greatly inhibited by the formation of solid surface films in solutions containing carbonates according to the following reactions [68]:

$$ZnO + 2H^+ \leftrightarrow Zn^{2+} + H_2O \quad \text{(Eq. 1.11.)}$$

$$Zn^{2+} + H_2CO_3 \leftrightarrow ZnCO_{3(s)} + 2H^+ \quad \text{(Eq. 1.12)}$$

$$5Zn^{2+} + 2HCO_3^- + 6H_2O \leftrightarrow Zn_5\ (OH)_6(CO_3)_{2\ (s)} + 8H^+ \quad \text{(Eq. 1.13)}$$

$$2H^2 + 2HCO_3^- + H_2O + 5ZnO_{(S)} \leftrightarrow Zn_5\ (OH)_6(CO_3)_{2\ (s)} \quad \text{(Eq. 1.14.)}$$

The presence of carbonates and bicarbonates extends the possible passivation region to near neutral pH values. In the presence of Cl^-, Zn^{2+} may be able to form various soluble species, such as $ZnCl_2$, $ZnCl_2^-$ and surface-confined $\beta - ZnOHCl$, that can lead to the formation of the main product of zinc hydroxychloride, $Zn_5(OH)_8Cl_2$. For this case, intermediate corrosion products formed on the surface can prevent the direct exposure to the environment. In particular, $Zn_5(OH)_8Cl_2 \cdot H_2O$ (simonkolleite) contributes to the improvement of corrosion resistance [71].

$$5ZnO + 2Cl^- + 6H_2O \leftrightarrow Zn_5(OH)_8Cl_2H_2O + 2OH^- \cdot 5ZnO + 2Cl^- + 6H_2O \leftrightarrow Zn_5(OH)_8Cl_2 \cdot 2H_2O + 2OH^- \quad \text{(Eq. 1.15.)}$$

In phosphate-containing solutions, the dissolution of Zn occurs through a solid surface film whose composition and structure are affected by the pH. At pH < 12 a solid-phase process

dominates. It has been reported that the presence of HPO_4^{2-} ions inhibits dissolution of Zn, forming insoluble phosphates such as $ZnHPO_4$. Protective films formed during Zn dissolution may have different compositions and various degrees of compactness and thus may significantly affect the dissolution process [68]. Since corrosion patterns are greatly affected by experimental parameters (e.g. composition of the testing solution, temperature, constancy of pH, duration of tests, etc.), a direct comparison between the reported researches can in some cases become uncertain.

Further, strength of the biodegradable Zn implants is desirable during the healing process and is critical for the postoperative rehabilitation. However, deterioration in mechanical integrity is expected as degradation progresses. Moreover, any mechanical load induced on the material may accelerate this process due to the dual effect of corrosion and stress, leading to premature cracking. Mostaed et al. [48] carried out compression tests on Zn, Zn-Mg and Zn-Al binary alloys before and after immersion to evaluate the effect of corrosion on mechanical properties. Compression specimens were immersed in Hanks' modified solution for two weeks. Results revealed that after immersion increasing Mg from 0.15 to 1wt.% led to larger reduction of compressive yield strength, from 8.7% and 20% respectively. This effect was attributed to the increased volume fraction of the second phase, resulting in localized corrosion. In the same report, it was found that Zn-Al alloys have a slower loss of mechanical integrity, which was due to the presence of Al in the solute form, causing more homogenous corrosion mode. Li et al. [50] investigated the tensile properties of the Zn-1Sr, Zn-1Ca and Zn-1Mg alloys for orthopedic applications after 2 and 8 weeks of immersion in Hanks' solution. Results revealed that alloys can retain their mechanical strength during the early implantation time.

1.4.3. *In vivo* performance

Table 1.4. summarizes the main literature outputs about *in vivo* tests carried out on biodegradable Zn and Zn-based alloys. Three zinc-based alloys (Zn-1X, X=Mg, Ca, Sr) have been evaluated for orthopedic applications within mouse femora to characterize the *in vivo* corrosion behavior as well as the bone response. Zn based alloys indicated good biocompatibility in bone.

Table 1.4. *Summary of animal tests for Zn and Zn-based biodegradable metals*

Material	Animal model	Duration (months)	Findings	Degradation rate ($mm \cdot year^{-1}$)	Ref
Zn-1X (X= Mg, Ca or Sr) pins, 0.7mm diameter x 5mm length	Mouse femora	2.0	No inflammation observed around the implantation site, distinct profiles indicate excellent radiopacity, implants promote new bone formation, the bone volume in Zn-1Mg, Zn-1Ca and Zn-1Sr pin groups is higher than that in the sham control group after week 1, and the bone volume in Zn-1Sr group is the highest.	Zn-1Mg = 0.17 Zn-1Ca = 0.19 Zn-1Sr = 0.22	[51]
Zn wire, 99.99% purity	Abdominal aorta of Sprague-Dawley rats	1.5 3.0 4.5 6.0	Critical aspects of biocorrosion – the rate of penetration and the immediate effects of generated products satisfy the requirements for biodegradable implant application; Zn wire remains intact for 4 months. Later corrosion accelerates, corrosion products on zinc after 4.5 and 6 months are compact mainly made of ZnO and $ZnCO_3$	After X months (X= 1.5, 3.0, 4.5, 6.0) 1.5: 0.012 3.0: 0.02 4.5: 0.042 6.0: 0.048	[47]
Zn wire, 99.99% purity		2.5 6.5	Excellent biocompatibility with arterial tissues, no inflammatory response, no progressive intimal hyperplasia nor necrosis.	-	[73]
Zn wires: -99.99% purity electropolished -oxidized -anodized		1.0 2.0 3.0	Zn corrosion rates vary with the different surface engineering of thin oxide films. Degradation rate depends on the quality and stability of the oxide film. Electropolished and anodized wires corroded slower compared to untreated ones.	-	[74]
Zn-Li extruded wires		2.0 4.0 6.5 9.0 12.0	Zn-Li retains about 70% of its original dimension after 12 months follow up. Alloy exhibits linear relationship between the percent of area reduction and time, ideal uniform gradual acceleration of biodegradation, moderate inflammation with non-obstructive neo intima.	After X months (X= 2, 4, 6.5, 9, 12) 2.0 =0.007 4.0 =0.015 6.5= 0.020 9.0=0.037 12.0=0.045	[50]

Results confirmed enhanced new bone formation around the implants. *In vivo* data showed that the corrosion rate of the Zn-1X binary alloys fits for orthopedic application and provides the suitable mechanical support during the tissue repair process [50]. So far, pure Zn, Zn-Al

and Zn-Li alloys have been investigated within blood vessels. Bowen et al. [46] developed and arterial wire implantation model by implanting Zn wire into rat artery lumens to simulate different arterial environments (i.e. stent blood contact and stent matrix contact). The degradation of Zn-based materials was found to be within the desired range with no chronic inflammatory response, localized necrosis or progressive intimal hyperplasia. Additionally, local tissue response to the Zn implant revealed evidences of early tissue regeneration around the biocorrosion area. It was proved that the Zn implant could remain almost intact for the first 4 months of implantation and afterward the corrosion accelerated, indicating timely degradation of the implant.

Zinc and its alloys were introduced as biocompatible and biodegradable metals just a few years ago and they still remain under this category after an upsurge of research activities in the biomedical field with this new class of biomaterials. Development of Zn alloys will continue toward getting proper compositions and meeting the strict clinical criteria for biodegradable implants applications such as excellent biocompatibility, prolonged mechanical integrity. and controlled corrosion rate.

1.5. Fe-based biodegradable metals

Fe is an essential trace element for the human body with a recommended intake between 8 and 18 mg/day for adults [73]. The distribution of Fe in the human body is shown in Fig. 1.6. Fe plays a key role in several enzymatic reactions involving electron transfer. Further it is crucial in the production of red blood cells. Moreover, Fe plays a vital role in metabolism, immunity and cognitive function. There is ~4-5 g of iron in the human body (~40mg/kg and ~50 mg/kg for women and men, respectively). ~2.5 g of Fe is present in the bloodstream and the rest in the ferritin complexes in all cells, liver and spleen.

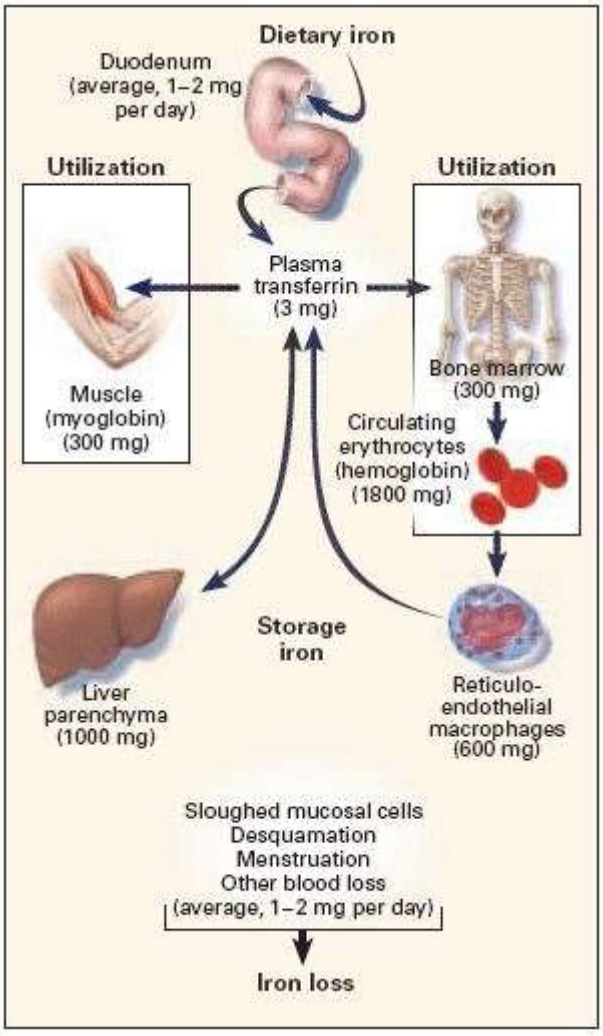

Figure 1.6. *Intake, distribution and excretion of iron in adults [72]*

In 2001, the first pioneering study on Fe as a potential BM was carried out by Peuster et al. [74]. An Fe stent was implanted in the descending aorta of New Zealand white rabbits. The authors found no long-term restenosis and inflammatory response in blood vessels, which are recognized as a clinical complication. Another study conducted by Waskman et al. [75] revealed no excessive formation of neointima. Fe and its alloys possess high radial strength, allowing to use stents with substantially thinner struts and thereby reducing the restenosis rate. Moreover, their high ductility facilitates stent delivery through catheter-based systems. On the other hand, there are two main concerns regarding the use of Fe as a degradable material. First, it cannot be fully degraded over its expected service period of up to two years, leaving a substantial portion of the implant intact even one year after implantation. More importantly, upon degradation it produces a relatively large volume of potentially hazardous iron oxide products which might not be comfortably metabolized in the body [76]. Despite several attempts made over nearly two decades that intended to accelerate the degradation of Fe through alloying with essential elements and/or low content of toxic elements, novel thermal treatments, processing and manufacturing routes including powder metallurgy and advanced forming techniques, further efforts are still required before Fe-based implants can progress to clinical trials [77,78].

1.5.1. Methods for strengthening Fe-based biodegradable materials

The microstructure and mechanical properties of Fe can be modulated and adjusted to suitable targets by controlling the phase composition and lattice features. Here, the relationship microstructure-mechanical properties and the strategies for strengthening of Fe-based BMs are briefly discussed. Strengthening of Fe-based biodegradable metals is reached by hindering the dislocation motion.

1.5.1.1. Work hardening

Work hardening consists in metal strengthening by plastic deformation (PD). PD induces dislocations movements and generation of new dislocations within polycrystalline structure of the metal. PD techniques such as rolling was used in the processing of Fe BMs [79,80], successfully increasing their mechanical strength, while keeping ductility.

1.5.1.2. Solution hardening

Solution strengthening occurs when heterogenous solute atom is introduced to a pure Fe hindering the dislocation movements. Nitrogen (N) and carbon (C) can be used to improve the strength of Fe. N or C, when added to the crystalline lattice of Fe from a solid solution. The local inhomogeneities in the Fe lattice makes plastic deformation more difficult to occur. Nitrided Fe and Fe-C with improved mechanical properties, compared to pure Fe have been investigated for BM applications [80–82]

1.5.1.3. Precipitation hardening

Precipitation hardening (known also as particle hardening or age hardening) is a common method to increase the strength and hardness of metals. Due to the thermal treatment, uniformly dispersed particles are precipitated. The formation of these precipitates occurs during solution treatment at high temperatures prior to a rapid cooling process. The precopitates hinder dislocation motion, altering the strength of the material. Hardening due to uniform dispersion of Pd-rich clusters was observed in Fe-Mn-Pd biodegradable alloys designed specifically for stent applications [83].

1.5.1.4. Grain refining hardening

Grain refinement is a well-known method to improve the mechanical and corrosion properties of metals. The grain refinement strengthening is defined by Hall-Petch relation based on which the yield stress σ_y consistently increases with decreasing the grain size by the following equation:

$$\sigma_y = \sigma_0 + \frac{K}{\sqrt{d}} \qquad \text{(Eq. 1.16)}$$

where σ_0 is the resistance of the lattice to dislocation motion, K is strengthening coefficient, which is a constant unique to each material and d is the average grain size. Grain refinement is mainly achieved by the addition of alloying element and applying thermomechanical treatments. However, the latter's effect is more pronounced, resulting in a remarkable improvement of mechanical strength. Variety of thermomechanical processing methods were applied to improve the performance of Fe-based biomaterials such as high-pressure torsion

(HPT) [84], equal channel angular pressing (ECAP) [85], and accumulative roll bonding (ARB) [79].

1.5.1.5. Composite strengthening / Particle dispersion hardening

Metal matrix composites (MMCs) which introduce micometer-sized reinforcing particles in a bulk matrix offer opportunities to tailor material's mechanical performances. With the emersion of nanomaterials, nanocomposites have developed with outstanding properties, suppressing the limitations for metals and conventional composites. The possibility of combining different materials (e.g. metal – ceramic – non-metal) provides the opportunity for infinite variations. The properties of these novel materials are arisen from the properties of their individual components. Fig. 1.7 shows the distribution of the composite materials into three distinct groups of materials. Reinforcing of Fe-based BMs would have various objectives which could be summarized as follows: (i) improvement of mechanical strength, while keeping acceptable ductility and toughness, (ii) increasing the fatigue resistance, (iii) increasing the Young's modulus, (iv) increasing corrosion rate in physiological environment resulting from micro-galvanic coupling and (v) improving the biocompatibility by introducing bioactive reinforcements. The improved mechanical performances of MMCs are arisen from several strengthening mechanisms such as: (i) load transfer effect, (ii) Hall-Petch strengthening, (iii) Orowan strengthening, (iv) mismatch in coefficient of thermal expansion (CTE) and elastic modulus (EM).

- **Load-transfer effect**

When composites having a strong bonding between the reinforcements and matrix is under loading, the applied load could easily transfer from the matrix to the particles. This effect is defined by the following model suggesting by Nardone and Prewo [86]:

$$\Delta\sigma_l = v_p \sigma_m \frac{(1+t)A}{4l} \qquad \text{(Eq. 1.17)}$$

where v_p is volume fraction of the reinforcing particles, σ_m is the matrix yield strength, l is the size of the particle parallel to the load direction, t is the particle thickness and A is the aspect ratio (l/t). It should be noted that when the reinforcements are equiaxial, their load

bearing contribution are independent from their size, which simplifies the aforementioned equation to the following one [87]:

$$\Delta\sigma_l = \frac{1}{2}\frac{v_p}{\sigma_m} \qquad \text{(Eq. 1.18)}$$

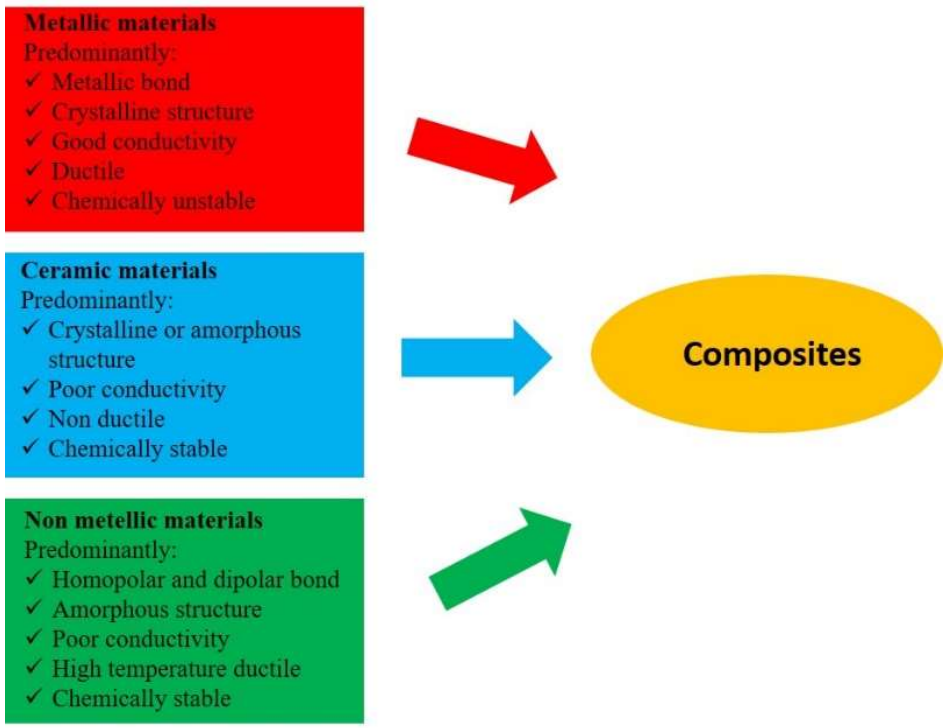

Figure 1.7. *Classification of composite materials within the group of materials[88]*

- **Hall-Petch strengthening**

Grain size has a crucial role in mechanical performances of metallic materials according to the Hall-Petch relation which is discussed in section 1.3.1.1. in MMCs, the reinforcements can restrict the growth of grains during thermal or thermomechanical treatments. The final grain size d_m in composites is defined by the Zener equation [89]:

$$d_m = \frac{4\alpha d_p}{3v_p} \qquad \text{(Eq. 1.19)}$$

where α is a proportionality constant, d_p the particle diameter, and v_p the volume fraction of the reinforcement.

- **Thermal expansion coefficient and elastic modulus mismatch**

In composites there is a difference in thermal expansion coefficient (CTE) and elastic modulus (EM) between the matrix and the reinforcement. When the composite is under loading, this mismatch leads to the formation of geometrically necessary dislocations (GND) [87]. GND density ρ_{CTE} can be estimated by the following equation [89]:

$$\rho_{CTE} = \frac{A\Delta\alpha\Delta T v_p}{b d_p (1-v_p)} \qquad \text{(Eq. 1.20)}$$

where $\Delta\alpha$ is the CTE difference, ΔT the difference in temperature between the processing and testing, A a geometric constant, b the magnitude of the Burger's vector, d_p the particle diameter, v_p the particle volume fraction;

$$\rho_{EM} = \frac{6v_p}{\pi d_p^3}\varepsilon \qquad \text{(Eq. 1.21)}$$

The increase in strength due to the two contributions is defined by the Taylor equation as follows:

$$\Delta\sigma_{CTE+EM} = \sqrt{\beta}Gb(\sqrt{\rho_{CTE}} + \sqrt{\rho_{EM}} \qquad \text{(Eq. 1.22)}$$

where G is the shear modulus.

- **Orowan strengthening**

When the reinforcements sizes are in nano-sized scale, they can hinder the dislocation movements. During the deformation, when a dislocation reaches a particle, it is forced to bow around the particle. This requires a higher energy for dislocations to pass the particles and thus, making the dislocation motion more and more difficult. The contribution of the Orowan effect to the strength can be defined as follows:

$$\sigma_O = M\frac{0.4Gb}{\pi(1-\nu)^{0.5}}\frac{\ln\frac{d}{b}}{\lambda} \qquad \text{(Eq. 1.23)}$$

where ν is the Poisson's ratio, M is the mean orientation factor and λ is the interparticle spacing. Several BMs Fe-based composites have been investigated so far. They will be discussed in detail in the next sections.

1.5.2. Pure Fe, its alloys and composites for BMs applications

Several types of iron-based alloys have been proposed for biomedical applications, including pure metallic Fe, binary Fe-metal alloys (metal = Mn, Co, Al, W, Sn, B, C, S), ternary ones (Fe–10Mn–1Pd , Fe–21Mn–0.7C, Fe–21Mn–0.7C–1Pd, Fe–Mn–Si), Fe-based bulk metallic glasses (BMG) and other Fe-based alloys obtained by elements forming intermetallic or second phases and Fe-based composites (Fe-W, Fe-CNTs (carbon nanotubes), Fe-Pt, Fe-Pd, Fe-Au, Fe-Ag, Fe-Fe_2O_3, Fe-HA (hydroxyapatite), Fe-TCP (tricalcium phosphate) and Fe-BCP (biphasic calcium phosphate)).

1.5.2.1. Pure Fe

Pure iron has been demonstrated as a potential candidate for biodegradable metal due to its appropriate biocompatibility, excellent mechanical properties and suitable biodegradation behavior [79,85,90]. Pure iron Armco was tested as reference material. It is a steelwork product commercially available with an iron content of 99.85% without the addition of other elements; the chemical composition is shown in Table 1.5. Obayi et al [79] studied the influence of the average grain size on its mechanical properties and degradation behavior. In this work the influence of combination of different cold working degree and annealing temperature on final mechanical properties were investigated. It was found that larger average grain size is detrimental to the desired strength, ductility and other beneficial grain-dependent properties. The degradation rate of polycrystalline pure iron is slightly dependent on grain size.

Table 1.5. *Concentration of impurity elements in the as-received Armco iron*

Element	C	Ni	Cr	Mn	Cu	Mo	S	Sn	P	Si	Al
Weight %	0.006	0.037	0.032	0.041	0.017	0.002	0.014	0.014	0.019	0.008	0.010

Moravej et al. [78,91]developed pure iron foils using an electroforming process. The electroforming technique was developed for fabricating iron foils and sheets for application as biodegradable cardiovascular stent. Fine grain pure iron (average grain size: ~4μm) produced by electrodeposition had a structure that affected the corrosion rate in Hanks' solution. Electroformed iron showed a faster degradation rate than iron fabricated by casting, with a more uniform degradation mechanism [91,92].

Nanostructured, nanocrystalline pure iron obtained by severe plastic deformation (SPD), was developed and investigated by Nie *et al*.[85]. It was reported that SPD processed iron exhibited higher strength and much stronger corrosion resistance than those of microcrystalline pure iron as seen in Table 1.6. Micro-hardness value and tensile strength variation for samples at distinct stages of the SPD process showed that mechanical and corrosion properties were strongly dependent on the grain size.

Table 1.6. *Summary of the mechanical properties of pure Fe for application as biodegradable metal*

	Materials	YS MPa	UTS MPa	Elongation %	Ref
Pure Fe	As-cast	170±2	270±5	49±3	[79]
	Rolled/annealed (550ºC)	246±10	283±6	34±3	[79]
	electroformed	360±9	423±12	8.3±2	[91]
	ECAPed (8 passes)	No data	470±29	No data	[85]
	PM/Hot rolled	385±3	420±8	22±6	[77]
	SPS	*220±7	800±14	No data	[93]
	Nitrided Fe	561.4	614.4	—	[82]

*Compression test

1.5.2.2. Fe-Mn system

Pure iron degrades too slow, and it can stay intact after 1-year implantation [74]. Furthermore, ferromagnetism also greatly restricts the compatibility for some specific imaging examinations, such as magnetic resonance imaging (MRI).

As listed in Table 1.7, so far, various iron-manganese alloys have been widely investigated for degradable biomaterial applications –Manganese (Mn) is an essential trace element for the body function of all mammals being necessary for the development of the metabolism and for the antioxidant system. Addition of Mn accelerates CR by decreasing potential of Fe-matrix, this making it more susceptible to degradation [94]. Furthermore, Mn tends to promote the formation of austenite phase which makes Fe-Mn alloys non-magnetic. Indeed, this effect is beneficial for medical implant applications, especially for stents.

Hermawan *et al*. [95] manufactured the Fe–Mn alloys-with different contents of Mn ranging from 20 to 35 wt%- and investigated systematically their mechanical performance and *in vitro* corrosion behavior. Fe-Mn alloys were prepared from pure Fe and Mn powders. Powders were mixed, compacted, sintered and cold-rolled. Fe–25Mn and Fe–20Mn alloys were mainly composed of γ and ε phases, while the alloys with higher Mn content (30 and

35 wt%) were composed of only γ phase. With an increasing content of Mn, the ultimate strength decreased, but the ductility increased significantly (Table 1.7.). Electrochemical test results showed that Fe–Mn alloys containing γ and ε phases corroded faster than those containing only γ phases. *In vitro* dynamic immersion test results showed that corrosion rate of Fe–Mn alloys was about 520 mm year^{-1}, which was about two times higher than that of pure Fe (220– 240 mm year^{-1}). The mechanical properties of Fe–35Mn (UTS = 550 MPa, YS = 228 MPa, A = 32%) were close to those of 316L SS and superior than those of pure Fe and Mg [96]. Furthermore, the magnetic susceptibility of Fe–Mn alloys was considerably reduced compared to that of 316L SS. Electrochemical test results showed that Fe–Mn alloys containing γ and ε phases corroded faster than those containing only γ phases. *In vitro* dynamic immersion test results revealed that corrosion rate of the alloys was about ~520 mm year^{-1}, which was about two times higher than that of pure Fe (220– 240 mm year^{-1}). *In vitro* cytotoxicity test results confirmed no inhibition of Fe– Mn alloys on 3T3 fibroblast cells [97].

Sing *et al*. fabricated Fe–35 wt%Mn alloy stents by laser cutting, annealing and descaling [98]. Their degradation behavior was tested in a simulated human coronary arterial bench system from 0.5 to 168 h. The results showed that corrosion occurred after 1 h on both crimped and expanded stents, mostly on the curvatures of the stents as seen in Fig.1.8. The corrosion rate of a stent was higher compared to the alloy, suggesting the influence of implant processing on its microstructural/surface properties. Therefore, Fe–Mn alloys were considered as appropriate degradable implant materials due to their good mechanical properties, accelerated corrosion rate, excellent paramagnetic features and biocompatibility.

Heiden *et al*. [99] developed as-cast Fe–33 wt%Mn alloy and investigated the influence of different deformation methods and heat treatment on its corrosion rate. Both annealing and cold working (CW) could accelerate the corrosion rate of as-cast Fe–33 wt%Mn alloy. Among the samples, the one that underwent SPD technique exhibited the fastest corrosion rate, as 2.4 times as high as that of as-cast Fe–33Mn. It was reported that up to a certain point the corrosion rate accelerated by increasing the strain level. Above this point, increasing the deformation strain no longer increased the corrosion rate. Heiden *et al*. [100] also developed Fe–20 wt% Mn alloy by arc melting and processed these alloys by cold rolling to 77% CW.

They found that 77% CW cold rolling suppressed the instantaneous corrosion rate compared with the cast structure.

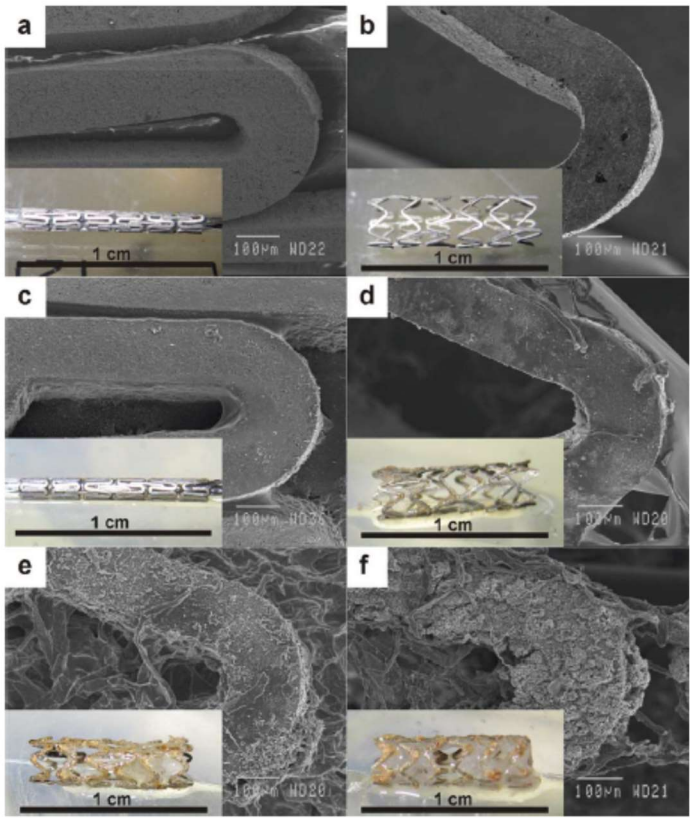

Figure 1.8. *SEM images and photographs of the Fe35Mn stents: (a, b) crimped and expanded stents before dynamic corrosion test, (c) crimped stent after 0.5h of dynamic corrosion test, (d, e, f) expanded stent after 1h, 24h and 168h of dynamic corrosion test, respectively [98]*

Drynda *et al*. [101] developed some Fe–Mn alloys with low content of Mn to avoid the toxicity of Mn, including Fe–0.5 wt%Mn, Fe–2.7 wt%Mn, and Fe–6.9 wt%Mn alloys. The formulated alloys exhibited good mechanical properties and biocompatibility, while the *in vitro* immersion test results revealed that the corrosion of the Fe–Mn alloys were slightly slower compared to pure iron. Moreover, the *in vivo* test in a mouse model showed no significant corrosion even after 9 months' implantation. Furthermore, Pd was introduced in the Fe-Mn alloys to tune their mechanical and corrosion properties [94]. The corrosion rate of Fe-10Mn-1Pd was ten times higher than that of SS316L.

Further, Schinhammer et al. [83,102,103] performed a research on Fe-Mn-C(-Pd) BMs. New alloys featured an accelerated corrosion rates.

The degradation behavior of Fe-based alloys depends on the method of manufacturing and processing techniques [6]. For example, Fe–Mn alloys produced by PM exhibited accelerated *in vitro* degradation compared to the same alloy fabricated by casting (as seen in Table 1.7).

Liu et al. [104] prepared Fe-30-Mn-6Si shape memory alloys by casting. It was established that this alloy consists of ε-martensite and γ-austenite. Further, its strength is superior compared to the cast Fe-Mn alloy (YS = 225 MPa, and UTS = 450 MPa). Elongation decreased noticeably with an addition of Si to Fe-Mn alloy (55% vs 18%) as reported in Table 1.7. Fe-30Mn-6Si exhibits higher corrosion rate than that of pure Fe because the addition of Si increases the contents of γ-austenite which is less corrosion resistant than α-Fe. For this .reason, this method is promising for the fabrication of other BMs with accelerated corrosion rate [105].

Table 1.7. *Summary of the properties of reported Fe-Mn system for biodegradable metals*

Materials	YS/MPa	UTS/MPa	Elongation/%	Hardness HV/10	Ref
Fe-20Mn/PM	420	700	8	230±1	[95]
Fe-25Mn/PM	360	720	5	200±1	
Fe-30Mn/PM	240	520	20	110±1	
Fe-35Mn/PM	230	430	30	106±2	
*Fe-35Mn, 27% porosity	No data	*50.7±4.21	*1.11±0.15	33.78±2.25	[106]
*Fe-35Mn, 40% porosity		*30.1±1.57	*0.95±0.21	27.72±2.01	
*Fe-35Mn,48% porosity		*20.2±2.54	*0.74±0.12	13.58±1.98	
Pure Fe	299±11	372±18	57±3	**96±4 (HBW)	[107]
Fe-30Mn/ hot forged	242±14	632±12	94±6	**175±7 (HBW)	
Pure Fe	207±19	313±6	37±2	No data	[101]
Fe-0.5Mn casting followed by forging	295±20	353±14	28±4		
Fe-2.7Mn	370±29	495±5	31±1		
Fe-6.9Mn	814±26	1041±7	11±1		
Fe-30Mn/cast	124.5	366.7	55.7	—	[104]
Fe-30Mn-6Si/cast	225	450	18	—	
Fe-30Mn/forged	169	569	60	—	[108]
Fe-30Mn-1C/forged	373	1010	88	—	
Fe-10Mn (sheet)	Samples failed before reaching uniform elongation			428±6	[94]
Fe-10Mn (heat treated)	800	1400	14	374±4	
Fe-10Mn-1Pd (sheet)	950	1500	2	432±8	
Fe-10Mn-1Pd (heat treated)	850	1450	11	384±5	
Fe-10Mn-1Pd (heat treated)	900	1550	7	437±3	

*Compression test, **Brinell hardness (HBW)

1.5.2.3. Other Fe-based alloys systems

Liu et al. demonstrated the effect the of alloying elements addition (such as W, Co, Al, Mn, Sn, C and B) on the biodegradability of Fe (Table 1.8). The results revealed that alloying with Co, W, C and S improved mechanical properties. Corrosion rates could be accelerated after the alloying with Co, W, C and S [80]. Addition of Co, B, W, Mn, S and C was found to enhance strength of Fe, while alloying with Sn resulted in substantial reduction of the strength and ductility.

Wang at al. formulated Fe-Ga alloys with an addition of B and TaC [109]. The $Fe_{81}Ga_{19}$ alloy contained A2 and $D0_3$ phases. In addition, Fe_2B and TaC second phases were detected in the $(Fe_{81}Ga_{19})_{98}B_2$ and $(Fe_{81}Ga_{19})_{99.5}(TaC)_{0.5}$ alloys, respectively. The results of the electrochemical measurements and static corrosion tests indicated a higher corrosion rate for Fe-Ga alloy compared to pure Fe in SBF at 37°C. The alloying with more reactive (compared to Fe) Ga reduced the corrosion potential of the Fe matrix, resulting in accelerated corrosion rate of new alloys. The addition of B or TaC resulted in the formation of multiple phases on the surface of the $Fe_{81}Ga_{19}$ alloy, shifting a corrosion mode to localized severe pitting.

Capek et al. [110] investigated Fe2Pd, Fe2Ag and Fe2C alloys, prepared by powder metallurgy techniques. The microstructural and chemical analyses of sintered materials revealed that the diffusion between Fe, C and Pd was strongly limited by processing parameters. A slight increase in porosity was observed in case of alloys. The presence of porosity deteriorated the mechanical properties of the alloys compared to pure Fe. Addition of Pd and C successfully accelerated the corrosion rate of Fe. Alloying with Pd resulted in higher corrosion rates in the long-term immersion compared to Fe2C. However, electrochemical measurements indicated the opposite trend. Alloying with Ag improve the corrosion resistance of Fe in both tests. The results suggested that the addition of Pd and C could be a promising approach to accelerate the corrosion rate of Fe-based biodegradable materials.

Others powder metallurgical Fe alloys were developed by Wegener at al. [111]. The degradable Fe-based alloys were prepared for matrix material of cellular structures application. Fe–C, Fe–0.6P, Fe–1.6P, Fe–B and Fe–Ag samples were manufactured. Phosphorus was found to have a beneficial effect on sintering. Therefore, the mechanical

strength of Fe-P was enhanced significantly. Although phosphorus is known to inhibit corrosion, no effect on the degradation rates was observed. Furthermore, no detrimental effects on the cell proliferation was noticed as well. Corrosion rates increased slightly in case of Fe-C alloy.

Table 1.8. *Summary of the properties of reported Fe-based alloys and Fe-based composites for biodegradable metals*

Materials	YS (MPa)	UTS (MPa)	Elongation (%)	Ref.
Fe-3Co rolled	460	648	5.5	[80]
Fe-3W rolled	465	712	6.2	
Fe-3C rolled	440	600	7.4	
Fe-3S rolled	440	810	8.3	
Fe-5W SPS	*220	940	—	[93]
Fe-1CNT/ SPS	*215	1260	—	
Fe-2.5HA	*68	*97	**3.5	[112]
Fe-5HA	*50.8	*60	**1.9	
Fe-10HA	-	*16	**0.1	
Fe-5Ag	*380	*1620	—	[113]
Fe-10Ag	*210	*1110	—	
Fe-5Au	*240	*1421	—	
Fe-10Au	*260	*1510	—	

*compression test

** fracture strain

Hrubováková et al. [114] prepared Fe foams alloyed with P. The foams exhibited an open, interconnected, microstructure. The presence of phosphorus improved their mechanical properties. Unfortunately, corrosion of Fe decreased after the addition of P.

Xie et al. [115], designed and developed Mg-Fe alloy through high energy ball milling, followed by spark plasma sintering (SPS) consolidation. The $Mg_{30}Fe_{70}$ alloys revealed excellent mechanical properties with ultrahigh strength - 1380 MPa and high hardness -424 HV. Moreover, their degradation rates were significantly improved compared to pure Fe. The major obstacle in fabrication of Mg-Fe alloys is immiscibility of Fe and Mg in both solid and liquid states. Moreover, their melting points and differences are significant. Therefore, Mg and Fe do not form intermetallic compounds by using conventional processing methods.

Porous Fe/Fe-xW (x= 0.5; 1; 1.5; 2 wt%) electrodeposited scaffolds featuring double-layer structured skeleton composed of a hollow Fe frame wrapped in a thin outer layer of Fe-W alloy were prepared by He at al. [116]. These scaffolds were characterized by a cellular morphology with a large surface area, comparable to that of cancellous bone.

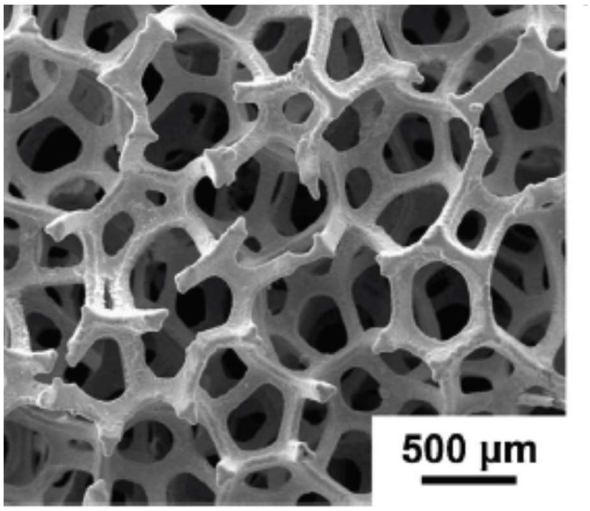

Figure 1.9. *Morphology of the 1.5FeW scaffold [116]*

Moreover, their tensile strength and the density were similar to those featured by cancellous bone. In vitro corrosion rates and biocompatibility varied with the chemical composition of the scaffold. The results of static immersion tests revealed the rapid corrosion at the beginning of the test. Subsequently, the corrosion rates decreased gradually (up to the end of the 30 days corrosion test) due to the protective film formation. Pure Fe exhibited slightly higher corrosion rates compared to Fe-W scaffolds. The extraction medium of the pure Fe featured the lowest cell viability. The cell viability was associated with a corrosion rates, therefore the extract of Fe-W scaffolds revealed better biocompatibility.

Fe-Zn alloys with different concentration of zinc (5, 10 and 15%) were prepared using electroforming by Wang et al [117]. The results revealed that the alloys consisted of single-phase Fe-Zn solid solution and had higher corrosion rate than pure Fe.

1.5.2.4. Iron-based biodegradable composites

To accelerate the corrosion rate of Fe and preserve or improve its mechanical strength to support the healing process, more complex compositions containing very low levels of noble and well dispersed component can be a satisfactory solution. Metal matrix composites

(MMCs) shows enhanced mechanical properties. A variety of secondary phases have been added into Fe matrix to generate micro-galvanic phenomena between the matrix and secondary phases, accelerating its corrosion rates.

Recently, variety of Fe matrix composites (Fe-W, Fe-CNT, Fe-Ag, Fe-Au, Fe-Fe_2O_3, Fe-Pt and Fe-Pd) were prepared by spark plasma sintering (SPS) [93,113,118,119]. Introduction of reinforcement could significantly improve the ultimate compressive strength of aforementioned MMCs. The addition of W, Fe_2O_3, Ag and Au only slightly enhanced the degradation rate (~2.8μg/cm^2/h) compared to pure Fe (2.62μg/cm^2/h) Introduction of CNT was the most effective in acceleration the corrosion rate of Fe (~4.3μg/cm^2/h). Subsequently, Huang et al. reported that Fe-5Pd and Fe-5Pt revealed enhanced corrosion rates, even higher than Fe–0.5 wt% CNT and Fe–5 wt% W. It was found that the reinforcement was uniformly distributed throughout Fe matrix. MMCs obtained after sintering by SPS showed high density. In addition, they did not induce any obvious cytotoxicity to L929 ECV304 cells. However, VSMC cell viability was reduced. Hemolysis percentage for all composites was less than 5%, and no thrombogenicity was observed.

Most of the studies on Fe BMs focused on optimizing their mechanical properties, accelerating their corrosion rates and enhancing the corrosion mode with no emphasis on enhancing their bioactivity. Ulum et al. [120] discussed the opportunity of promoting bioactivity by introducing various bioactive ceramics into Fe matrix. Fe-based composites composed by Fe-matrix and ceramic reinforcement, such as– hydroxyapatite (HA), tricalcium phosphate (TCP) and biphasic calcium phosphate (BCP) were prepared by powder metallurgy (mechanical milling followed by sintering process). These three composites exhibited an accelerated corrosion rates. However, their mechanical properties in terms of mechanical strength deteriorated. From the biological point of view, favorable reactions with bone growth were observed. *In vitro* cytotoxicity results revealed enhanced cellular activity when rat smooth muscle cells interacted with the corroding composite samples compared to pure Fe. X-ray radiography pictures clearly indicated a coherent *in vivo* degradation progression. Even after 70 days of implantation, a positive tissue response in sheep animal model was observed.

Several kinds of Fe–HA composites were manufactured by powder metallurgy methods. The samples were prepared using different amount (2.5, 5, 10 wt%) and particle size (1 μm, 1–10 μm, 100–200 μm) of hydroxyapatite (HA) as a bioactive phase in the iron matrix [112]. X-ray diffraction did not indicate the formation of new phases after powder sintering process. Mechanical properties such as yield strength, tensile strength, and ductility of the composites deteriorated with the higher reinforcement content and lower particle size. The corrosion rates showed increasing tendency with higher HA fraction. The strongest composite was Fe–2.5 wt% HA (100–200 μm) with YS = 81.7 MPa, UTS = 130.1 MPa, fracture strain of 4.87%, and *CR* = 0. 23mm·year^{-1}. In contrast, the weakest composite was Fe–10 wt% HA (1 μm) which did not exhibit a plastic deformation, fractured at YS= 16.1 MPa with 0.11% strain, and showed the highest *CR* =1.07 mm·year^{-1}.

Iron-matrix composites containing substantial amounts (20-40%) of calcium silicate (CS) ceramic particles were successfully prepared by means of powder metallurgy processes. Pure Fe and Fe-CS were fully consolidated, exhibiting relative sintered density ~98% and uniformely distributed reinforcement in case of composite material. The bending strength of pure iron was only slightly decreased when the content of CS was limited to 20%. Homogenously distributed CS particles in the composites induced enhanced deposition of CaP on the surfaces of specimens after immersion in the SBF solution for seven days. In addition, the degradation rates of the Fe-CS composites were significantly higher than that of pure iron, owing to the high solubility of the CS bioceramic in SBF[121].

1.5.2.5. Surface modifications for enhanced degradation rate of Fe-based alloys

Silver ions were implanted into the surface of pure Fe by metal vapor vacuum arc (MEVVA) technique in order to enhance the degradation rate of the substrate [122]. The analyses revealed 60 nm depth of an Ag implantation. In the outer layer the presence of Ag_2O was confirmed, while zero-valent Ag was detected for increasing implantation depths. The implantation of Ag ions could increase the corrosion rate of the pure Fe. In addition, Ag-containing samples exhibited uniform degradation mode. However, the results of platelet adhesion tests suggested an increasing risk of the thrombosis.

The same method (MEVVA) was adopted to implant Zn ions [123]. The implantation depth for Zn ions was (similarly as in case of Ag) about 60 nm. The degradation rate of pure iron was found to be accelerated after zinc ion implantation.

Magnetron sputtering followed by UV-lithography was employed to manufacture Fe-Au multilayer foils. [124,125]. A homogenous microstructure with finely distributed Au precipitates was obtained after annealing of Fe-Au foils. The mechanical testing revealed a high tensile strength in a range of 550-800 MPa depending on the Au content and parameters of heat treatment. In addition, the Fe-Au foils showed a significantly accelerated corrosion compared to pure iron samples.

Huang at al. [126] coated two unique designs of platinum disc arrays on the surface of pure Fe as shown in Fig. 1.10. Disc arrays were deposited through photolithography combined with electron beam evaporation.

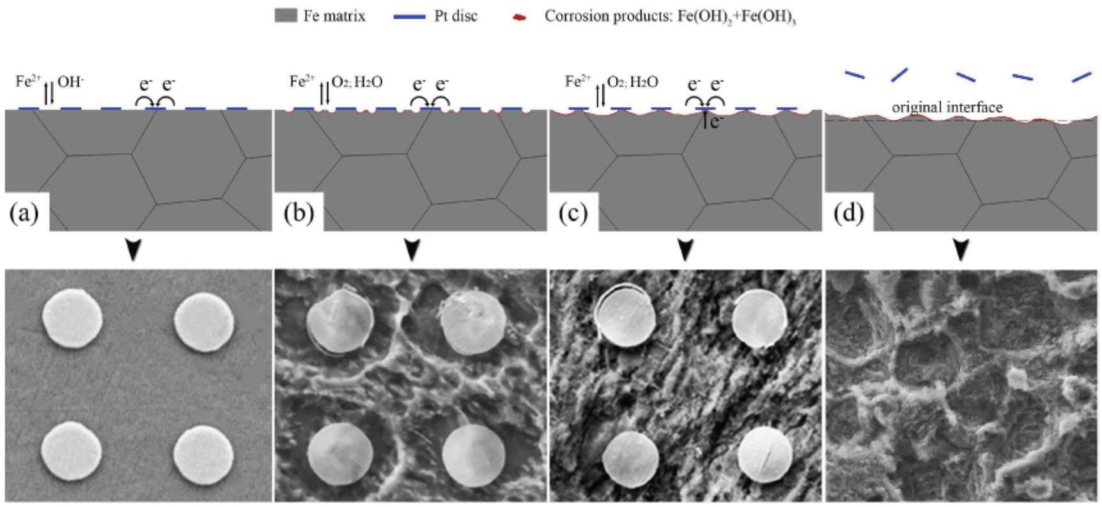

Figure 1.10. *Scheme of the degradation mechanism for Pt discs patterned pure iron: **(a)** corrosion initiation; **(b)** and **(c)** formation of hydroxide layer; **(d)** after Pt discs fell off, the enhanced degradation rate of Fe is observed due to the formation of several uniformly distributed pits on its surface [126]*

With progressing corrosion, number of galvanic cells was formed around Pt discs, resulting in considerable enhanced degradation rate compared to untreated samples. Simultaneously, because of the possibility to modulate and adjust the shape, size and distribution of Pt discs, not only degradation rate but also degradation mode could be effectively controlled. Pt disc

pattern as the one presented in the Fig. 1.10. showed almost no toxic effects on human umbilical vein endothelial cells. However, a considerable inhibition on proliferation of vascular smooth muscle cells was observed. The hemolysis rate of Pt patterned samples was lower than 1%. The number of adhered platelets was significantly reduced in a presence of Pt discs.

Another technique to tailor corrosion behavior of Fe is introducing biodegradable polymers into the metal matrix. Porous pure iron (PPI) was vacuum infiltrated by poly(lactic-*co*-glycolic acid) (PLGA) to form fully dense infiltrated porous iron (PIPI). PIPI samples were dip coated into the PLGA forming partially dense PLGA-coated porous iron (PCPI). The results of mechanical tests revealed improvement in terms of mechanical properties of containing polymers Fe samples (PIPI and PCPI). In addition, PIPI and PCPI samples showed enhanced corrosion rates compared to PPI. Faster degradation rates were attributed to the effect of PLGA hydrolysis. More importantly, the accelerated corrosion of PIPI did not influence the viability of human fibroblast cells [127].

1.5.3. Manufacturing and processing techniques for fabrication of iron-based BMs.

To enhance the mechanical properties and the corrosion rate of Fe-based biodegradable metals, many novel fabrication and processing methods were developed, such as electroforming, equal channel angular pressing (ECAP), metal injection molding (MIM), cold gas dynamic spraying (CGDS) and 3D printing.

1.5.3.1. Electroforming

Electroforming enables the deposition of a thin metallic films. This technique has been previously exploited to deposit coatings on the substrate surface with the electroforming process, it is possible to produce thin metallic layers (in range of 10 μm to 500 μm).
The feasibility of developing this strategy to fabricate Fe tubes as a stent precursor was firstly investigated by Moravej et al. [128]. Fig. 1.11. shows the stent made of electroformed Fe mini-tubes at each processing step. The results proved that mini-tube electroforming followed by laser cutting is a promising method for manufacturing of thin walled implants such as stents.

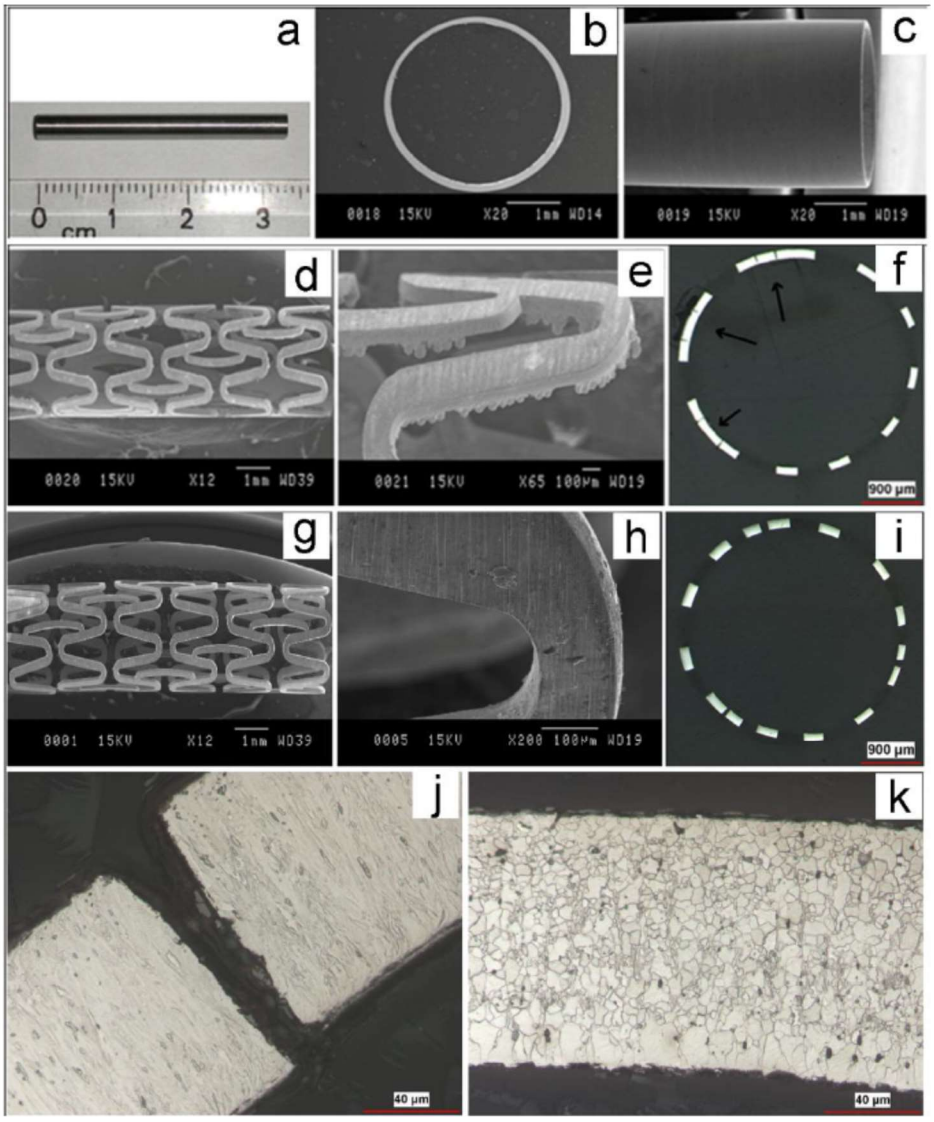

Figure 1.11. *Morphology of Fe electroformed mini-tube/stent at different processing steps:* ***(a–c)*** *ground mini-tube;* ***(d–f)*** *laser cut mini-tube;* ***(g–i)*** *final stent;* ***(j, k)*** *cross section of the stent [128]*

1.5.3.2. Severe plastic deformation techniques

New generation of thermomechanical methods known as severe plastic deformation (SPD) techniques are proved as novel grain refiners (down to submicrometric regime), resulting in markedly improvement of mechanical strength in metallic materials. In SPD techniques such as equal channel angular pressing (ECAP), high-pressure torsion (HPT), accumulative roll bonding (ARB) and asymmetric rolling (AR) massive deformation is imposed to the materials at relatively lower temperatures than those of conventional thermomechanical

treatments. This results in an achievement of reasonably equiaxed ultrafine grains (UFG) within the whole volume of the samples. The potential of generating UFG structure in metallic materials aimed at obtaining improved mechanical properties opens new opportunities for materials in applications where conventional treatments have failed to introduce [129–132]. Nie *et al*. obtained nanosized grain pure Fe with employing ECAP processing. The material exhibited higher strength and corrosion resistance than its coarse-grained counterpart. So that in the latter case many big and deep corrosion pits were observed. The number of corrosion pits considerably decreased after two- and four-pass ECAP. Eventually, after eight passes, the surface of pure iron had fully distributed corrosion pits, but these pits were smaller and shallower than that of the untreated pure iron. *In vitro* cytotoxicity test results showed that nanoscale pure iron could stimulate growth of ECV304 cell and L-929 cells but inhibited proliferation of VSMCs.

1.5.3.3. Metal Injection Molding

Metal injection molding (MIM) is a metalworking process where metal powderes are converted into complex shapes. More importantly, precise and reproducible parts can be manufactured at a considerably lower cost as compared to conventional processes. Besides of the high final density, MIM products have properties that are equivalent to those achieved with other manufacturing techniques. The other attractive feature of the MIM process is its potential for metal matrix composite manufacturing. This process was developed and commercialized in 1970-80s. The MIM process usually involves following steps: (i) feedstock mixing and granulating, (ii) molding, (iii) binder removel and (iv) sintering. Mariot *et al*. [90] for first time fabricated injection-molded Fe with relative density values around ~ 95% for potential BMs applications. The results showed that the MIM Fe exhibited yield strenght in a range 80-140 MPa (depending on initial powder loading and sintering conditions). and very high ductility (up to 40%). Its degradation rate in Hanks' solution was reported to be higher than that of as-cast pure Fe. More uniform degradation mode was observed in the most densified samples. The specimens made from the feedstock containing 66% of iron powder showed the highest elongation and an accelerated *in vitro* degradation rate.

1.5.3.4. Cold Gas Dynamic Spraying

Frattolin *et al*. [133] adopted CGDS technology that fabricated 316L SS, 20Fe–80SS, 50Fe–50SS, and 80Fe–20SS (all in wt%) and pure iron through 316L SS and pure iron mixed powders. Since relatively low temperature can limit the growth of grains, the grain size of metallic materials fabricated by CGDS is notably small. The grain sizes of materials fabricated in this research were less than 10 μm. As mentioned earlier, reducing the grain size of metallic materials is an effective way to improve both strength and ductility. Therefore, these experimental materials exhibited good mechanical properties. The corrosion rate of these materials was tested by static immersion. The corrosion rates increased by increasing the concentration of iron. The authors considered that there was galvanic corrosion in Fe–SS composites for different corrosion potentials between Fe and 316L SS. The 80Fe–20SS composite was also processed for stenting by femto-laser cutting. Its corrosion rate was measured by both static and dynamic immersion tests. The dynamic corrosion rate of the stent was faster than that of the static one, but both were slower than that of pure iron.

1.5.3.5. 3D Printing

Additive manufacturing (AM) is another laser technology having an enormous potential in implant fabrication which is customized for a specific patient's body. This technique uses a high-energy laser as the source of power to sinter metal powder particles to build subsequent layers, generating desired geometries. AM process based on powder bed fusion stands out as a promising and attractive option, which can be used to produce stent precursors or orthopedic implant (such as screws or foams) directly from powders, thus eliminating laser micro cutting and machining. Additive manufacturing of metallic biomaterials can be classified in three broad sections as: a) laser energy based, b) electron beam based and c) powder bed inkjet-based manufacturing techniques. The high energy associated with the laser and electron beam assisted manufacturing ensures complete melting or welding of powder particles, ensuring good strength property. As the local temperature fluctuation for a printed element is too rapid between two consecutive layers, the microstructure is characterized by heterogeneous phase formation and rough morphological features, leaving detrimental effect on strength reliability. In contrast, the 3D inkjet powder bed printing is a low temperature manufacturing technique, which involves room temperature processing, has seamless

possibilities towards printing of a broad spectrum of biomaterials. Chou *et al*. [105] adopted 3D printed Fe–30Mn porous bones, as shown in Fig. 1.12. The diameter of pores was between 0.5 mm and 1 mm. Alongside a lower corrosion potential the corrosion rate of 3D printed Fe–30Mn was recorded faster than pure iron. This is ascribed to the porosity of 3D printed samples. Moreover, their tensile strength and ductility largely decreased but were closer to natural bone.

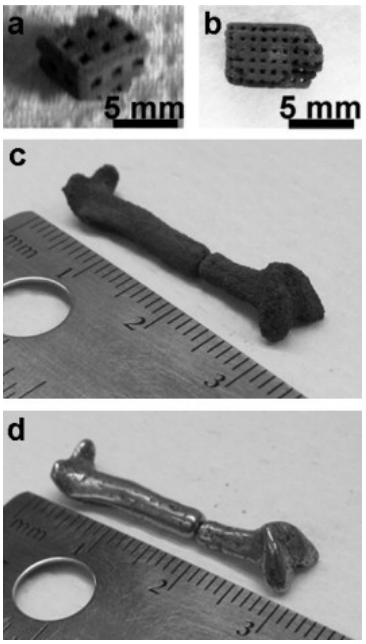

Figure 1.12. *Photographs 3-D printed samples from Fe–30Mn powder after sintering: parts with square pore sizes of lengths (a) 1 mm and (b) 500 μm; miniature human femur (c) before finishing and (d) after finishing [105]*

1.5.4. *In vitro* corrosion mechanism

Fe alloys undergo corrosion in aqueous environments. Body fluids are aqueous solutions consisting of inorganic and organic compounds and ions. Their combined effect is a key factor affecting the degradation of Fe-based alloys and composites [134]. The degradation of Fe is a phenomenon triggered by surface conditions and it depends on the chemical composition of the corrosive medium, pH, temperature, and solubility of metallic ions released from the substrate [135]. When Fe is immersed in a solution, it is oxidized to Fe^{2+} based on the following reaction [78,128]:

$$Fe \rightarrow Fe^{2+} + 2e \qquad \text{(Eq. 1.24)}$$

Some of Fe^{2+} can be transformed to Fe^{3+} because of alkaline pH and the presence of oxygen in Hanks' solution; $Fe(OH)_3$ is produced according to the following reactions:

$$^1/_2O_2+H_2O+2e^-\rightarrow 2OH^- \quad \text{(Eq. 1.25)}$$

$$Fe^{2+}+2OH^-\rightarrow Fe(OH)_2 \quad \text{(Eq. 1.26)}$$

$$Fe^{2+}\rightarrow Fe^{3+}+e^- \quad \text{(Eq. 1.27)}$$

$$Fe^{3+}+3OH^-\rightarrow Fe(OH)_3 \quad \text{(Eq. 1.28)}$$

Because of the presence of chloride ions, $Fe(OH)_3$ is hydrolyzed and goethite (α-FeOOH) is formed. According to the Pourbaix diagram with increasing pH, the local H^+ concentration at the metal-solution interface decreases, resulting in a formation of Fe oxides and hydroxides on the iron surface [136]. $Fe(OH)_2$ and $Fe(OH)_3$ are solid phases with a low solubility (respectively K_{sp} $(Fe(OH)_2) = 8\times10^{-16}$, K_{sp} $(Fe(OH)_3) = 4\times10^{-38}$) [137]. The stability of these compounds is limited by the presence of carbonates/bicarbonates and phosphates, chloride ions and changes in the concentration of the degradation products[138,139]. Subsequently, after immersion, apart from the contact with Cl^-, HCO_3^-, HPO_4^{2-}, Fe is also exposed to an environment rich in cations (such as Ca^{2+}, Mg^{2+}, Na^+, K^+ *etc.*), dissolved oxygen and CO_2. Therefore, in addition to the deposition of a Fe hydroxide layer, the presence of HCO_3^- , Cl^- and HPO_4^{2-} in solution also promotes thermodynamically the precipitation of other phases. The corrosion deposit is thus reconstructed into layers of oxides, hydroxides, Fe and Ca carbonates and phosphates. Chloride, carbonate and sulfate anions, present in the body fluid are responsible for the formation of intermediate phases in the iron oxidation process. $Fe_6(OH)_{12}CO_3$, $Fe_4(OH)_8Cl$ and $Fe_6(OH)_{12}SO_4$ complexes, known as green rust (GR), might be formed during Fe biodegradation [140]. GR rust forms on the substrate surface in a pH range of 7 to 9 and has a substantial contribution to the degradation of Fe based biomaterials [140]. The nature of the protective film (chemical composition and thickness) depends not only on the environmental parameters such as the buffer solution, pH, and temperature. Microstructural features (such as grain size, uniformity) and chemical composition of the substrate have a significant contribution to the corrosion susceptibility of Fe-based BMs.

A uniform corrosion is rather expected for BMs. Ideally, degradation of implants starts on the surface to the bulk (layer by layer). A non-uniform corrosion process might result in the

lost of mechanical integrity under cyclic mechanical loads. In addition, a non-homogenous stress distribution in an implant is another factor triggering localized corrosion. Further, the prediction of implant life-time is considerably more difficult in case of materials exhibiting non-uniform dissolution mode. Corrosion of Fe through pit formation is a self-catalytic process, so that pitting occurs in the vertical direction (Fig. 1.13a).

Fig. 1.13b presents a scheme of a corrosion mechanism and an ideal corrosion process of Fe BMs in physiological environment [80]. Pits should form as much as possible at the beginning of the corrosion pattern. As the pits grow they should develop horizontally and connect, forming a uniform layer of degradation product or degraded surface.

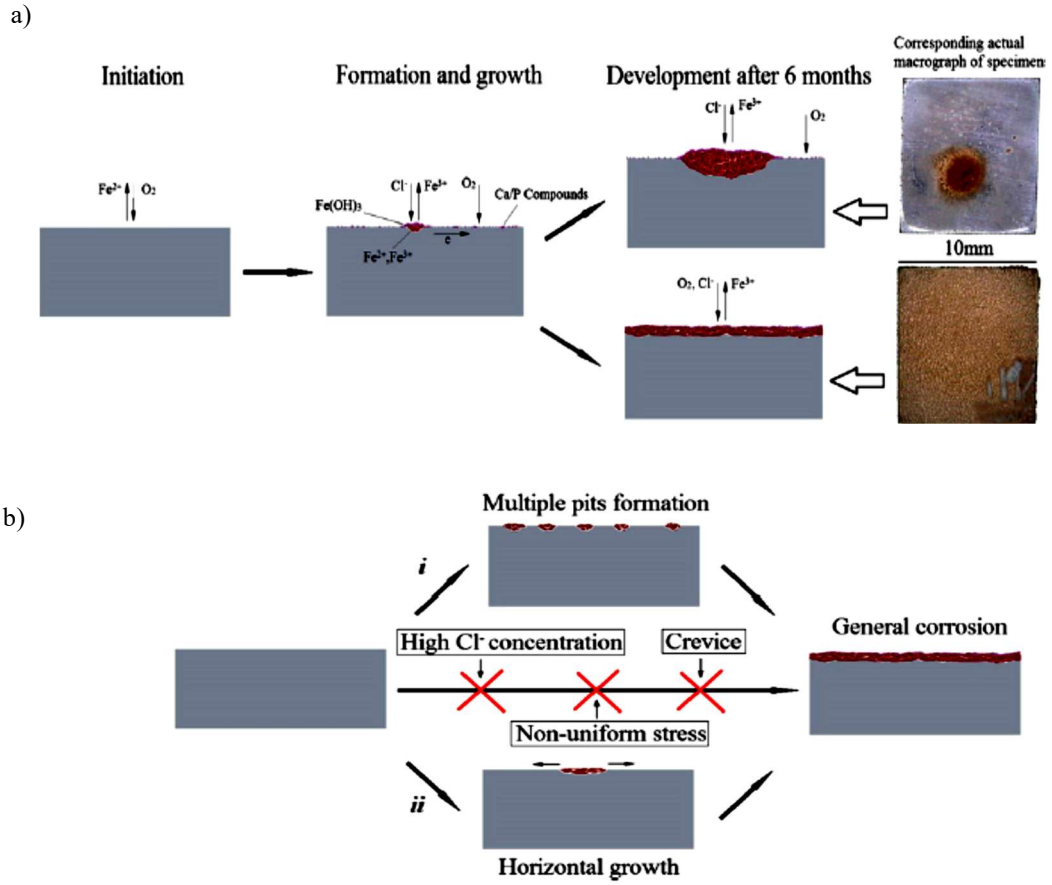

Figure 1.13. *Schematic diagram illustrating a) corrosion mechanism of Fe-based BM in Hanks' solution, b) ideal corrosion process of Fe-based BM [80]*

A detailed investigation on the corrosion mechanism and the formation of *in vitro* corrosion products for this biodegradable metal candidate remains largely unexplored. Commercial Hanks', modified Hanks' balanced salts, simulated body fluids, Dulbecco's phosphate

buffered saline solutions are among the most common solutions adopted to conduct *in vitro* tests on recently investigated Fe-based alloys (Table 1.9). These solutions represent different ionic compositions, constituents and concentrations of the buffering agents.

Table 1.9. *Summary of the corrosion rate data available in literature for Fe and Fe-based biodegradable alloys*

Alloy	Corrosion rate ($mm \cdot year^{-1}$)		Solution	Other conditions	Time of immersion test (days)	Ref.
	Static immersion test	Potentiodynamic test				
Pure Fe as-cast	0.27	0.08	Hanks'	Specimens 10x10x2mm R=25ml/cm^2 T=37ºC	30	[93]
annealed (550ºC)	0.243±0.029	0.144±0.006	Modified Hanks'	Specimens 10x20x2mm R=20ml/cm^2 T=37ºC pH=7.4 5%CO_2	14	[79]
Electroformed Fe		0.85±0.05	Modified Hanks'	T=37ºC pH=7.4	14	[91]
ECAPed Fe (8 passes)		0.02			14	[85]
SPS pure Fe	0.32	0.016	Hanks'	Specimens 10x10x2mm R=25ml/cm^2 T=37ºC	30	[93]
Nitrided Fe		0.225	PBS	T=37ºC pH=7.4 5%CO_2 FlowRate:25cm/s	2	[81]
Fe-3Co/rolled		0.142	Hanks'			[80]
Fe-3W/rolled		0.148				
Fe-3C/rolled		0.187				
Fe-3S/rolled		0.145				
Fe-5W/ SPS	0.35	0.138	Hanks'	Specimens 10x10x2mm R=25ml/cm^2 T=37ºC	30	[93]
Fe-1CNT/ SPS	0.46	0.117				
Fe-20Mn	PM, cold rolled ~0.23-0.24	0.5	Modified Hanks'	T=37ºC pH=7.4	15	[96]
Fe-25Mn		0.5				
Fe-30M		0.7				
Fe-35Mn		0.7				
*Fe-35Mn, 27% porosity	0.82	1.99	SBF	T=37ºC R=60 ml/cm^2 Corrosiob products removed by brushing in 15% H_2SO_4	14	[106]
*Fe-35Mn, 40% porosity	0.85	3.72				
*Fe-35Mn,48% porosity	0.9	5.26				

Pure Fe	0.217mg/cm^2/day	0.041	SBF	T=37ºC R=150ml/cm^2 Solution renewed every 7 days	70	[107]
Fe-30Mn/ hot forged	0.058 mg/cm^2/day	0.899				
Pure Fe	*10%	-	0.9% NaCl	Discs (d=15 mm, 2.5mm thick), every 5 days up up a total time 84 days samples were taken out of the solution, and etched with picric acid to remove corrosion products	84	[101]
Fe-0.5Mn Casting followed by forging	*9.5%					
Fe-2.7Mn	*8%					
Fe-6.9Mn	*7%					
	*Mass loss					
Fe-30Mn/cast		0.12	SBF	T=37ºC pH= 7.4	-	[104]
Fe-30Mn-6Si/cast		0.29				
Fe-30Mn/forged	-	0.12	SBF	T=37ºC pH= 7.4	-	[108]
Fe-30Mn-1C/forged		0.2				
Fe-10Mn (sheet)	**0.36	-	SBF	3 mm thick discs, d=8mm, mechanically polished up P1200 grit paper	28	[94]
Fe-10Mn (heat treated)	**0.38					
Fe-10Mn-1Pd (sheet)	**0.45					
Fe-10Mn-1Pd (heat treated)	**M0.44					
Fe	No data	0.13	SBF	T=37ºC pH=7	28	[109]
$Fe_{81}Ga_{19}$		0.48				
$(Fe_{81}Ga_{19})_{98}B_2$		0.63				
$(Fe_{81}Ga_{19})_{99.5}(TaC)_{0.5}$		0.33				
Fe	0.49	0.41	SBF	T=37ºC pH=7 R=1/170		[110]
Fe-2Pd	0.79	0.43				
Fe2Ag	0.14	0.33				
Fe2C	0.65	0.51				
Fe	0.17	No data	SBF	T=37ºC pH=7	7	[111]
Fe-0.6%P	0.27					
Fe-1.6%P	0.25					
Fe-0.05%B	0.24					
Fe-1%Ag	0.26					
Fe-5%Ag	0.32					

*R: ratio of surface area to solution volume in (cm^2/ml)
**Mass loss (%)
***Mass loss rate (mg cm^{-2}d^{-1})

Since corrosion patterns are greatly affected by experimental parameters (e.g. composition of the testing solution, temperature, constancy of pH, duration of tests, etc.), a direct comparison between the reported research works can in some cases become uncertain.

1.5.5. *In vivo* performance

During the last 17 years, a number of researches on *in vivo* performance of Fe and Fe-based BMs was published (as listed in Table 1.10.).

Table 1.10. *Summary of animal tests for Fe-based biodegradable metals*

Material	Animal model	Duration	Findings	Ref.
Pure Fe stent	Descending aorta of rabbit	6-18 months	No thrombogenicity, no significant neointimal proliferation and systemic toxicity, faster degradation at junctions of the stent; locally discoloration of intima	[74]
Pure Fe stent	Descending aorta of pig	360 days	Complete coverage of neointima after 14d; accumulation of degradation product adjacent to the stent struts and within adventitia, disintegration of struts after 1 year with large stent's residue, no sign of Fe overdose or Fe-related toxicity	[141]
Pure Fe stent	Descending aorta of pig	28 days	Locally discoloration of the vascular wall adjacent to the stent; degradation was evidenced at 28d; similar vessel parameters to Co-Cr stent	[142]
Pure Fe wire	Artery of rat	1-9 months	Fe wire experienced substantial corrosion within artery matrix, whereas experienced minimal biocorrosion in blood-contacting environment	[76]
Pins of: -pure Fe -Fe-10Mn-1Pd -Fe-21Mn-1Pd	Sprague-Dawley rat growing skeleton	1, 3, 6, 12 months	Slowly proceeding degradation. There are no significant diffrences between the materials. Dense layer of deradation products formed on the surfaces. No signs of local toxicity and no clinical abnormalities were observed. No significant diffrences betweend degradation rates of Fe and Fe-Mn-Pd.	[143]
Nitrided Fe stent	Porcine arteries	12 months	A nearly intact endothelial cells layer formed on the stented vessel wall; a decreased inflammation scoring, ~30% loss of in-stent luminal diameter, ~47% reduced strut thickness and corrosion product accumulation 12 months postimplantion	[84, 85]
-Pure Fe -Fe-5%HA -Fe-5%TCP -Fe-5%BCP	Indonesian thin tailed sheep, bone	3,9, 14, 35, 50, 70 days	Superiority of the composite implants in terms of bone healing and formation because of the enhanced bioactivity compared to that of pure Fe. The thicker degradation layer was observed on the surface of composites confirming their higher bioactivity. Fe-BCP was found to be the most active among the composites.	[120, 144]
Cylindrical plates, -pure Fe	NMRI mice, Charles River (Sultzfeld)	3.6.9. months	Even after 9 months no significant corrosion was detectable. SEM investigations showed that passivation	[101]

-Fe-x%Mn (x=0.5, 2.7 ,6.9)		layers (FeMn phosphates) might be the reason for corrosion resistance.	
Pieces 2x4x0.5mm Fe-Mn-Si	Wistar Rat's bone	No adverse biological reactions, normal evolution of bone fracture After 2 weeks significant fibrous tissue and transformation of fibroblast into osteoblast was observed. Comparation of the histological samples sustained a favorable trend accelerate bone restoration as compared to positive control implant.	[145]

These important studies have become an urgent topic in the field of cardiovascular and orthopedic applications. In 2001, Peuster et al. implanted cardiovascular stents made of pure iron into the descending aortas of New Zealand white rabbits [141]. After 18 months of the test, neither thrombogenicity, nor significant neointimal proliferation and nor systemic toxicity were observed. Accelerated, localized corrosion with local intima discoloration were noticed at junctions of the stent. Subsequently, Fe stent was implanted into the descending aortas of 29 mini-pigs for a period of 12 months. Histopathological analyses did not reveal any toxicity or Fe overload. Other researches confirmed the biosafety of Fe stent after 28 days of implantation into the porcine coronary arteries. No signs of degradation without evidence of embolization or thrombosis were observed in proximity of Fe stent. Kraus [143] assessed *in vivo* corrosion behavior of Fe and two Fe-based alloys (Fe-10Mn-1Pd) and (Fe-21Mn-0.7C-1Pd) in a growing rat skeleton; the material was implanted into the femur and monitored over a period 1 year. No signs of local cytotoxicity or abnormal clinical observations were noticed. The implants were found to be well-integrated into the bone.

2. Strategies, objectives and structure of the thesis

****

Chapter 2 presents in detail the objectives of this research project as well as the methodologies applied.

****

2.1. Importance of research on development of biodegradable implants

According to a survey (reported by MarketsandMarkets), the global biomaterials market (for the largest device sectors – Fig. 2.1) from US$164 billion in 2010 reached to US$228 billion in 2015. The value of the biomaterials market is constantly growing due to the increasing demands for new materials [146].

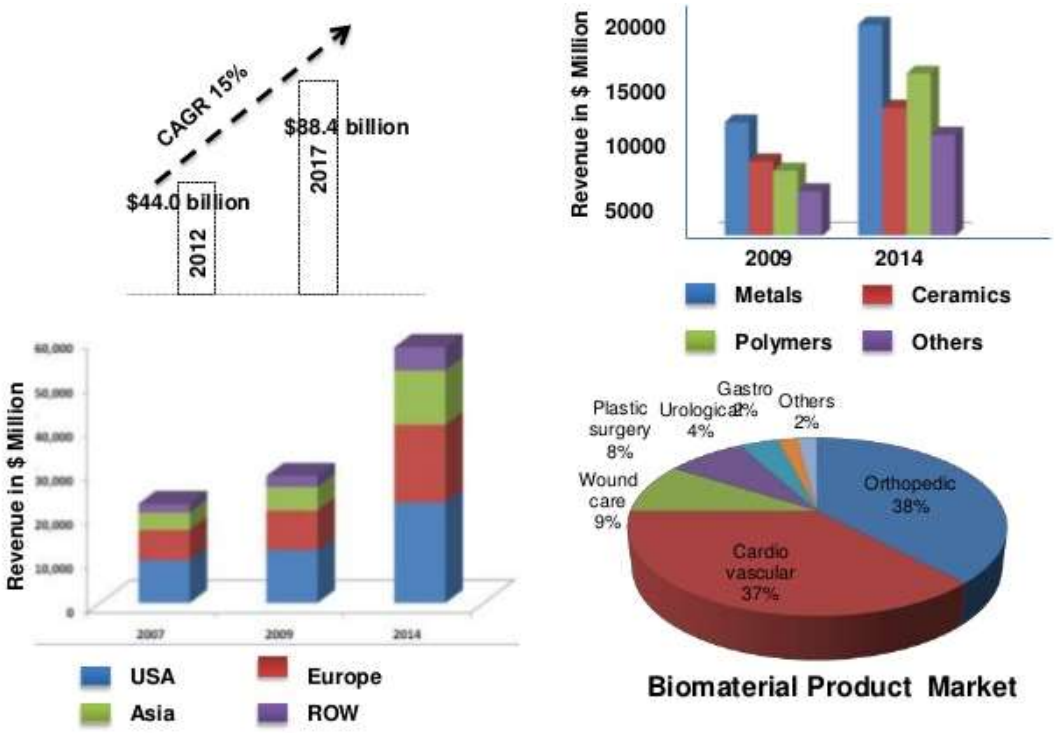

Figure 2.1. *Biomaterials market – status [146]*

The national institutes of health and science foundation programs are producing remarkable progress in the research on a development of new materials for medical devices. The focus is put on the development of the engineered implants that can improve the quality of life and decrease the cost of health care.

Since 2000, biodegradable metallic implants have been investigated. These materials have several advantages in specific applications over permanent implants used nowadays. BMs can adapt the human body and eventually dissolve when no longer needed. Such materials would help patients suffering from fractures of long bones or limb length discrepancies.

Further, the expenses of multiple procedures including implantation, removal, and re-implantation of the permanent implant could be avoided. Another example are metallic stents, used for millions of people to treat blockages in the coronary artery. This small implant can cause an immune response that leads to the growth of scar tissue and the formation of blood clots. If blockages form again, the stent is difficult to be removed, thus additional stents must be implanted, and re-operation is needed. Using BM stents could minimize the risk of invasive procedures. BM stents as well as bone fixation implants have other advantages in pediatric applications showing the ability to adjust to the tissue growth.

2.2. Main challenge for iron-based BMs- objective of the project

Fe and Fe-based alloys feature very slow corrosion rate in physiological environment. Therefore, controlling their corrosion mode and rates is a key challenge. Substantial number of detailed studies have been conducted to overcome the limitations of these biomaterials. However, their corrosion rates are still far from levels required for translation in clinical applications [7]. Early results and *in vivo* animal experiments have validated the suitability of pure iron as a degradable medical implant [4,128]. High strength and high ductility make iron-based alloys attractive for implant applications. Iron is considered safe although the process of degradation and the absorption of degradation products should be studied more widely. Additionally, the alloying elements must be non-toxic [94,147]. Another critical aspect to be improved for achieving higher performances of biodegradable iron is the control of the corrosion kinetics to enhance their degradation rate. *In vitro* studies in simulated physiological fluids have shown that corrosion rate and the corrosion processes depend on a variety of factors including, but not limited to alloy composition, surface treatments, coatings and composition of testing solution [94]. In addition to concerns about biocompatibility and corrosion control of the alloys, a detailed knowledge on processing routes and on resulting properties is also required. Strategies to improve the performance of biodegradable stents are namely; tailoring the microstructure to improve the mechanical and corrosion performances [78] and adopting surface

modifications to temporarily insulating the bulk metallic structure [148,149] as shown in Fig. 2.2. The key issues of this study are tailoring biocompatibility, corrosion resistance and mechanical properties in Fe-based material.

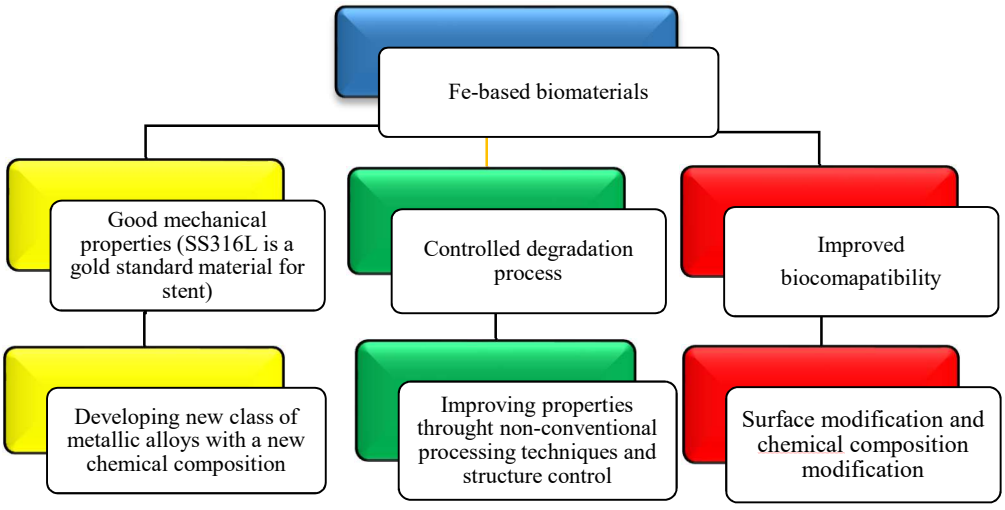

Figure 2.2. *Design strategy for biodegradable Fe-based alloys for medical applications*

The objective of this work is to carry out a research project on design and development of a new iron-based degradable biomaterial.

2.3. Objectives

Designing materials with appropriate mechanical properties and adjustable degradation behavior is a key for the development of biodegradable metals. The main objective of this research is to design, validate and develop an improved metallic Fe-based material with controlled degradation rate specifically designed for biodegradable metallic stent.

In this work magnesium silicide was added to iron to enhance its mechanical properties and corrosion rate.

The specific objectives are as follow:

- to design new material having appropriate mechanical properties and a suitable fabrication process with an improved degradation rate in a more uniform manner and to optimize their microstructure, physical and mechanical properties.

- to synthesize and optimize the processing parameters for the generation of Fe-Mg_2Si composite powders using high energy ball milling or mixing processes followed by hot rolling.
- to study the effect of Mg_2Si addition to Fe matrix and understand the short-term degradation behaviour to explore the potential of these composites as novel biodegradable material systems.
- to study the effect of Mg_2Si addition as reinforcement of Fe matrix and understand the long-term degradation behaviour and corresponding corrosion mechanism/products.

Fig. 2.3 illustrates the flowchart of the project activities. The research and experimental work of this project was conducted as following:

- Primarily, the literature review on the current status of degradable metallic biomaterials and fabrication methods was completed.
- The second stage of the project was to design and prepare a powder metallurgy set-up for the manufacturing of iron composite. Iron-based composite was produced using the developed set-up and then a series of preliminary experiments were carried out.

  The specimens were fabricated in the form of flat sheets.
- Subsequently, corrosion testing using potentiodynamic polarization technique and immersion test was performed to evaluate the corrosion rates of Fe-Mg_2Si composites and to compare to the other materials previously studied for degradable biomaterials. The results of this stage of the project including microstructural, mechanical and corrosion studies on new composites are presented in the first article.
- Since in the previous stage of the project Fe-Mg_2Si composites showed certain interesting mechanical properties and corrosion rates, a more profound study on their degradation mechanism was necessary. Corrosion initiation mechanism of prepared composites was explored in detail. The results from this part of the project will be published in the second article.
- Finally, the fundamental study on long-term corrosion behaviour of Fe and its composites was performed to provide a basis about the processes and the sequence of

protective film formation in physiological media. The influence of Mg_2Si on the Fe corrosion was explored, and corresponding mechanism of the degradation was proposed.

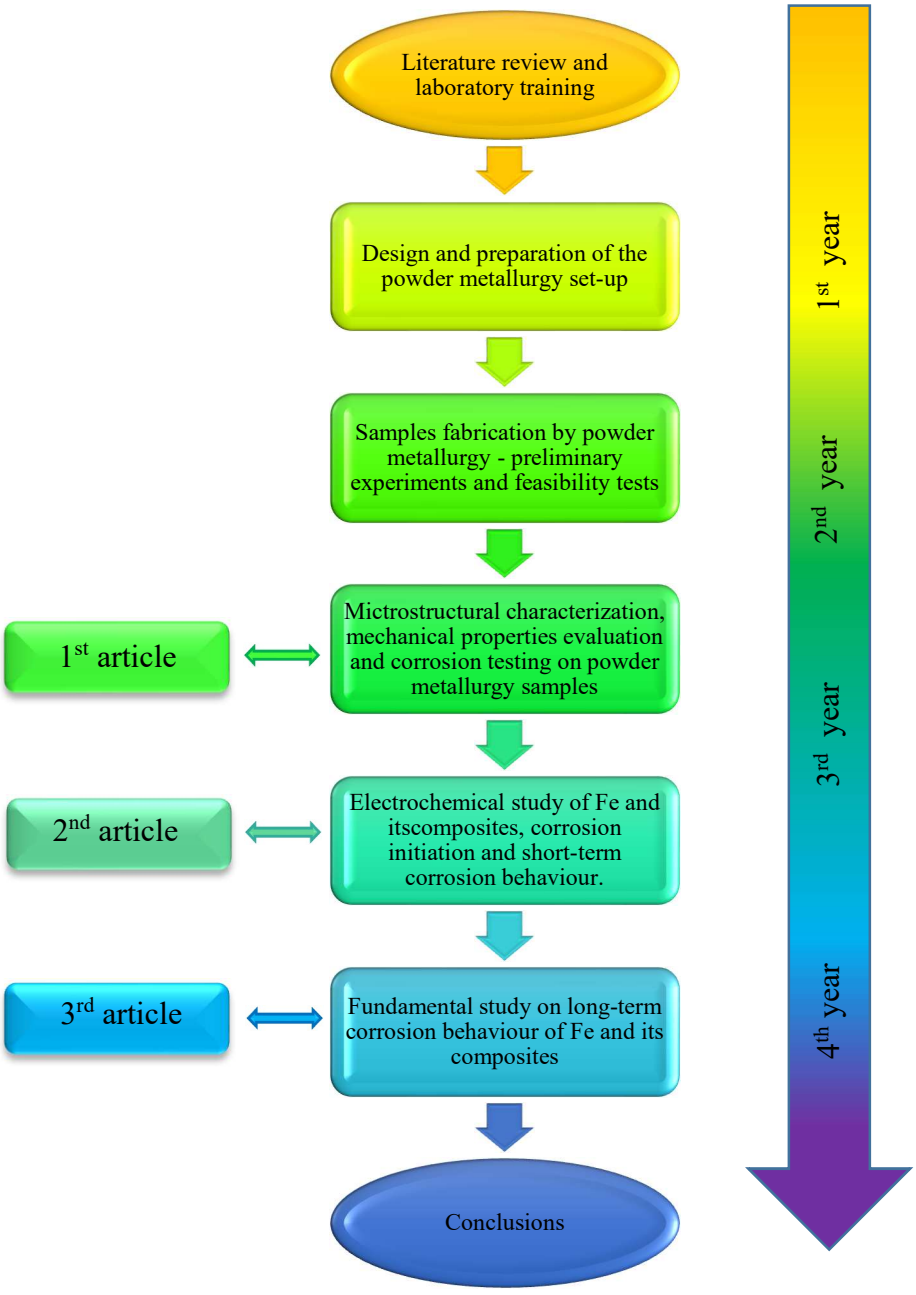

Figure 2.3. *Flowchart diagram of the experimental strategy of the project*

2.4. Material selection

Alloying elements play a key role in biodegradable iron alloys design. In biodegradable metals field, factors such as biocompatibility and modulable corrosion rate are essential. The materials that will be released from the biodegradable implants to the surrounding tissues and body fluids must be safe and cannot exhibit any allergic, inflammatory or toxic reactions [4]. The high content of Fe and other potentially harmful alloying elements may result in cytotoxicity. The amount of released ions depend on the biodegradation rate [150]. The released metallic ions may cause general toxicity in the human body or a local toxicity affecting the surrounding tissues [151,152]. Table 2.1 summarizes the pathophysiology and toxicology of Fe and Mg and other alloying elements used to manufacture BMs [4]. It is worth to notice that even a toxic element can be tolerated by the body below its toxicity limit [151]. Controlling the amount of the released metal ions at the implantation site is a key issue for the design of the BMs [4,7].

Table 2.1. *The summary of the pathophysiology and toxicology of Fe, Mg, Si and the common used alloying elements in biodegradable Fe, Mg and Zn alloys [4,5,7]*

Element	Human amount	Blood serum level	Pathophysiology	Toxicology	Daily allowance
Fe	**4-5 g**	**5.0-17.6 g/l**	**component of several metalloproteins; be crucial in vital biochemical activities, i.e. oxygen sensing and transport**	**iron toxicity gives rise to lesions in the gastrointestinal tract, shock and liver damage**	**10-20 mg**
Mg	**25 g**	**0.73-1.06 mM**	**activator of many enzymes; co-regulator of protein synthesis and muscle contraction; stabilizer of DNA and RNA**	**excessive Mg leads to nausea**	**0.7 g**
Ca	1100 g	0.919-0.993 mM	more than 99% has a structure function in the skeleton; the solution Ca has a signal transmission function, including muscle contraction, blood clotting, cell function	inhibit the intestinal absorption of other essential minerals	0.8 g
Zn	2 g	12.4-17.4 μM	trace element; appears in all enzyme classes; Most Zn appears in muscle	neurotoxic and hinder bone development at higher concentration	15 mg
Mn	12 mg	<0.8 μg/l	trace element; activator of enzyme; Mn deficiency is related to osteoporosis, diabetes mellitus, atherosclerosis	excessive Mn results in neurotoxicity	4 mg
Si	**1-2 g**	-	**cross linking agent of connective tissue; necessary for growth an bone calcification**	**silica and silicate caused lung diseases**	**25-33 mg**
Zr	<250 mg		probably excreted in feces; low systematic toxicity to animals	high concentration in liver and gall bladder	3.5 mg

2.4.1. Iron matrix reinforced by magnesium silicide particles

In this study, it is proposed that incorporation of a small quantity of magnesium silicide (Mg_2Si) into iron matrix increases the degradation rate while preserving its biocompatibility. By uniform dispersion of Mg_2Si into iron matrix a homogenous degradation of a new material can be achieved.

Table 2.2. *Properties of Fe and Mg_2Si powders selected to design new BMs*

	Iron	**Magnesium Silicide**
Molecular formula	Fe	Mg_2Si
Density	7.874 g cm^{-3}	1.988 g cm^{-3}
Melting point	1538°C	1102°C
Particle size	10 µm	840µm

In this context, a series of Fe/Mg_2Si alloys were produced with the objective to obtain uniform corrosion mode and accelerated corrosion rate. Compared with their unreinforced counterpart, iron matrix composites offer higher hardness, improved wear resistance and higher elastic modulus. On the other hand, as in all metal matrix composites – reduction in the fracture properties (ductility and toughness) is expected [153,154]. However, recently there has been a series of breakthroughs in strategies that could result in good ductility, while keeping an substantially high tensile strength [155].

2.5. Manufacturing process selection and equipment set-up.

Powder metallurgy techniques have been selected as a manufacturing route aimed at making new Fe/Mg_2Si biodegradable composites. Fe-based composites consist of a metal matrix filled by secondary particles featuring entirely different physical and mechanical properties from those of the matrix. The introducing of reinforcing particles to the iron matrix leads to enhance the mechanical strength, degradation rate as well as achievement of more uniform corrosion mode [154]. By homogeneously dispersion of small quantity of Mg_2Si into iron matrix an uniform degradation of new composite can be achieved. It is well established that porous alloys show less corrosion resistance than their fully dense counterparts in simulated body fluid solutions [156]. In porous structures due to the big true

surface area resulted from pores, the electrolyte is trapped and stagnated and thus, leads to the localized corrosion.

Particularly, the main concern of producing the proposed composites is the low wettability of the secondary particles which does not allow the production by convectional casting methods. On the other hand, small powder aggregates are prone to form clusters, losing their capability to be homogenously dispersed through the matrix for an optimal exploitation of the strengthening potential. For this reason, several alternative methods have been proposed in order to overcome this problem [157]. Variety of solid state methods were studied and developed for preparing metal matrix composites. Some investigations focused on mechanical alloying which is a powder metallurgy (PM) technique consisting in repeated cold welding and re-welding of powder particles in a high energy ball mill [77,158,159]. The general sequence of operations involved in powder metallurgy process is shown schematically in Fig. 2.4.

PM involves the compaction of metallic powders, followed by a heat treatment to increase the density. First, the metal powders are mixed together. Then, the powder mixture will be compacted in a die by pressing. This step provides form, structure and the necessary strength to handle the material before sintering. Pressing can be done under cold and hot conditions. Finally, the sintering process is performed to consolidate the metallic particles at a temperature of $T \approx 0.5T_m$ where T_m is a melting point. This condition results in atomic diffusion and neck formation between the powder particles in the solid state. This method is used for metals with high melting temperatures and difficult to cast. The main challenge in PM is to obtain a high-density product and keep the grain size in the desired range. Higher process temperatures lead to higher densities but also result in grain growth [160–162]. Control over heating rate, time, temperature and atmosphere is required for the optimum. Moreover, in this process the size, morphology and purity of initial metal powders, mixing time and conditions, pressing load and process atmosphere influence the properties of the final products [161]. Stir casting and PM are two widespread methods which have been utilized in various works and both have advantages and drawbacks – Table 2.3 [157,162]. PM is superior to casting in precisely control the chemical composition, impurity and the final grain size by determining the size of starting powders and following process parameters [162].

Table 2.3. *Advantages and disadvantages of powder metallurgy and casting methods regarding fabrication of composite materials*

Methods	Advantageous	Disadvantageous
Powder metallurgy	-Better bonding of matrix and reinforcing particles -Better distribution of reinforcement -Easier control of matrix structure	-Discontinues matrix media -High complexity -High portions of porosity -Expensive
Casting	-Continues matrix media -Low cost -Simplicity of instrumentation -High production rate	-Complex process control -Non- uniform distribution of reinforcement -Weaker bonding of matrix and nanoparticle -Large free zone of reinforcement

2.5.1. Fabrication of the specimens

The composites with a Mg_2Si content ranging from 0.5 to 1.5 wt% were explored in this study. Their microstructure, mechanical properties, as well as degradation behavior were carefully investigated. The powders were mixed and/or mechanically milled to make iron composite reinforced by Mg_2Si particles. Mechanical milling (MM) was also employed to decrease the size of Mg_2Si particles and to produce the composite where the particles Mg_2Si are embedded in iron matrix and uniformly distributed. MM is now widely used to synthesize a variety of non-equilibrium alloys. The transfer of mechanical energy to the powder particles results in introducing strain through generation of dislocations and other defects, facilitating diffusion. Additionally, during this process, refinement of particles and grain sizes occur and consequently the diffusion distances are reduced. Further, a slight rise in powder temperature occurs during milling. All these effects lead to alloying of the blended elemental powders during the milling process [158,159]. The result could be constitutional changes – formation of solid solutions (equilibrium and supersaturated), intermetallic phases (equilibrium or metastable), and amorphous phases – or microstructural changes leading to development of ultrafine-grained and nanostructured phases [159]. Planetary ball milling is a technique employed in this work. It is a common system to reduce the particle size. With this technique, jars filled by powders and balls of various hard materials (stainless steel, agate, tungsten, carbide, silicon nitride, etc.). The repeated shear and impact forces between the balls and jar walls break down the particulates. Processed powders were consolidated by hot rolling. Hot rolling, which is carried out above the recrystallization temperature of the matrix powder, has advantages over cold rolling such as lower residual stresses and limited residual

porosities [160,161]. The detailed description of manufacturing process of investigated specimens and the other details are presented in the next chapters.

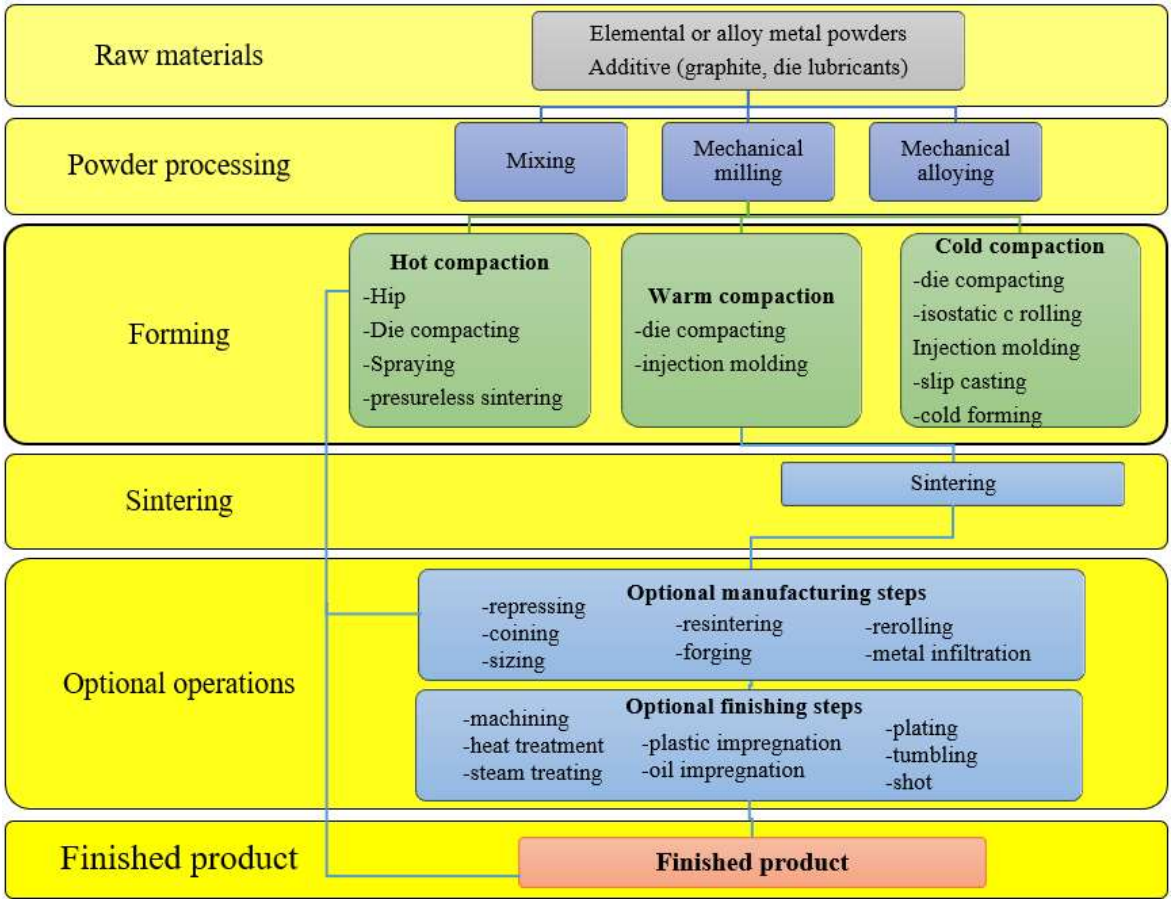

Figure 2.4. *Powder metallurgy process -schematic view*

3. Synthesis, mechanical properties and corrosion behavior of powder metallurgy processed Fe/Mg_2Si composites for biodegradable implant applications

****

A focus of this study was to develop a high-strength Fe-based composite with accelerated degradation rate, compared to pure Fe. Addition of reinforcement is a common and widespread method to increase the hardness of metals and it plays an important role in modern metallurgy. Moreover, the corrosion properties of newly developed materials are here discussed in general.

****

Synthesis, mechanical properties and corrosion behavior of powder metallurgy processed Fe/Mg_2Si composites for biodegradable implant applications

M. Sikora-Jasinska[1,2], C. Paternoster[2], E. Mostaed[1], R. Tolouei[2], R. Casati[1], M. Vedani[1], D. Mantovani[2*]

[1] *Department of Mechanical Engineering, Politecnico di Milano, Milan, Italy.*

[2] *Lab. for Biomaterials & Bioengineering (CRC-I), Dept. Min-Met-Materials Engineering & Research Center CHU de Québec, Laval University, Québec City, Canada.*

Keywords: Fe-based composites, Magnesium silicide, Mechanical properties, Biodegradable, Corrosion, Powder consolidation, Rolling, Mechanical milling

This chapter was published in the journal of Materials Science and Engineering C

3.1. Résumé

Récemment, le Fe et ses alliages ont montré leur potentiel en tant que matériaux dégradables pour des applications biomédicales. Néanmoins, la vitesse de corrosion lente limite leurs performances dans certaines situations. Les matériaux composites à matrice de fer représentent une approche possible, non seulement pour améliorer leurs propriétés mécaniques, mais aussi pour accélérer et ajuster la vitesse de corrosion dans un environnement physiologique.

Dans ce travail, des composites à base de Fe renforcés par des particules Mg_2Si ont été proposés. Les poudres initiales ont été préparées par différentes combinaisons de procédés de mélange et de broyage, et finalement consolidées par laminage à chaud. L'influence de la microstructure sur les propriétés mécaniques et le comportement à la corrosion de Fe/Mg_2Si a été étudiée. La microscopie électronique à balayage et la diffraction des rayons X ont été utilisées pour l'évaluation de la structure composite. Des tests de traction et de dureté ont été réalisés pour caractériser les propriétés mécaniques. Des essais de corrosion potentiodynamique et statique ont été effectués pour évaluer le comportement de la corrosion dans un environnement pseudo-physiologique.

Les échantillons contenant des particules Mg_2Si plus petites présentaient une distribution plus homogène du renforcement. Le rendement et l'état limite ultime à la traction ont augmenté par rapport à ceux du Fe pur (de 400 MPa et 416 MPa à 523 MPa et 630 MPa, respectivement). Des mesures électrochimiques et des tests d'immersion ont indiqué que l'ajout de Mg_2Si pourrait augmenter le taux de corrosion du Fe à deux fois (de 0,14 à 0,28 mm · an-1). Il a été constaté que la méthode de préparation des composites selon les poudres initiales jouait un rôle majeur dans le processus de corrosion ainsi que dans le mécanisme de corrosion du composite final.

3.2. Abstract

Recently, Fe and Fe-based alloys have shown their potential as degradable materials for biomedical applications. Nevertheless, the slow corrosion rate limits their performance in certain situations. The shift to iron matrix composites represents a possible approach, not only to improve the mechanical properties, but also to accelerate and tune the corrosion rate in a physiological environment. In this work, Fe-based composites reinforced by Mg_2Si particles were proposed.

The initial powders were prepared by different combinations of mixing and milling processes, and finally consolidated by hot rolling. The influence of the microstructure on mechanical properties and corrosion behavior of Fe/Mg_2Si was investigated. Scanning electron microscopy and X-ray diffraction were used for the assessment of the composite structure. Tensile and hardness tests were performed to characterize the mechanical properties. Potentiodynamic and static corrosion tests were carried out to investigate the corrosion behavior in a pseudo-physiological environment.

Samples with smaller Mg_2Si particles showed a more homogenous distribution of the reinforcement. Yield and ultimate tensile strength increased when compared to those of pure Fe (from 400 MPa and 416 MPa to 523 MPa and 630 MPa, respectively).

Electrochemical measurements and immersion tests indicated that the addition of Mg_2Si could increase the corrosion rate of Fe even twice (from 0.14 to 0.28 $mm \cdot year^{-1}$). It was found that the preparation method of the initial composite powders played a major role in the corrosion process as well as in the corrosion mechanism of the final composite.

3.3. Introduction

A new class of biomaterials called biodegradable metals (BMs) was recently developed as a substitute to metals for permanent biomedical implants [7]. BMs are expected to degrade uniformly till the full recovery of the impaired tissue and simultaneously to preserve the mechanical integrity of the device they are used for [4]. At the same time, the chemical composition of the alloy does not have to affect the hosting tissue by the release of toxic ions and the formation of harmful degradation products. The degradable device is finally supposed to dissolve completely after having accomplished its mission [4,7].

Mg, Zn, Fe and their respective alloys attracted the attention of the scientific community as suitable materials for degradable implants [4]. Although the interest for Mg-based alloys is continuously large, the use of these materials generally presents some drawbacks, such as limited mechanical properties, high degradation rates in physiological environment and a significant hydrogen formation during the corrosion process [64,163,164]. Zn-based alloys have recently shown attracting characteristics, making them a potential candidate for biomedical applications. However, the mechanical properties of Zn still need to be significantly improved [48,53,165]. Among the three kinds of alloy families above mentioned, Fe-based alloys are considered to offer some advantages because of their tunable mechanical properties, general biocompatibility and flexibility in processing [6]. Fe-based BMs have similar mechanical properties to those of AISI316L stainless steel and they are more attractive from a structural point of view, when compared to Mg-based BMs [7]. Their cytocompatibility was already successfully tested in animal models (rats, pigs, etc.), but they have a slow degradation rate. Peuster et al. [166] reported that, after 12-months, parts of a pure Fe cardiovascular device were found in the blood vessel wall, without being affected by any degradation process.

Researchers focused on the development of Fe-based alloys with new and more appealing features, by modifying their chemical composition, microstructure and surface properties [94]. The presence of phases with a difference in corrosion potential from that of the base material can promote micro-galvanic corrosion. Gold, silver [113], tungsten [93], platinum and palladium [119] addition as alloying elements has already been explored in literature to accelerate the degradation rate of Fe-based BMs. Indeed, it is proved that they can also improve the mechanical properties

through the solid solution and second phase strengthening mechanisms. The addition in a Fe matrix of carbon nanotubes, Fe_2O_3 [118], hydroxyapatite, tricalcium phosphate or biphasic calcium phosphate [120] showed the possibility to tune mechanical and corrosion properties, determined by the selection of the reinforcement material [4]. The amount, distribution and size of the reinforcement phase affect relevantly the mechanical and the degradation properties of Fe MMCs.

Different manufacturing processes including casting [167], powder metallurgy (PM) [113], electroforming [78] and inkjet 3D-printing [105] are available to achieve materials with selected properties. These production methods affect the features of the final product: for example, Fe-Mn alloys showed a faster *in vitro* degradation rate compared to the same alloy produced by casting. This behavior can be attributed to the unavoidable small amount of porosity found in materials obtained by PM processes. Powder metallurgy is an attractive fabrication method because it allows the direct production of relatively complex shapes. The porosity that can be found in this kind of products can also affect the mechanical properties [168]. Materials with finely tailored properties can be obtained with this technique, through the variation of some fabrication parameters in a wide range (for example, the reinforcement particle size and its amount). In addition, metal–reinforcement interface reactivity can be controlled by using solid-state processing methods, limiting process temperature and/or adopting special additives [169,170].

In this research, the effect of the addition of 1.5 wt.% Mg_2Si particles into a pure Fe matrix is systematically investigated, considering the effect of different powder preparation methods on the microstructure formation, the mechanical properties and the corrosion behavior. Mg_2Si was selected as a reinforcement phase, on the basis of microstructural and toxicological consideration, since it increased the overall material corrosion rate, compared to that one of pure Fe, while preserving its biocompatibility [171–173].

3.4. Materials and methods

Powder metallurgy was selected as a fabrication route to produce several kinds of specimens. Table 3.1 offers a detailed description of the relevant conditions used for samples fabrication and their corresponding codes hereafter adopted.

Table 3.1. *Samples investigated in the present study and their denotation*

Sample name	Composition (wt.%)		Starting powders	Powder preparation
AR (As received)	Fe	100	as received	
MX (Mixing)	Fe	98.5	as received	8 hours of mixing
	Mg_2Si	1.5	as received	
BM (Ball milling + Mixing)	Fe	98.5	as received	8 hours of mixing
	Mg_2Si	1.5	32 hours of high energy ball milling	
MM (Mechanical Milling)	Fe	98.5	as received	16 hours of high energy mechanical milling
	Mg_2Si	1.5	32 hours of high energy ball milling	

AR samples were composed only by Fe powders (99.9% purity supplied by Alfa Aesar) and used as reference materials (Table 3.1). All the kinds of samples were compacted by hot rolling, using the following procedure. Rectangular-section carbon steel profiles, having an inner size of 6 mm × 16 mm, a length of 100 mm and a thickness of 2 mm, were used as powder containers. The cans were filled with the powders, plugged and subjected to multi-step hot rolling using a laboratory rolling mill, up to a total nominal reduction in thickness of 50%. Before each rolling step, samples were preheated to 700 °C in a resistance furnace for 20 min. The cans were then machined to extract the compacted material used for the subsequent experiments. In case of composites, corresponding to MX, BM and MM conditions, samples were obtained by a blend of Fe and Mg_2Si powders (99.5% purity, supplied by Sigma Aldrich). For MX condition, the powders were mixed in a conventional horizontal cylindrical mixer for 8 hours without any previous pre-treatment, while for BM and MM conditions, the Mg_2Si powders were milled before the mixing and compaction process. BM samples were produced with as received pure Fe and ball-milled 1.5 wt. % Mg_2Si powders. The reinforcement was milled in an 80mL stainless steel jar using n-hexane as a process control agent. Ball milling was carried out in a planetary ball mill (PM 400 Retsch®), in an argon atmosphere for 32 hours with a milling speed of 300 rpm. The balls and jars used in this experience were made of hardened steel. Ball diameter was 10 mm; the initial balls to powder and fluid to powder mass ratios were 40:1 and 4:1, respectively. After milling, powders were dried in vacuum for 30 hours prior to their exposure to air. Ball-milled Mg_2Si powders were also used for the preparation of MM samples (Table 3.1) using the similar milling parameters set for BM

samples. Fe and milled 1.5 wt. % Mg_2Si powders were subsequently mechanically milled in a planetary ball mill for 16 hours with a milling speed of 300 rpm; the initial balls to powder and fluid to powder ratios were respectively 10:1 and 2:1. Eventually, MX, BX and MM powders were dried, canned, hot rolled and machined as already described for the AR samples.

3.4.1. Characterization

The samples were prepared before etching with the following procedure: their surface samples' surfaces were ground and polished following the standard metallographic procedure. Then, they were washed 5 min in an ethanol ultrasonic bath to remove residuals of abrasive particles, and finally rinsed with distilled water for 10 min before the corrosion testing.

The polished specimens were then etched in a 2% Nital solution. A Carl Zeiss AG - EVO® 50 Series scanning electron microscope (SEM), equipped with an INCA, *Oxford Instruments*, Uedem, *Germany* energy dispersive X-ray spectrometer (EDS), was used to investigate the microstructure and morphology of the samples and to analyze the phase chemical composition. The grain size was evaluated according to ASTM E112-96 standard, following the linear intercept procedure [174]. Phase identification was carried out on as-received samples and degraded surfaces by X-ray diffractometry (XRD). The Siemens D5000 diffractometer was set-up with a Brentano-Bragg configuration. It was equipped with a curved graphite crystal monochromator, and it was operated with a Cu anode ($\lambda_{Cu\ K\alpha}$ = 1.54184 nm), an acceleration voltage of 40 kV and a current of 30 mA. The acquisitions were carried out at a scanning rate of 0.02°/1.2 s^{-1}. The scanning range was 10 – 90°. The density of the samples was measured on the basis of the Archimedes' principle, and the porosity was calculated with the same technique described by Yu et al. [175].

Tensile specimens were cut along the rolling direction, according to ASTM E8/E8M standard [176]. The tensile specimens had a gauge length of 30 mm and a rectangular cross section of 6 mm × 1.5 mm. Tensile tests were carried out using a universal testing machine MTS Alliance RT/100, USA, at a strain rate of 2×10^{-3} s^{-1}. Average and standard deviation of tensile properties were calculated on the base of three tests per each condition. Additionally, Vickers macro-hardness test was performed according to ASTM E92 standard [177]. The applied load on the indenter was 49 N.

3.4.2. Corrosion behavior

The corrosion behavior of Fe and Fe/Mg_2Si composites was studied in Hanks' modified solution. The solution composition and its preparation is reported by Lévesque et al. [70]. The solution pH was adjusted to 7.4, by the addition of 1M HCl or 1M NaOH, where appropriate. The samples surfaces were polished in the same way as above described for metallographic analyses. Both potentiodynamic polarization tests and static immersion tests were performed to investigate the corrosion behavior [178,179]; the tests were carried out according to the corresponding standards, that is respectively ASTM G59–97 and ASTM G31-72.

The potentiodynamic test was performed using a conventional three-electrode cell (Princeton Applied Research Model K47) with a platinum counter electrode of 1 cm^2 in surface area, a saturated calomel reference electrode and the prepared Fe-based working electrode. The experiment was performed after the open circuit potential settled for 30 minutes. A scan rate of 0.166 mV/s, with an applied potential range of 1V, was used. The experiments were carried in an aerated environment at 37±1°C; the solution was mechanically stirred (80 rounds/min). For each type of material, three specimens were tested using the same conditions.

For static immersion tests, five 16 mm × 8 mm × 0.7 mm samples for each condition were immersed for 14 days in 90 mL of Hanks' modified solution [70]. The containers were stored in a controlled environment (T = 37±1°C), with a CO_2 atmosphere content of 5vol. % and a relative humidity of 85%. The amount of solution for each sample is specified by the aforementioned standard, for a total of around 90 mL for sample. The whole volume of solution was changed every 48 hours to keep the pH value close to 7.4 and to maintain the working conditions as constant as possible. Subsequently, the samples were brushed and washed with 70% ethanol in an ultrasonic bath for 5 minutes, in order to remove the corrosion products on the surface before measuring the final weight. The samples were either sonicated 3 times, or after two consecutive weightings provided the same weight. Insoluble corrosion products, found at the bottom of each bottle, were collected with a small amount of solution and centrifuged. The extracted deposit was then added to a solution of 50% ethanol and 50% nanopure water and vortexed, again centrifuged, dried and characterized by SEM and EDS. The corrosion rates of the alloys were calculated using the weight loss method.

3.5. Experimental results

3.5.1. Microstructure

SEM micrographs in Fig. 3.1a, b and c depict as received Fe and as received/mechanically milled Mg_2Si powders. In the inset of Fig. 3.1b, a representative picture of an as-received Mg2Si powder showing small particles (~ 80% of particles are in the range of 1.7 – 19.4 μm), large particles (~ 19.5% of particles are in the range of 19.4 – 222 μm) and markedly coarse particles (0.5% of particles are in the range of 222 – 750 μm) is provided. The particle size of Fe and mechanically milled Mg_2Si powder was measured by analyzing an average of 10 SEM micrographs.

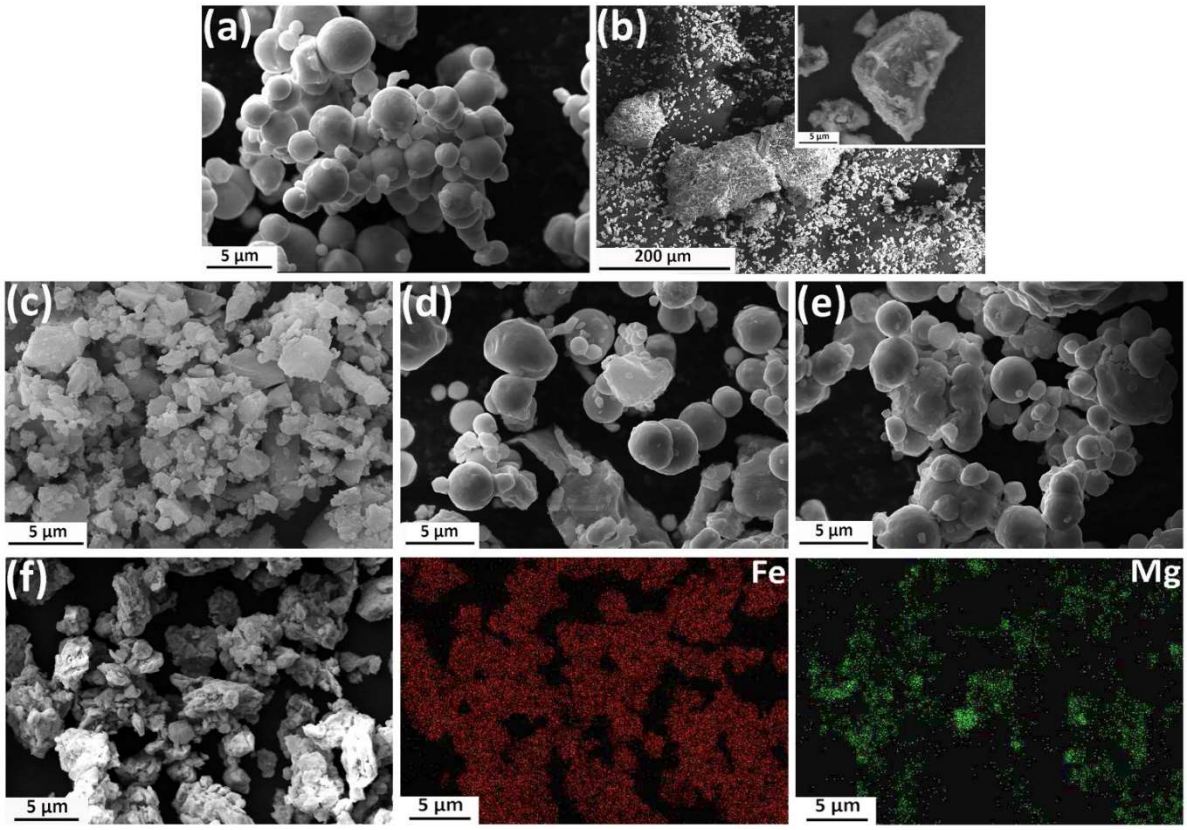

Figure 3.1. *SEM morphology of the powders used in this study: a) as-received Fe powder, b) as-received Mg_2Si powder, c) high energy ball milled Mg_2Si powder, d) MX, e) BM, f) MM and its corresponding elemental maps for Fe and Mg, respectively*

As seen in Fig. 3.1a, the as-received Fe powder has a spherical shape with an average particle size of 2.8±0.3 μm. Fragmentation induced by high energy ball milling led to a decrease of the Mg_2Si particles to ~1.5±0.2 μm (Fig. 3.1c). Fig. 3.1d-f show Fe/1.5%Mg_2Si powder mixtures

respectively for MX, BM and MM samples. As evidenced by the micrographs, the mixing process did not lead to a relevant change in the morphology of the initial powders. Moreover, combined observation of Fig. 3.1d and Fig. 3.1e indicates that a uniform component distribution could not be obtained by the mixing process. In contrast, mechanical milling process considerably influenced the reinforcement distribution throughout the matrix (see Fig. 3.1f). In this case, Fe particles underwent plastic deformation, while Mg_2Si was affected by fragmentation, both of which could not be achieved during the mixing process. A more homogenous reinforcement distribution was obtained in the case of MM samples. Fig. 3.1f shows that ball milling caused the coarser Mg_2Si particles to break down into fine pieces embedded on the surface of deformed and cold-welded Fe powders. EDS elemental maps of Fe and Mg, for the MM condition presented in Fig. 3.1f confirms the homogeneous distribution of the reinforcement phase in the Fe powders.

Fig. 3.2 represents the typical microstructures on the transversally cross-sectioned hot rolled samples. Hot rolling resulted in fine-grained consolidated samples with an average grain size of 2.3 µm, 2.1 µm, 1.3 µm and 0.9 µm for AR, MX, BM and MM samples, respectively. Moreover, as shown in Table 3.2, the relative porosity for AR, BM and MM samples are lower than 0.79%. Only MX samples exhibited a higher porosity (2.08%) which is attributed to the presence of coarser Mg_2Si particles, preventing the full consolidation of the matrix and promoting reinforcement cracking. Moreover, as seen in Fig. 3.2b, for this condition, Mg_2Si particles are heterogeneous in size and dispersion. This suggests that the reinforcement distribution varied with different powder processing methods and various combinations of matrix/reinforcement powder size.

Table 3.2. *Density and porosity of Fe and Fe/Mg_2Si composites*

Sample	Density g/cm^3	Porosity %
AR	7.78±0.01	0.79±0.09
MX	7.36±0.05	2.08±0.59
BM	7.46±0.04	0.95±0.43
MM	7.47±0.01	0.89±0.12

In the case of BM samples, Mg_2Si particles were remarkably refined and homogeneously spread within the Fe matrix. Mechanical milling (samples MM) resulted in the formation of a much finer reinforcement particles (mainly submicron in size, Fig. 3.2d).

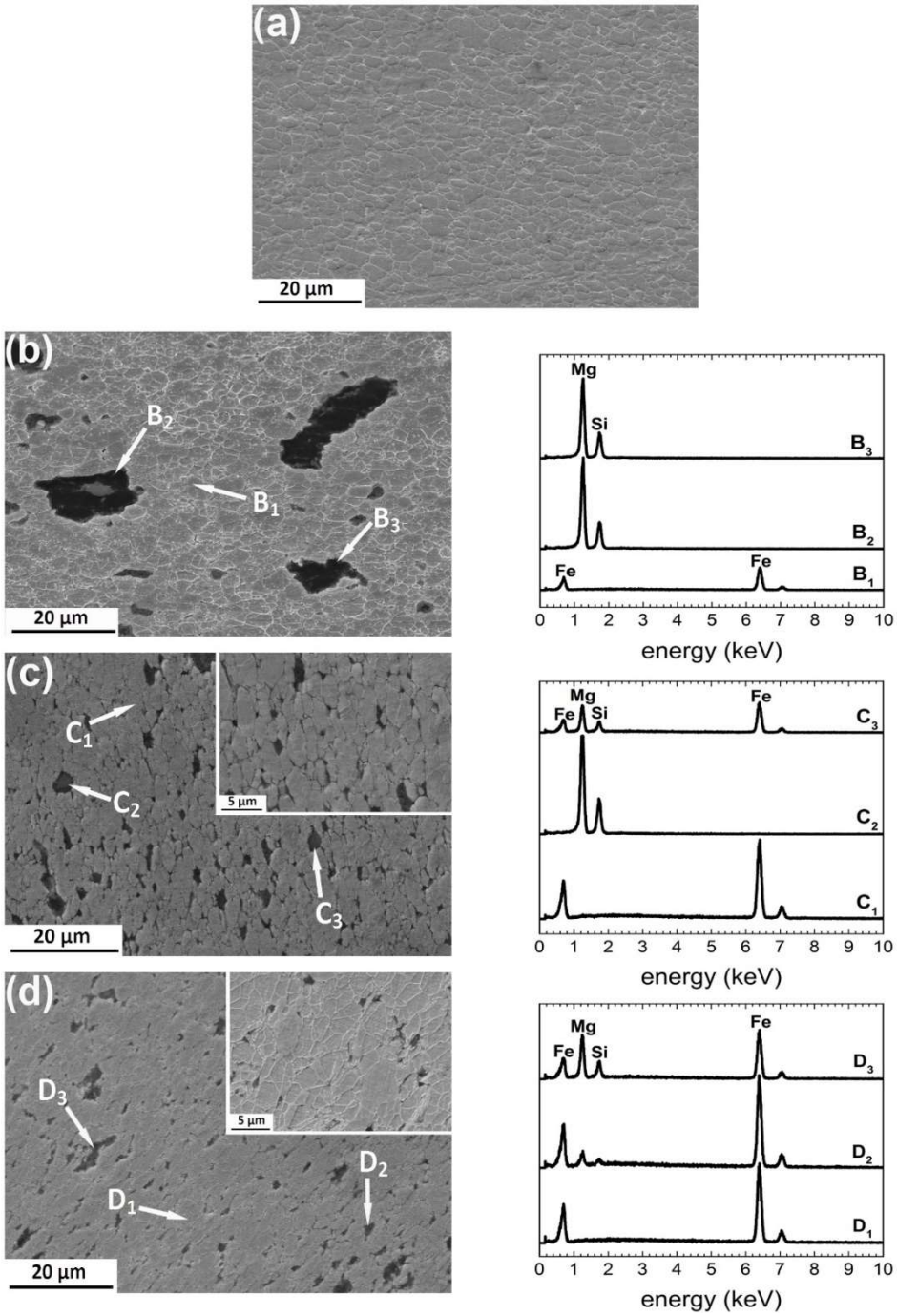

Figure 3.2. *SEM micrographs of hot rolled Fe, Fe/Mg_2Si composites and corresponding EDS spectra, a) AR, b) MX, c) BM and d) MM samples*

XRD patterns (Fig. 3.3) confirms the presence of α-Fe (JCPDS #06-0696*)* with BCC structure as the only detectable phase. For pure Fe, the most common grain orientation belongs to (200) reflection. After the addition of the reinforcement, the grain orientation of the (200) plane

decreased, while that of (110) increased. The presence of Mg_2Si (JCPDS #35-0773) in each composite sample was detected.

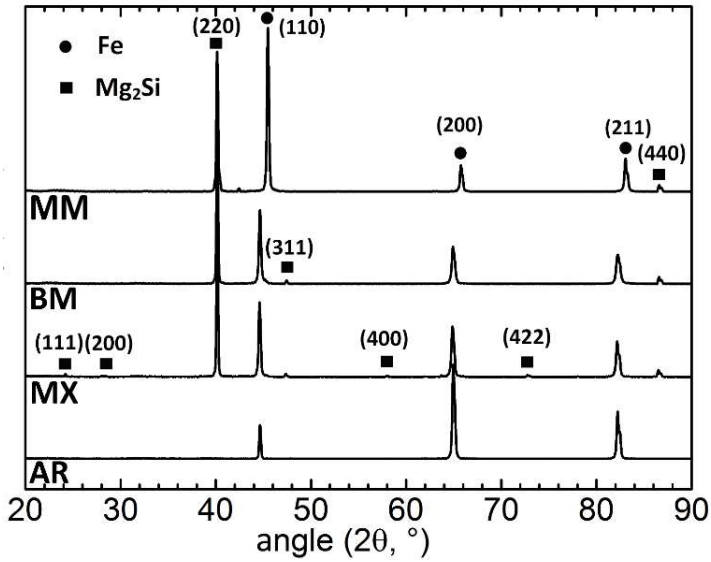

Figure 3.3. *X-ray diffraction patterns of Fe and Fe/Mg_2Si composites.* ***Table 3.1*** *shows the preparation details for AR, MX, BM and MM samples, respectively*

3.5.2. Mechanical properties

Fig. 3.4a presents the tensile properties of the investigated samples including 0.2% yield strength (YS), ultimate tensile strength (UTS) and fracture elongation (A). As seen, for MX samples, the addition of coarse Mg_2Si particles by simple mixing leads to an evident decrease in the tensile properties of YS, UTS and A from 400 MPa, 416 MPa and 21% for pure Fe to 290 MPa, 321 MPa and 5%, respectively. Similarly, the value of hardness (Fig. 3.4b) decreased compared to its unreinforced counterpart (AR sample). Only by using mechanically milled Mg_2Si particles during mixing (BM samples), meaningful improved mechanical properties were achieved (481 MPa and 570 MPa, for YS and UTS, respectively). In the case of MM samples, a further enhancement of YS and UTS (523 MPa and 630 MPa, respectively) was recorded, whereas fracture elongation was concurrently reduced to about 4%.

Additionally, as indicated in Fig. 3.4b, the average hardness of sample MM (270 HV) is notably higher than those measured for other investigated samples (~140 HV, ~120 HV and ~220 HV for AR, MX and BM samples, respectively). The assessment of the mechanical properties for all the conditions highlighted the outstanding mechanical strength achieved by the MM. This result can

be ascribed to the effect of the MM process on the matrix powders and the effect caused by the markedly fragmentation/better distribution of reinforcement particles.

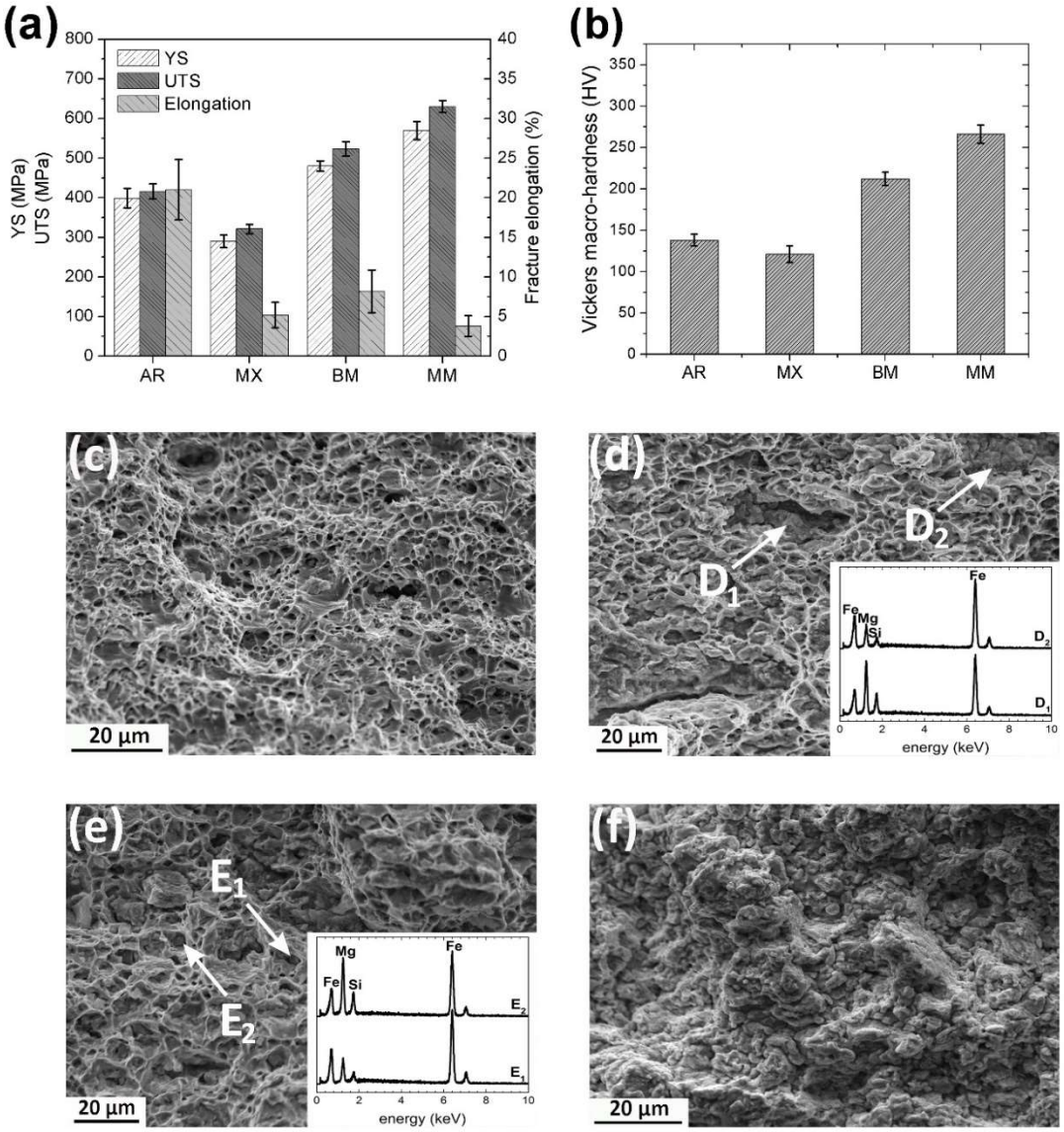

Figure 3.4. *Mechanical properties: a) tensile properties, b) macro-hardness results and SEM morphology of the tensile fracture surface of the investigated samples, c) AR, d) MX, e) BM and f) MM samples*

Fig. 3.4c-f represents SEM micrographs of the tensile fracture surfaces of the tested samples. As seen, AR exhibits a typical dimple-mode ductile fracture, whose features are in good agreement with the high measured tensile elongation value (~21%). With the addition of Mg_2Si particles, the amount of surface covered by dimples consistently decreases, showing a ductility diminution. The fracture morphology of MX and BM type samples show several cleavage planes very often

associated to the presence of Mg_2Si particles, suggesting a mixed ductile–brittle fracture. The fracture mode observed in these samples are attributed to the reinforcement distributions [180,181]. Particle/matrix interface decohesion could be found not only in composite reinforced with coarse Mg_2Si particles(MX), but also in other conditions. This behavior can be ascribed to the poor bonding strength between matrix and particles. Mg_2Si particles can also be observed on the fracture surface of the composites in Fig. 3.4d and 3.4e (white arrows). Particles could be damaged during composite fabrication or subsequently fractured during straining. This observation supported the interpretation previously given for the decreased strength of MX samples. In case of BM samples, in spite of dimples formation by plastic deformation around reinforcement particles, a smaller amount of them were exposed to the fracture surface. The MM sample fracture surface is almost fully covered by tiny cleavage planes, representing essentially a brittle fracture mode. It is supposed that the distribution of very small particles prevented the occurrence of extensive plastic deformation of the matrix.

3.5.3. Corrosion behavior of Fe and Fe/Mg_2Si composites

The addition of Mg_2Si particles into a Fe matrix is responsible for a change in the corrosion properties of the material.

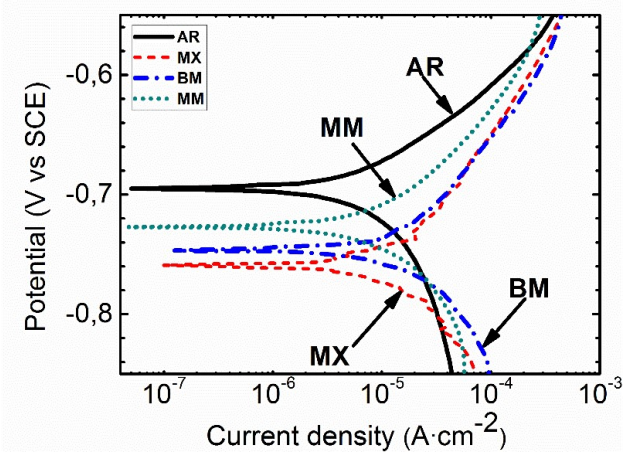

Figure 3.5. *PTD curves for Fe/Mg_2Si composites compared to the pure Fe*

For all the Mg_2Si reinforced samples, E_{corr} was always below that of pure Fe (Fig. 3.5). Corrosion current densities showed higher values for MX, BM and MM composites (24.5, 26.5 and 22.3 $\mu A/cm^2$, respectively) compared to pure Fe (Fig. 3.5 and Table 3.3). Furthermore, the corrosion rates of all composites calculated on the base of the weight loss after static immersion in Hanks' solution were higher than that of AR (Table 3.3). As shown in Table 3.3, BM samples reinforced

with a finer particulate showed the highest mass loss (0.28 mm·year^{-1}). Among the three investigated composites the slowest corrosion rate was recorded for MM (0.19 mm·year^{-1}).

Table 3.3. *Summary of corrosion data obtained from potentiodynamic polarization and static immersion tests for Fe and Fe/Mg_2Si composites*

Material	Potentiodynamic polarization test			Static immersion test
	E_{corr} (V)	i_{corr} (µA/cm^2)	Corrosion rate (mm year^{-1})	Corrosion rate (mm year^{-1})
AR	-0.698 ± 0.003	21.17 ± 0.8	0.25 ± 0.01	0.14±0.01
MX	-0.760 ± 0.002	24.52 ± 1.6	0.30 ± 0.03	0.22±0.03
BM	-0.748 ± 0.004	26.47 ± 1.4	0.31 ± 0.04	0.28±0.04
MM	-0.732 ± 0.001	22.32 ± 0.4	0.27 ± 0.02	0.19±0.01

Fig. 3.6 displays the SEM surface morphologies of the samples, after the static immersion test. AR samples showed a uniform corrosion mode. This is consistent with the findings of other researchers for cast and rolled pure Fe in similar conditions [79]. Obayi et al. showed the effect of static immersion test of cast pure Fe. The morphology of the degraded surfaces was affected by the grain size, which depends on the fabrication route [79]. Localized corrosion could be observed on MX sample surfaces with the presence of corrosion products partially covering the exposed surface. The Mg_2Si particles seem to be partially dissolved, forming shallow craters (an example is given in Fig. 3.6b – point B_2 showing a partially dissolved Mg_2Si particle).

EDS analyses for BM revealed that the corrosion process could be localized, affecting the composition of Mg_2Si particles. As expected, the measured atomic Mg/Si ratio for not degraded powders was close to 2:1. The analysis performed on reinforcement particles after the static immersion test showed a relevant change of the reinforcement chemical composition: in particular, the total amount of Mg decreased (Fig. 3.6e – point B_2) and the atomic ratio of Mg/Si was 0.1:10 for the points shown in Fig. 3.6b. Mg/Si ratio changed when measured for different particles after the corrosion test. In degraded samples, a generally lower Mg concentration for Mg_2Si particles could be caused by ion-selective depletion of this element. For BM samples, corrosion products almost covered the whole surfaces. Where surface products were not present, a series of pits were distributed all over the sample surface: this corrosion morphology could be associated to the small size of particles used during the compaction process, the presence of deformed grains and the residual porosity after powder compaction.

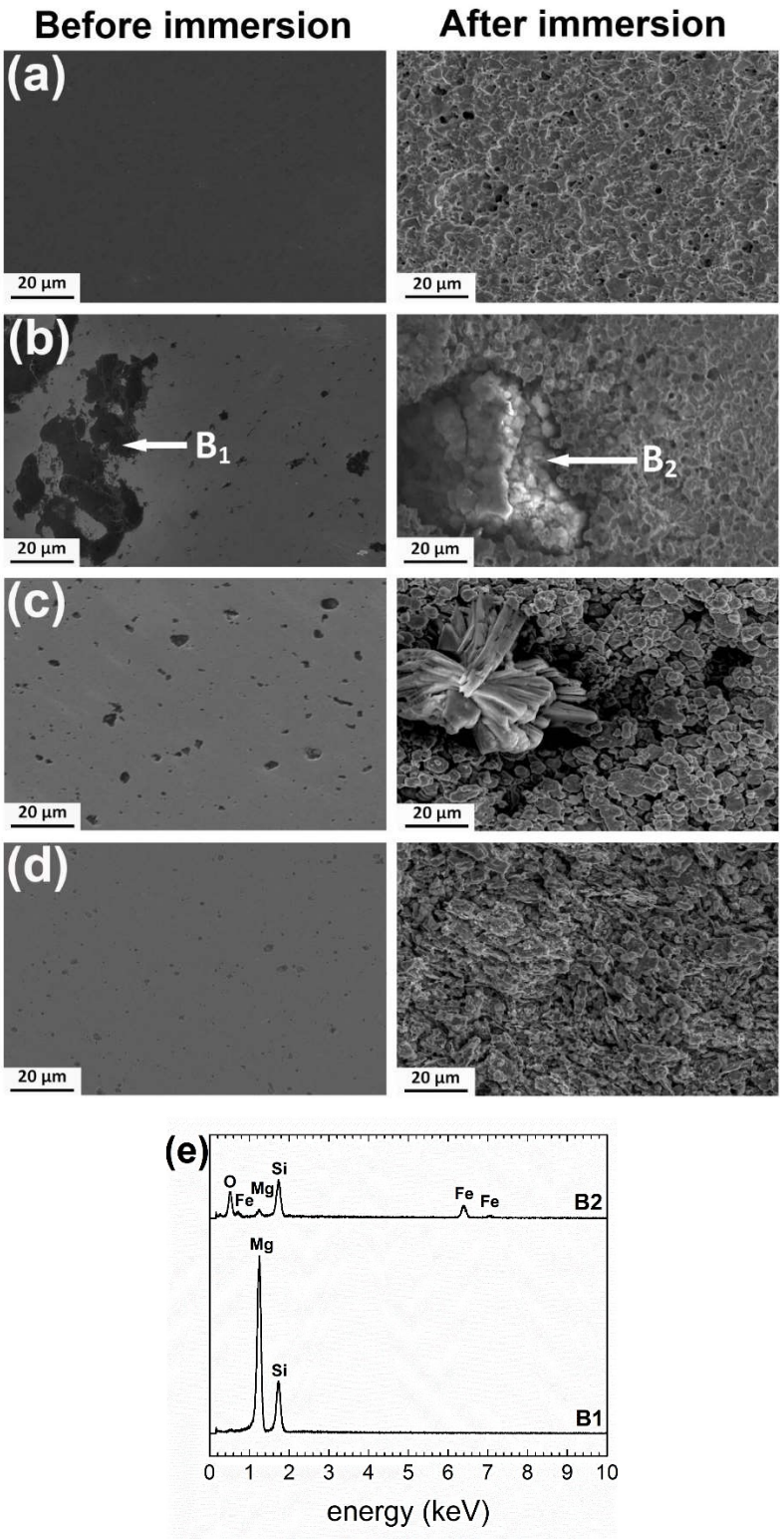

Figure 3.6. (a) to (d). *SEM images of samples' surface morphology before and after static immersion test in Hanks' solution for 14 days a) AR, b) MX, c) BM, d) MM,* ***(e).*** *EDS analyses related to points B_1 and B_2 of Fig. 3.6 (b).*

The corrosion of MM samples led to the formation of a more homogeneous distribution of corrosion products on the surface (Fig. 3.6d). This surface layer reduces the contact of the material with the electrolyte and thus, restricting the release of Fe ions into the solution due to a barrier effect. Accordingly, MM samples revealed the lowest mass loss compared to MX and BM. The effects of the reinforcement size and distribution on the corrosion behavior of the composites are better assessed after removing the corrosion products as shown in Fig. 3.7. SEM observations showed the presence of specific corrosion morphology, corresponding to dimples often localized at grain boundaries in AR samples (Fig. 3.7a). Cross sections of AR degraded samples revealed the presence of small size shallow pits. The addition of Mg_2Si markedly affected the composite corrosion pattern. The surface morphology of MX samples after the static corrosion test was clearly non-uniform, showing the presence of deep pits between metal matrix and coarse Mg_2Si particles. Such features could be attributed to a micro-galvanic activity between the matrix and the reinforcement. SEM micrograph of the cross-sectional view of MX samples revealed deep pits having a narrow opening exposed toward the surface; the cavity expanded in the material bulk, to encompass the size of the reinforcement particle (Fig. 3.7b'). EDS analyses revealed the presence of Si and O in the pits, confirming the dissolution of reinforcement and a formation of SiO_2. Micro-galvanic effects were attributed to the size and distribution of local anodes (Mg_2Si) and cathodes (Fe matrix): for MM samples, in which the reinforcement phase had a smaller size and a more homogeneous distribution, smaller and closer local electrodes reduced the overall pH of the samples leading to a more uniform corrosion. MM samples showed a more homogenous morphology of the degraded material surface compared to those of MX and BM. Indeed, the formation of galvanic micro-cells between Fe and Mg_2Si caused a more intense and widespread dissolution of the composite surface, as it is evident after removing corrosion products by brushing. Fig. 3.7d' shows that with increasing the corrosion time the pits grew and became interconnected, forming a homogenously corroded surface. MM sample cross-section evidenced the presence of open and shallow pits (Fig. 3.7d and 7d').

XRD patterns (Fig. 3.8) show the presence of α-Fe and $FeCO_3$ (siderite*,* JCPDS #29-0696*)* in BM and MM samples. The $FeCO_3$ peaks corresponding to (012) and (014) planes were the most intense reflections. Other low intensity siderite peaks corresponded to (113), (022), (018) and (116) planes. α-Fe (110), (200) and (211) reflections were also evident.

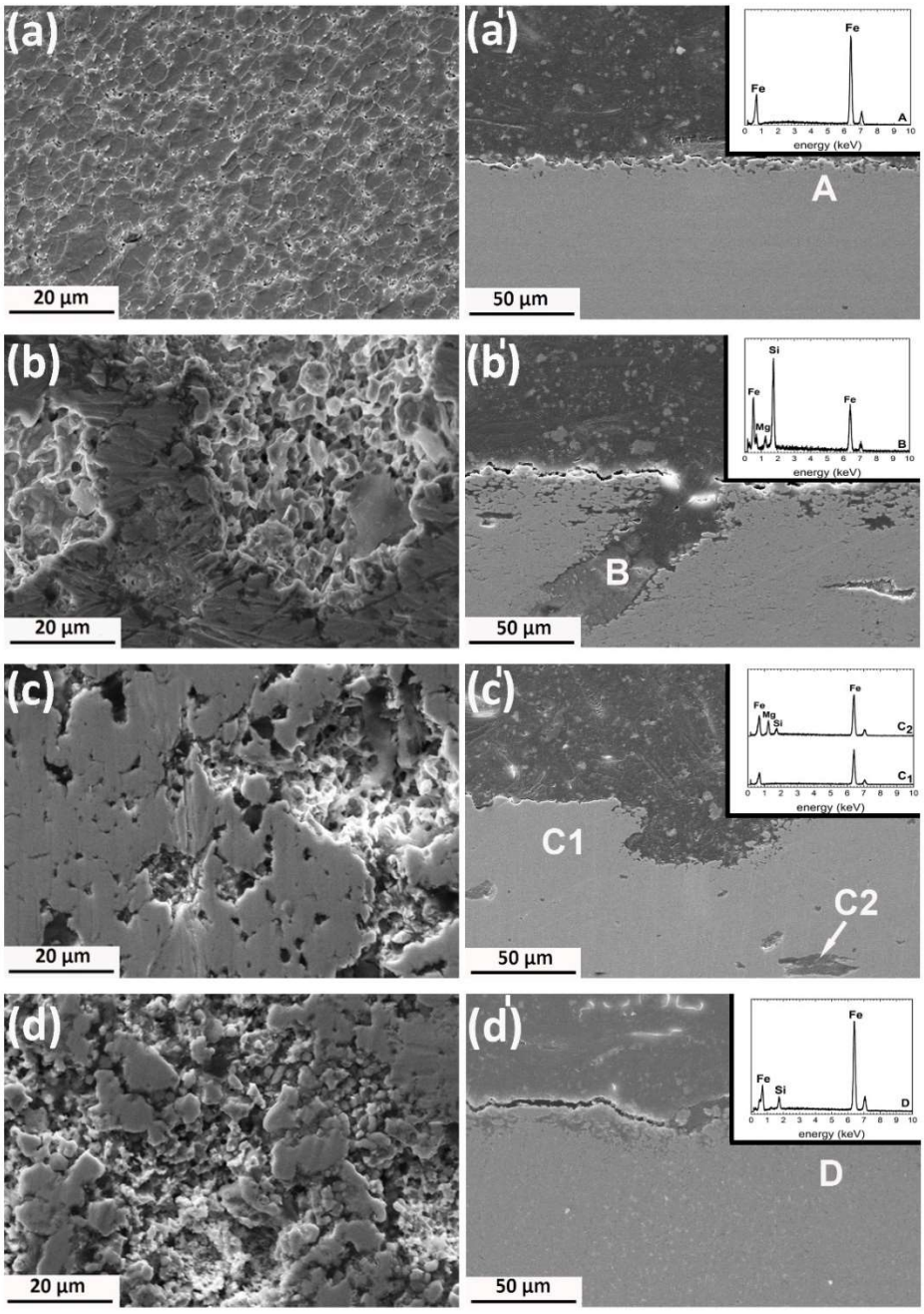

Figure 3.7. *Degraded surfaces after cleaning in ethanol and brushing a) AR, b) MX, c) BM, d) MM and corresponding cross section of the investigated samples (a'-d') with EDS analyses related to the points A-D*

The same α-Fe peaks were found in the as-received samples (Fig. 3.3). In the case of AR and MX samples, XRD analysis showed only the presence of α-Fe. For all the degraded samples, no peaks corresponding to the Mg_2Si phase was found. Despite the presence of corrosion products on the samples surfaces, as evidenced by SEM studies, no peaks corresponding to phosphate compounds

or iron oxides, hydroxides or hydro-oxides were present. The presence of O and P, highlighted by EDS analyses, is due to the formation of insoluble phosphates so that this corrosion layer could be amorphous, nanocrystalline or very thin and therefore, not detectable by X-ray diffraction studies.

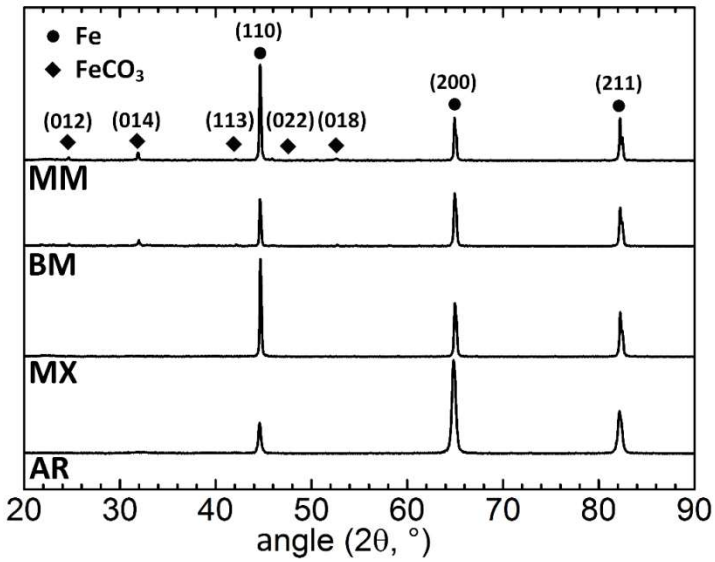

Figure 3.8. *XRD patterns of samples after immersion test in modified Hanks' solution. Table 3.1 shows the preparation details for AR, MX, BM and MM samples, respectively*

3.5.4. Corrosion products characterization

The precipitates, collected at the bottle bottom, were analyzed by SEM and EDS. The morphology of the particles extracted from the solution at the end of the immersion test is shown in Fig. 3.9a. The corrosion products of the Fe-composites were essentially composed of Fe, O, P and Si. Mg was not detected as a component of the precipitates (Fig. 3.9b). Other found elements were Na, Cl and Ca, that can be found in the pseudo-physiological medium. Some cations, such as Ca, can precipitate in the form of phosphates, The absence of Mg in the precipitate composition was also reported for the corrosion of high-Ti content Mg-Ti alloys in saline solution [182]. This might be due to high solubility of Mg^{2+} ions in solution containing Cl^- ions. According to Mg Pourbaix diagram, $Mg(OH)_2$ cannot be formed in solutions with pH values lower than 10 [183]. Furthermore, some Si from Mg_2Si was detected among the corrosion products, showing that Si was less soluble than that of Mg.

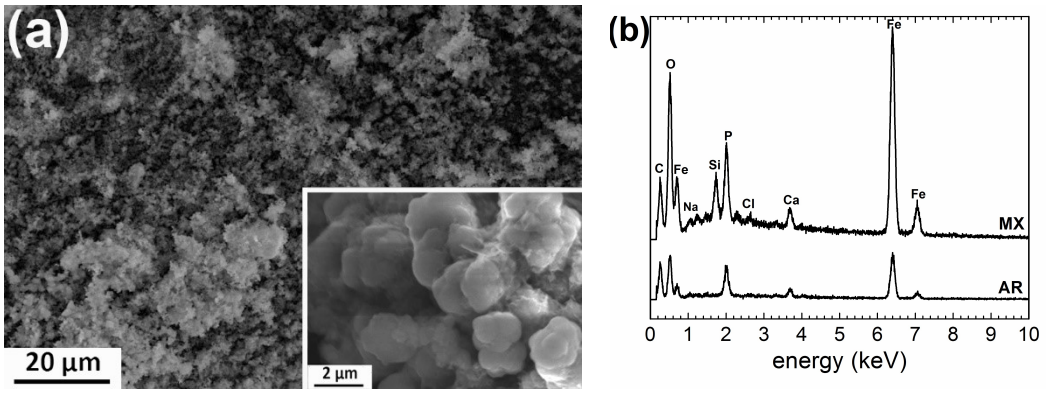

Figure 3.9. *a) Morphology of degradation products precipitated from solution after static immersion tests of sample MX, b) EDS analyses of the same degradation precipitates for samples AR and MX*

3.6. Discussion

3.6.1. Microstructure and mechanical properties

The mechanisms contributing to the strengthening of a particle reinforced composite are of different natures: (i) load transferring from the soft matrix to the stiff and hard reinforcement via shear stresses at the interface [86], (ii) increasing of the dislocation density generated during temperature change, arisen from the difference in coefficient of thermal expansion (CTE) between Fe ($13 \cdot 10^{-6} \cdot K^{-1}$ [184]) matrix and Mg_2Si reinforcement ($7 \cdot 10^{-6} \cdot K^{-1}$ [185]) [87], (iii) hindering of dislocation motion by reinforcement particles, a mechanism known as "Orowan strengthening" [186] and (iv) increased initial work hardening rate of the composite due to the presence of the Mg_2Si particles [187]. All the strengthening mechanisms, from a theoretical point of view, seem suitable to take place in Fe/Mg_2Si matrix composites. Results confirmed that they became less efficient as the particle size increased. Coarse reinforcement size in MX samples reduced the mechanical performance of this composite. For finer particulate reinforced samples (MM), CTE mismatch and Orowan strengthening might be the most effective strengthening mechanisms. For BM samples, the CTE mismatch tends to become the most effective contribution. It should be noted that in all the investigated samples, load transfer had surely a minor role in increasing strength since the amount of the reinforcement (1.5 wt. %) was very low to create significant effects. The outstanding strength of MM samples was at the expense of its fracture elongation. The small reinforcement size produced not only a relevant grain refinement, but also had an effect of higher amount of dislocations. Moreover, the particle shape of the powders used for MM samples

was rather irregular, and the matrix milled powders were subjected to a heavy work hardening [188]. These features are supposed to affect the recrystallization behavior during powder consolidation and the final microstructure of the material [158,189]. It is worth to mention that obtaining a high density by hot rolling of the compacted powders does not always mean that a complete consolidation was achieved and a good interparticle bonding was reached [49,51].

3.6.2. Corrosion behavior

The corrosion led to an increase in local pH at sample surface due to the increasing concentration of OH^- ions generated by water reduction at Mg_2Si-solution interface and at Fe-solution interface by oxygen reduction. Fe matrix for MX, BM and MM samples was more reactive than for the AR samples, where only pure Fe was the constituent as confirmed by the lower corrosion resistance at pH 7.4. The reactions describing the mechanism of Fe oxidation are related to tests carried out in Hanks' solution as follows: [78]:

$$Fe \rightarrow Fe^{2+} + 2e^- \qquad \text{(Eq. 3.1)}$$

$$Fe(OH)_2 + 2FeO(OH) \rightarrow Fe_3O_4 + H_2O \qquad \text{(Eq. 3.2)}$$

Once the solubility limit of $Fe(OH)_2$ is exceeded, hydroxides form on the sample surface along with the formation of a siderite layer or isolated siderite spots. Siderite is not stable at the relatively low pH (~7.4), temperature and pressure used in the present work and thus, they are an intermediate product in Fe oxidation pattern. It was already found that pH is one of the most important factor in siderite formation and the degree of supersaturation strongly increases with increasing pH [190]. The formation of $FeCO_3$ was discussed in detail by Postma et al. and Pfennig et al. [190,191]; it can be described by the following reactions:

$$Fe^{2+} + 2HCO_3^- \rightarrow Fe(HCO_3)_2 \qquad \text{(Eq. 3.3)}$$

$$Fe(HCO_3)_2 \rightarrow FeCO_3 + CO_2 + H_2O \qquad \text{(Eq. 3.4)}$$

An XRD analysis revealed the presence of siderite only on the surface of BM and MM samples. More importantly, the surface morphology of MM samples appeared porous and full of small cavities, more homogenously distributed than those present on BM samples. The difference between the degraded surface morphology of these two conditions led to the conclusion that the

kinetics of siderite formation was not the similar in the two composites. This different corrosion pattern can be explained by the increased concentration of Fe hydroxides, which is related to the dissolution of the reinforcement. The homogeneous distribution of small size particles obtained for the MM condition was responsible for raising the local pH near the surface and for the formation of a siderite corrosion layer. The formation of $FeCO_3$ deposits on the surface of MM samples was more regular than that for the other samples; this mechanism was supported by experimental observations (Fig. 3.6d.). Due to the presence of chloride anions in the Hanks' solution, the insoluble corrosion products may be partially transformed into soluble chlorides, accelerating the corrosion process.

A mechanism associated with the composite dissolution in modified Hanks' solution could be described by the following steps: (i) selective Mg leaching from the reinforcement particles, triggering a complete dissolution of Mg_2Si, (ii) pitting corrosion of Fe in correspondence with the matrix-reinforcement interface, after the dissolution of Mg_2Si, (iii) pure Fe matrix dissolution (by uniform corrosion and linkage of pits) at later stages of corrosion. As seen in fig. 3.6b, the partial dissolution of Mg_2Si particles was evident after static immersion test. The EDS analyses of degraded surfaces showed that the presence of Mg_2Si affected the corrosion pattern of the whole material. In fact, as seen in Fig. 3.8, XRD analyses after the static corrosion test did not reveal the presence of Mg_2Si phase, which confirms the dissolution of the reinforcement. The decrease in the concentration of Mg was caused by the selective ion leaching of Mg from Mg_2Si. The local dissolution of Mg_2Si particles in chloride aqueous solution was previously observed in aluminum-based alloys [192–194], according to the following reaction:

$$Mg_2Si + 4H_2O \rightarrow 2Mg(OH)_2 + SiH_4 \qquad \text{(Eq. 3.5)}$$

This reaction is followed by SiH_4 hydrolysis and by the formation of silicon hydroxides:

$$SiH_4 + nH_2O \rightarrow SiO_2 \cdot mH_2O + 4H_2 \uparrow \qquad \text{(Eq. 3.6)}$$

Mg preferential dissolution for Mg_2Si is responsible for the formation of Si or SiO_2, due to the anodic activity of the Mg_2Si:

$$Mg_2Si + 2H_2O \rightarrow Mg^{2+} + SiO_2 + 4H^+ + 8e^- \qquad \text{(Eq. 3.7)}$$

The corrosion potential value of Mg_2Si for the previous reactions highlights the anodic behavior of this compound, compared to that of the Fe matrix. The anodic dissolution starts from the surface due to selective leaching of Mg. Neutral or local acidic pH might form close to Mg_2Si particles, after Mg depletion, because of the increased Si amount that transforms into silicates:

$$SiO_2 + 4OH^- \rightarrow SiO_4^{4-} + 2H_2O \qquad \text{(Eq. 3.8)}$$

$$Mg^{2+} + 2OH^- \rightarrow Mg(OH)_2 \qquad \text{(Eq. 3.9)}$$

The results of EDS analyses shown in the Fig. 3.7 and 3.9 are in good agreement with the proposed corrosion pattern. The oxygen reduction at the matrix surface might coincide with the local rise of pH promoting surface passivation:

$$O_2 + 2H_2O + 4e \rightarrow 4OH^- \qquad \text{(Eq. 3.10)}$$

The hydroxide formation on Mg_2Si might form a barrier preventing its further decomposition. Reinforcement particles dissolved or detached from the matrix with the corrosion advancement, initiating at the matrix-reinforcement interface; the formation of such cavities is the first step for the nucleation and growth of pits. Pitting corrosion triggered by Mg_2Si dissolution influenced the surrounding metallic matrix, and the phenomenon could then be promoted by the local acidification mechanism. The proposed mechanism is well consistent with the observations and the mechanisms of the localized corrosion found for Fe-based materials in a chloride-rich medium discussed in literature [6,93,113].

3.7. Conclusions

A series of Fe/Mg_2Si composites were prepared by different routes, for example mixing and/or mechanical milling of powders. Specimens were fabricated by powder metallurgy, using hot rolling as a consolidation method. The addition of Mg_2Si particles was selected to obtain a faster corrosion rate of Fe-based composites through a micro-galvanic coupling mechanism. The introduction of a second phase was found to significantly modify the mechanical properties of the base material, that is pure Fe. The simple addition of coarse Mg_2Si particles, such as for MX samples, led to a decrease in tensile properties of ~75% and even a more relevant ductility reduction. The composites made by small size reinforcement, that is BM and MM, showed

a general increase of tensile properties, with MM samples presenting better tensile performances (YS = 523 MPa, UTS = 630 MPa), but the lowest ductility compared to that of pure Fe, that is ~4%. Concerning potentiodynamic and static immersion tests, a higher corrosion rate was obtained in general when Mg_2Si particles were added to the pure Fe matrix; both the tests showed the same trend for the different studied conditions. The lower corrosion rate was obtained for pure Fe (CR = 0.25±0.01 mm/year for potentiodynamic test, CR = 0.14±0.01 mm/year for static immersion test), while the highest one was found for the BM condition (CR = 0.28±0.04 mm/year for potentiodynamic test, CR = 0.31±0.04 mm/year for static immersion test). The potentiodynamic test corrosion rate was basically the same for MM and BM samples. The corrosion mode of Fe/Mg_2Si composites varied with the powder preparation method and reinforcement size/distribution. A more uniform corrosion pattern, found for example in MM samples, replaced the predominant localized pitting corrosion evident in MX samples.

3.8. Acknowledgements

MSJ was awarded a doctoral scholarship from the Italian Ministry of Education, Universities and Research (Ministero dell'Istruzione, dell'Università e della Ricerca, MIUR). The research involved in this work was partially supported by the Natural Science and Engineering Research Council (NSERC) of Canada. MSJ, CP, DM and MV were recipients of the Linkage Grant from Quebec/Italy sub-commission of the Quebec Ministry of International Relations and the Italian Ministry of Foreigners Affairs.

4. Understanding the effect of the reinforcement addition on corrosion behavior of Fe/Mg_2Si composites for biodegradable implant applications

****

The aim of this paper is to examine how corrosion develops on Fe and its Fe/Mg_2Si composites during the initial stages of exposure to modified Hanks' solution. The corrosion initiation and the role of Mg_2Si particles at early stages of degradation is explained.

****

Understanding the effect of the reinforcement addition on corrosion behavior of Fe/Mg_2Si composites for biodegradable implant applications

M. Sikora-Jasinska[1,2], P Chevallier[2], S Turgeon[2], C Paternoster[2], E Mostaed[1], M Vedani[1], D Mantovani[1]

[1] *Department of Mechanical Engineering, Politecnico di Milano, Milan, Italy.*

[2] *Lab. for Biomaterials & Bioengineering (CRC-I), Dept. Min-Met-Materials Engineering & Research Center CHU de Québec, Laval University, Québec City, Canada.*

Keywords: Biodegradable metals, Fe-based composites, Localized corrosion, Magnesium silicide, Potentiodynamic polarization, Static immersion test, Galvanic coupling

This chapter is under review

Journal: *Materials Chemistry and Physics, Elsevier*

4.1. Résumé

Les matériaux à base de fer ont montré un fort potentiel pour les applications de biomatériaux dégradables. Cependant, leur vitesse de corrosion lente limite leur utilisation en tant que matériau biodégradable pour l'implantation. Une approche pour contrôler et modifier leurs propriétés mécaniques est l'utilisation de particules de renfort, pour créer des composites à matrice métallique dans lesquels la seconde phase vise à ajuster non seulement les propriétés mécaniques mais aussi la façon et la vitesse de corrosion dans un environnement physiologique.

Dans ce travail, des composites à base de Fe ont été produits par métallurgie des poudres à partir de poudres de Fe et de Mg_2Si. Les différentes conditions ont été fabriquées par diverses combinaisons de procédés de broyage ou de mélange suivies d'une consolidation par laminage à chaud. L'effet de l'addition de Mg_2Si sur le comportement à la corrosion des composites Fe/Mg_2Si a été étudié en effectuant des tests de polarisation potentiodynamique cyclique et de corrosion statique pour un temps d'immersion de 24 et 240 heures.

La présence des particules de renforcement a joué un rôle crucial dans la susceptibilité à l'attaque de corrosion localisée dans les composites à base de Fe. L'initiation de la corrosion et son développement ont été systématiquement suivis. La microscopie électronique à balayage, la diffraction des rayons X et la spectroscopie d'émission atomique ont été utilisées pour étudier le mécanisme de corrosion. L'importance des particules de Mg_2Si dans le déclenchement des processus de corrosion a été expliquée.

Des mesures électrochimiques et des tests d'immersion statique ont indiqué que l'ajout de Mg_2Si pourrait augmenter le taux de corrosion du Fe. Il a été constaté que la taille et la distribution des particules de renfort jouaient un rôle crucial à l'uniformité de l'attaque de corrosion.

4.2. Abstract

Iron-based materials showed a high potential for degradable biomaterial applications. However, their slow corrosion rate limits their use as a biodegradable implant material. One approach to control and modify their mechanical properties is the use of reinforcement particles, to create metal matrix composites in which the second phase is aimed at tuning not only the mechanical properties but also the corrosion mode and rate in a physiological environment.

Here, Fe/Mg_2Si composites were produced via powder metallurgy from pure Fe and Mg_2Si powders. The different conditions were fabricated by various combinations of milling or mixing processes followed by hot rolling consolidation. The effect of the Mg_2Si addition on corrosion behavior of Fe/Mg_2Si composites was studied by performing cyclic polarization and static corrosion tests for an immersion time of 24 and 240 hours.

The presence of the reinforcement particles played a crucial role in the susceptibility of Fe-based composites to localized corrosion attack. The corrosion initiation and its development were systematically monitored. Scanning electron microscopy, X-ray diffraction, and atomic emission spectroscopy were employed to investigate the corrosion mechanism. The importance of Mg_2Si particles in the triggering of corrosion processes was explained.

Electrochemical measurements and static immersion tests implied that the introduction of Mg_2Si particles could accelerate the corrosion rate of Fe. It was confirmed that the size and distribution of the reinforcement influenced considerably the uniformity of the corrosion attack.

4.3. Introduction

Over the past two decades, biodegradable metals (BMs) have been the subject of comprehensive research as a potential alternative to permanent biomedical implants. The raised interest for this material is still alive in the scientific community. BMs emerged as a promising candidate for cardiovascular and orthopedic applications, showing an alternative where permanent implants could result in complications such as inflammatory reactions or inability to adapt to pediatric patient growth [7].

Magnesium, iron, zinc and their alloys have been investigated as potential metallic materials for BMs [7]. Nevertheless, the use of Mg as a degradable implant is still challenging due to its poor, anisotropic mechanical behavior and rapid, inhomogeneous degradation, which leads to the formation of a high amount of hydrogen in a physiological environment [64,134,195]. Recently, Zn has been introduced as a potential candidate to the biomedical community due to its excellent biocompatibility and an appropriate corrosion rate. The main concern related to the use of Zn is due to its poor mechanical properties [48,53].

Fe and Fe-based alloys, because of their superior mechanical properties to those of Mg and Zn alongside their good biocompatibility and ease of processing, seem to be promising materials for medical applications [82,128,196]. An *in vivo* research conducted by Peuster et al. [74] found no inflammation, systemic toxicity, and tissue proliferation after 18 months of pure Fe implantation. In spite of this, the implantation of a pure Fe stent in a porcine descending aorta showed that even after one year of implantation a large portion of the device remained unchanged, because of a very slow degradation rate [141]. Liu et al. [80] investigated the *in vitro* effects of Fe alloyed with common elements such as C, Mn, Si, P, B, and Cr, and they found that all the alloys exhibited a good hemocompatibility and no significant cytotoxicity. To date, many attempts have been made for the purpose of accelerating the degradation of Fe by the modification of the chemical composition, thermal treatments and surface modifications [94]. The presence of secondary phases with a pronounced difference in corrosion potential relative to that of the bare metal can promote the micro-galvanic coupling and therefore accelerates corrosion. Thus far, a variety of alloying elements (e.g. Au, Ag, W, Pt, Pd etc.) have been used to increase the corrosion rate [93,113,119,143]. Moreover, from a mechanical point of view, the addition of alloying

elements leads to a considerable improvement of the mechanical performance due to the formation of a solid solution and/or second phase strengthening mechanisms. Furthermore, recent studies have reported that adding non-metallic or metallic particles to Fe results in simultaneously modulate the mechanical and corrosion properties of the final material. Size, volume fraction, and particle distribution play a fundamental role in the definition of material properties [77,154,157]. Further, manufacturing processes (e.g. casting [102], electroforming [78], powder metallurgy (PM) [95] and 3D printing [197]) could selectively tune the mechanical and electrochemical material properties. For instance, Fe-Mn alloy fabricated by PM showed increased *in vitro* corrosion rate than its counterparts produced by casting. Such enhanced degradation rate was to the presence of porosity which is an inevitable feature of PM processes. PM is an appealing manufacturing technique, allowing the production of samples with complex geometries.

Corrosion susceptibility of metallic materials relies on the formation and stability of degradation products on the surface. Over the last decade, despite extensive corrosion studies have been performed on the degradation behavior of Fe in a physiological environment, the corrosion pattern is not yet completely clear. The study of the corrosion behavior is still a critical aspect of BMs science. Thus, a fundamental understanding of corrosion initiation, protective film formation, and growth on Fe and Fe-based material surfaces leads to a design of smarter and surface responsive BMs with controlled degradation rates, at distinct stages of the degradation process.

The aim of this work is to examine how corrosion develops on Fe and Fe/Mg_2Si composites during the initial and further stages of exposure to modified Hanks' solution. Here, the corrosion initiation and the role of Mg_2Si particles at the early stages of immersion is addressed. Thus, in this study, for a better understanding of the corrosion initiation on Fe and Fe/Mg_2Si composites, electrochemical measurements and immersion tests (for a duration of 24 and 240 hours) were performed. Corroded surfaces were investigated in detail using X-ray diffraction (XRD) and scanning electron microscopy equipped with an electron dispersive X-ray spectrometry (SEM-EDS). Ion release was assessed by atomic emission spectroscopy (AES). Finally, the corrosion mechanism for Fe and Fe/Mg_2Si composites was proposed.

4.4. Materials and methods

4.4.1. Sample preparation

Fe and Fe/Mg_2Si composites were fabricated via powder metallurgy (PM) process as reported in [77]. Table 4.1 summarizes the detailed description of the investigated powder conditions and their corresponding denotation. Mixed or mechanically milled powders were put in rectangular sectioned steel containers, pressed, sealed, and finally consolidated by hot rolling, with a final thickness reduction of 60%. Before each rolling pass, the containers were preheated in a furnace at 700°C for 20 min.

Table 4.1. *Investigated samples' conditions and their corresponding denotation*

Sample denotation	Composition		Starting powders	Powder processing
PF	Fe	100 wt.%	as received	-
MX	Fe	99 wt.%	as received	24 h mixed
	Mg_2Si	1 wt.%	32 h mechanically milled	
MM	Fe	99 wt.%	as received	24 h mechanically milled
	Mg_2Si	1 wt.%	32 h mechanically milled	

4.4.2. Metallographic examination

Samples for microstructural observation were cut and mechanically polished according to the standard metallographic procedure. Subsequently, specimens were etched in 2% Nital solution for microstructure evaluation. A FEI Quanta 250 SEM with a tungsten filament equipped with an EDS was employed to evaluate the microstructure and morphology of the samples and to investigate their chemical composition. The acceleration voltage was in the range of 10-30kV. The grain size was calculated as stated in ASTM E112-96 standard, according the linear intercept procedure [23]. SEM micrographs were analyzed using Microstructure Characterizer software in order to evaluate the reinforcement size distribution. Feret's equivalent diameter was chosen to estimate the size of the reinforcement. The phase composition of as-received and degraded specimens was analyzed by XRD. The Siemens D5000 diffractometer with a curved graphite crystal monochromator operated with a Cu anode ($\lambda_{Cu\ K\alpha}$ = 1.54184 nm), an acceleration voltage

of 40 kV and a current of 30 mA. The acquisitions were carried out at a scanning rate of 0.02°/1.2 s^{-1}. The scanning range was 0 – 90°. The density of Fe and Fe/Mg_2Si composites was measured following Archimedes' principle, and the porosity was calculated according to the same method described by Yu et al.[175].

4.4.3. Corrosion behavior

The corrosion susceptibility of Fe and Fe/Mg_2Si samples was investigated in Hanks' modified solution. The solution composition and its preparation was previously reported by Lévesque et al. [70]. Its ionic composition in comparison to blood plasma is shown in Table 4.2.

Table 4.2. *Ionic composition of a blood and modified Hanks' solution*

Ion	Blood plasma (mg/L)	Testing solution (mg/L)
Na^+	3266	24
K^+	156	170
Ca^{2+}	100	32
Mg^{2+}	24	14
Cl^-	3657	3542
HCO_3^-	1708	1654
SO_4^{2-}	78	9
HPO_4^{2-} / $H_2PO_4^-$	346	48
D-glucose	714	800

The pH of the solution was adjusted to 7.4 using 1 M NaOH or HCl. Prior to corrosion tests, the samples' surfaces were polished according to the procedure mentioned in the previous section. Cyclic polarization and static immersion tests were performed to evaluate the electrochemical behaviour of composites according to ASTM G59–97 and ASTM G31-72 standards, respectively. The electrochemical measurements were carried out using a conventional three-electrode cell (Princeton Applied Research Model K47) with a platinum counter electrode of 1 cm^2 in surface area, a saturated calomel reference electrode and the Fe-based working electrode. The open circuit potential (OCP) was recorded for 30 minutes. A scan rate of 0.166 mV/s, with a reverse in scan direction when anodic current density reached 1 $mA \cdot cm^{-2}$ or potential -0.8 mV vs. SCE. The experiments were performed in an aerated environment at 37±1°C; the solution was mechanically

stirred (80 rounds/min) during the tests. For each type of material, three specimens were tested using the same conditions. Corrosion rates were obtained based on the calculated corrosion current density (i_{corr}), using the following equation:

$$CR_P = 3.27 \cdot 10^{-3} \frac{i_{corr} EW}{\rho} \quad \text{(Eq. 4.1)}$$

where CR_P is the corrosion rate (mm year^{-1}), i_{corr} is the corrosion current density (μA cm^{-2}) obtained on the base of potentiodynamic curves using Tafel extrapolation method, EW is the weight equivalent and ρ is the material density (g cm^{-3}).

Further, Mg_2Si was coupled with Fe in a modified Hanks' solution. During the coupling test, the coupling current was measured. After a test duration of 240 h, coupled electrodes were disconnected, and potentiodynamic polarization tests on respective electrodes were performed.

For static immersion tests, 18 mm × 9 mm × 1 mm samples were immersed for 24 and 240 hours in 80 mL of Hanks' modified solution [70]. The containers were placed in the incubator (T = 37±1°C, 5 vol. % of CO_2 and a relative humidity of 90%). After the test, samples were cleaned in 70% ethanol ultrasonic bath for 5 minutes in order to remove the corrosion precipitates formed on the surface before measuring the final weight. Corrosion rates were calculated using the weight loss method, following the equation:

$$CR_S = 8.74 \cdot 10^{4} \frac{W}{A \cdot t \cdot \rho} \quad \text{(Eq. 4.2)}$$

CR_S is the corrosion rate (mm·year^{-1}), W is the weight loss (g), A is the exposed area (cm^2), t is exposure time (h) and ρ is the material density (g·cm^{-3}). Four specimens were tested for each condition and the average values and relative standard deviations were calculated.

4.4.4. Corrosion characterization

The surface morphology, chemical composition and phase composition of the degraded samples were examined by SEM, EDS and XRD. Further, atomic emission spectroscopy (AES) was performed (model 4200 MP-AES, Agilent Technologies) to assess the release of Fe and Mg ions. A 10% HNO_3 was used to clean glassware for the digestion procedure, to avoid any kind of contamination.

4.5. Experimental results

4.5.1. Microstructure

Fig. 4.1 displays microstructures of specimens prepared by hot rolling. Hot rolling resulted in fine-grained samples with an average grain size of 2.1 µm, 1.5 µm, and 1.1 µm respectively for PF, MX and MM samples. In addition**,** as seen in Table 4.3, the relative porosity of PF and fine particulate reinforced composites was not higher than 0.93%.

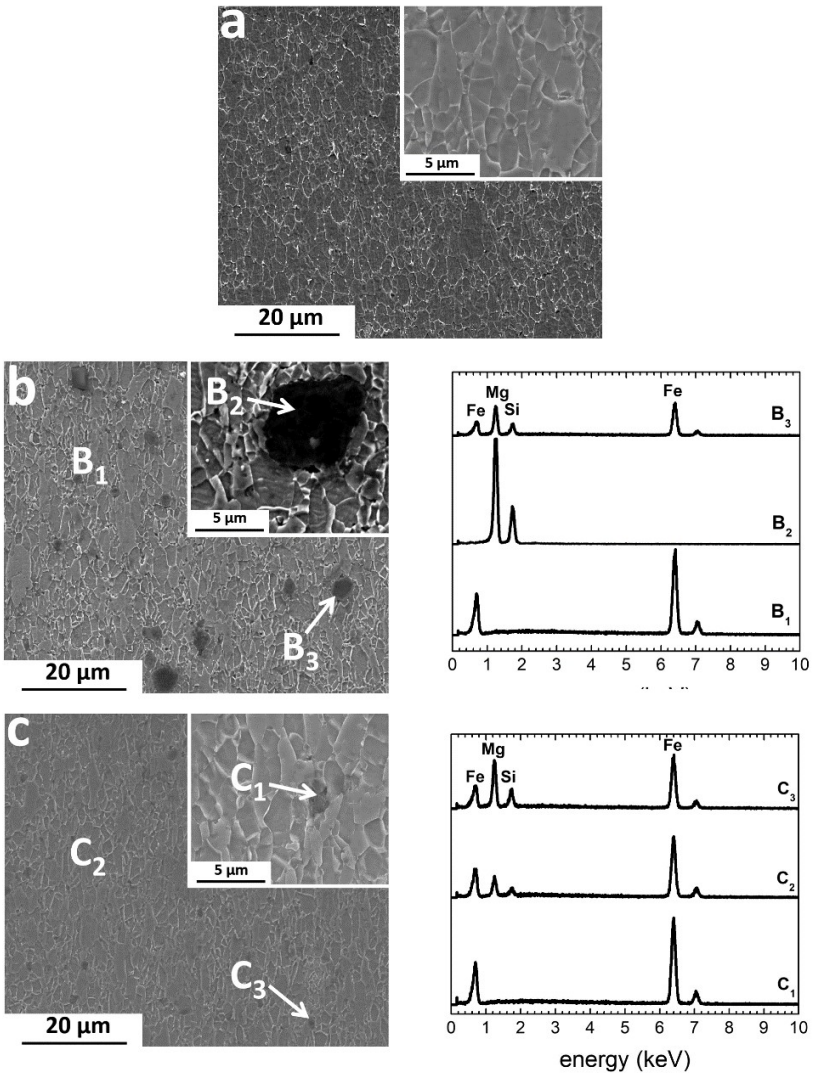

Figure 4.1. *SEM micrographs of powder metallurgy Fe, Fe/Mg_2Si composites and corresponding EDS spectra a) PF, b) MX, c) MM*

The distribution of reinforcement varies with powder processing methods. In case of MM samples, Mg_2Si particles were considerably refined and homogenously spread within the Fe matrix. As expected, this behavior was not seen in the sample prepared by conventional mixing. The size distribution of Mg_2Si was calculated using image analysis. The results showed the presence of coarse (~12% in the range of 5-10 μm) and small (~50% in the range of 1-4.9 μm and ~38% in the range 0.3-0.99 μm) Mg_2Si particles for MX samples. In contrast, high energy ball milling resulted in significantly decreased reinforcement size down to the sub-micrometer regime (Fig. 4.1c). For MM samples, ~83% of reinforcement particles were in a range of 0.1-0.99 μm) and 17% particles exhibited size between 1-3 μm).

Table 4.3. *Density and porosity of the investigated specimens*

Sample denotation	Hot rolled specimens	
	Density ($g \cdot cm^{-3}$)	Porosity (%)
PF	7.78±0.01	0.79±0.09
MX	7.40±0.04	0.93±0.03
MM	7.48±0.09	0.85±0.12

XRD patterns (Fig. 4.2) confirmed the existence of α-Fe (JCPDS #06-0696).

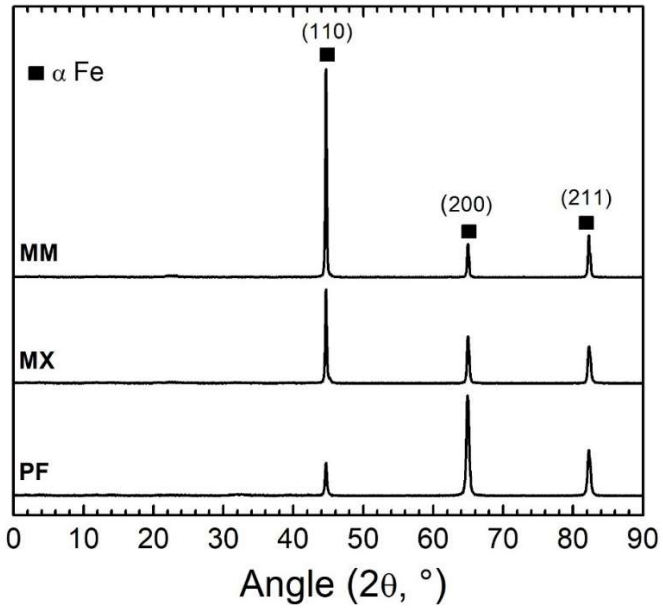

Figure 4.2. *X-ray diffraction patterns of Fe and Fe/Mg_2Si composites*

For PF, the most intense peak belonged to (200) reflection. With the addition of Mg_2Si particles, the intensity of the (200) peak decreased, while that of (110) increased. Magnesium silicide was not detected by XRD because of the low amount of the added powder (1 wt. %), which is below the detection limit.

4.5.2. Electrochemical measurements

The influence of the reinforcement in the polarization behavior for all the conditions was investigated at 37˚C in modified Hanks' solution. The respective polarization plots and their kinetic parameters are shown in Fig. 4.3. and Table 4.4. After Mg_2Si particles addition, the potential (E_{corr}) became lower showing more active behavior of Fe matrix in the presence of reinforcement (respectively -0.65, -0.75 and -0.71 V for PF, MX, and MM). From the observed data, PF showed a minimum corrosion current density I_{corr} = 22.1 µA compared to MX and MM ones, respectively 35.3 and 29.4 µA. MX samples exhibited significantly higher corrosion rates compared to pure Fe.

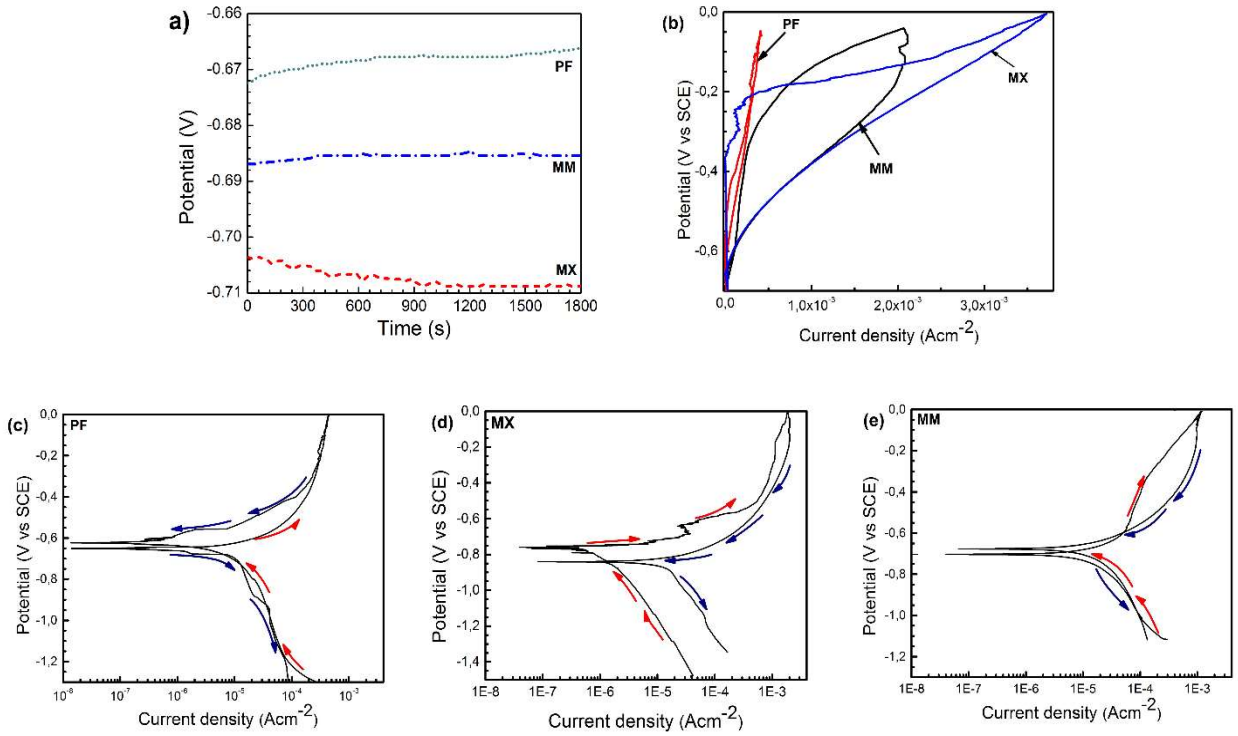

Figure 4.3. *Electrochemical measurement plots for Fe/Mg_2Si composites compared to pure Fe a) OCP, b) hysteresis loop, and cyclic polarization curves for c) PF, d) MX, and e) MM samples*

A typical hysteresis loop is seen on the polarization curve, indicating the presence of a corrosion mechanism mainly due to pitting triggering and development. The area under the loop indicates the amount of localized corrosion incurred by the material. The smallest hysteresis loop area for PF (the forward and reverse scans almost overlap – Fig. 4.3b, c) implied that the surface of the area affected by pitting was lower compared to that one in Fe/Mg_2Si composites. As seen in Fig. 4.3b, the addition of Mg_2Si increased the loop area, suggesting that the pitting corrosion preferentially occurs near Mg_2Si particle.

***Table 4.4**. Summary of corrosion data obtained from the electrochemical measurements for Fe and Fe/Mg_2Si composites*

Sample denotation	E_{corr} (V)	i_{corr} (µA/cm^2)	CR_p (mm year^{-1})
PF	-0.65 ± 0.01	22.1 ± 0.8	0.26 ± 0.01
MX	-0.75 ± 0.04	35.3 ± 1.4	0.41 ± 0.04
MM	-0.71 ± 0.08	29.4 ± 0.4	0.35 ± 0.02

Fig. 4.4 describes the electrochemical behavior of Fe and Mg_2Si, which were coupled together for 240 h. Fig. 4.4c and 4.4d show respectively the coupled current and coupled potential variation for the Fe/Mg_2Si system during the considered period. Potentiodynamic tests on pure Fe and pure Mg_2Si samples were carried out before (fig. 4.4a) and after (fig. 4.4b) the galvanic coupling test. SEM micrographs of Mg_2Si and of pure Fe after 240 days of coupling in modified Hanks' solution are shown in fig. 4.4e and 4.4f, respectively.

Initially, corrosion potential of bulk Mg_2Si was lower (- 1.09 V) compared to the one of pure Fe (- 0.65 V), as shown in Fig. 4.4a. Meanwhile, the corrosion current of Mg_2Si is much greater than the Fe one, 48 µA vs 22.1 µA, respectively. These results indicate that Mg_2Si particles were more susceptible to corrosion than Fe matrix at the beginning of the corrosion process. Potentiodynamic curves of Fe and Mg_2Si after coupling test are shown in Fig. 4.4b. E_{corr} of Mg_2Si moved towards a positive direction to about −0.63 V from the initial value of about −1.09 V, resulting in a remarkable potential increase. E_{corr} of Fe did not show significant changes after 240 h, it decreased slightly down to ~-0.72 V. The potential of Mg_2Si electrode increased because of the preferential dissolution of Mg and the enrichment of Si. EDS analyse of Mg_2Si phase after the coupling test showed that the amount of Mg content decreased considerably (Fig. 4.4e).

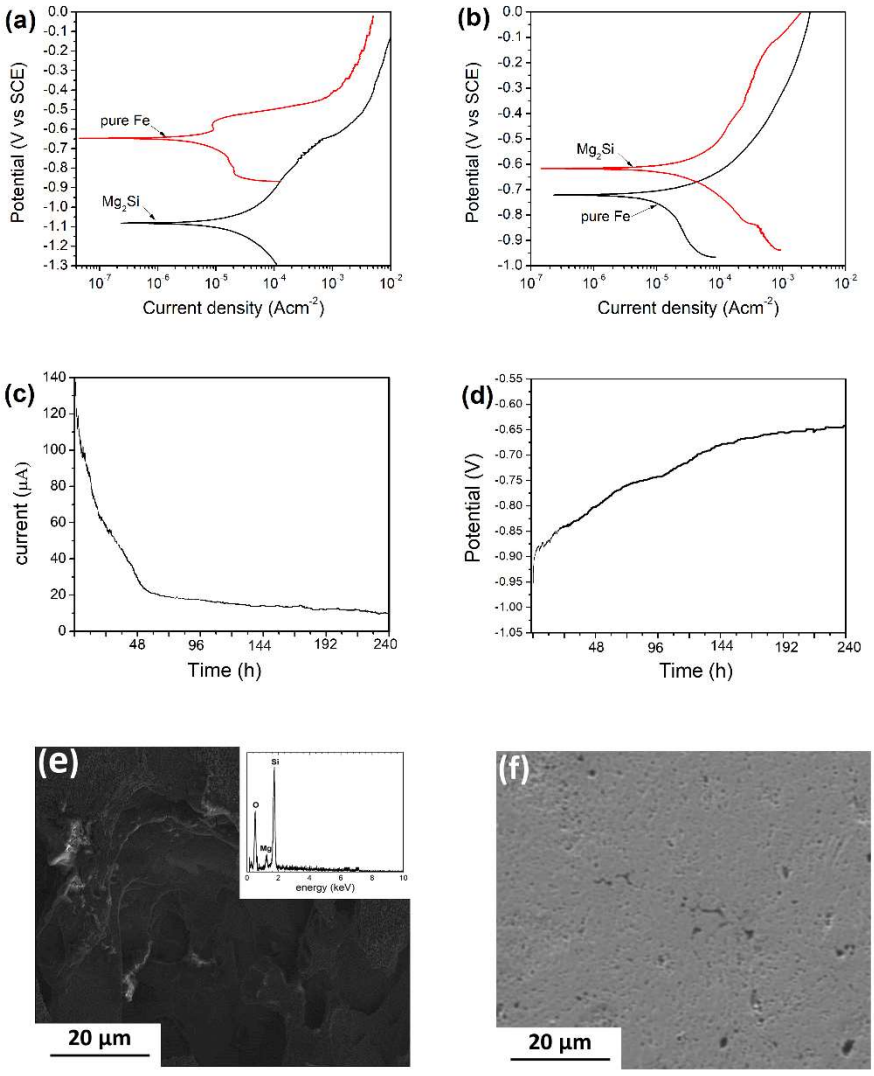

Figure 4.4. *Potentiodynamic scanning curves for individual Fe and Mg_2Si in modified Hanks' solution a) at the beginning and b) after coupling for 240 h, c) evolution over the time of galvanic current density and d) mixed potential resulting from the galvanic coupling between Mg_2Si and pure Fe, f) morphology of Mg_2Si and e) pure Fe after 240 hours of galvanic coupling test*

At the beginning of the coupling process, the potential of Mg_2Si electrode was lower than that of Fe electrode, it acted as an anode subjected to a relatively high anodic current. The potential of Mg_2Si electrode increased, resulting in a potential switch of Fe. Fig. 4.4c shows the coupling current of the Mg_2Si - Fe system. It is clearly seen that at the initial stages of the test Mg_2Si was subjected to an anodic current in the coupling system of around 140 µA. The potential of Mg_2Si became more positive with ongoing experiment, and the current dropped after 48h reaching a value

of ~ 20 μA. Afterwards, it decreased slower until the end of the experience (until a stable final current of ~10 μA was reached). The preferential dissolution of Mg in Mg_2Si was also found in Mg_2Si containing Al-based alloys and it was described in details elsewhere [193,198].

4.5.3. Static immersion tests

Fig. 4.5 displays SEM surface morphologies of PF and its composites after static test for an immersion time of 24 hours. PF exhibited uniform corrosion and there was no noticeable localized corrosion. However, higher magnification images highlighted that PF samples experienced more pronounce grain boundary corrosion compared to the other investigated materials (Fig. 4.5a, inset). In fact, localized corrosion could be seen on the surfaces of MX and MM samples. Many isolated pits were formed on the MX and MM surfaces. The composite materials experienced differences in pit formation compared to PF due to the addition of Mg_2Si. The average pit depth for MX samples was much higher compared to MM condition (4.82±0.72 μm vs 2.7±0.41μm). Mg_2Si particles partially dissolved forming shallow craters. The MM samples revealed a more homogenous corrosion. In addition, the number of pits per surface area was higher in case of MM samples. There are always many pits with small orifices on the surface of MM samples, while for MX samples several pits with larger orifices were observed (Fig. 4.5b, inset). Micro-galvanic effects might be associated with the size and distribution of local anodes (Mg_2Si) and cathodes (Fe matrix).

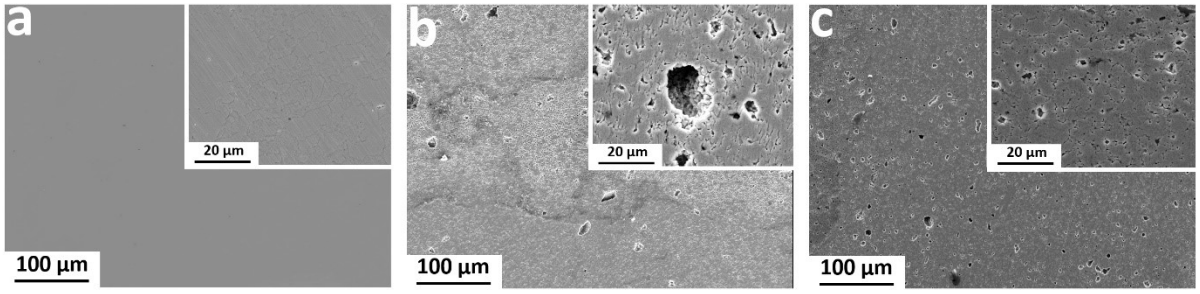

Figure 4.5. *SEM images of sample surface morphology after 24 hours of static immersion test in modified Hanks' solution a) PF b) MX, c) MM samples*

Subsequent effect Mg_2Si addition on the corrosion susceptibility of Fe could be better assessed after 240 hours of static immersion test (Fig. 4.6). The surface of PF samples was covered by numerous flower-like islands, about 100 μm in size. EDS analyses confirmed the presence of

P, Fe, and O (as seen in Fig 4.6a-a'). Cross sections of PF corroded samples revealed the existence of shallow pits (Fig. 4.6').

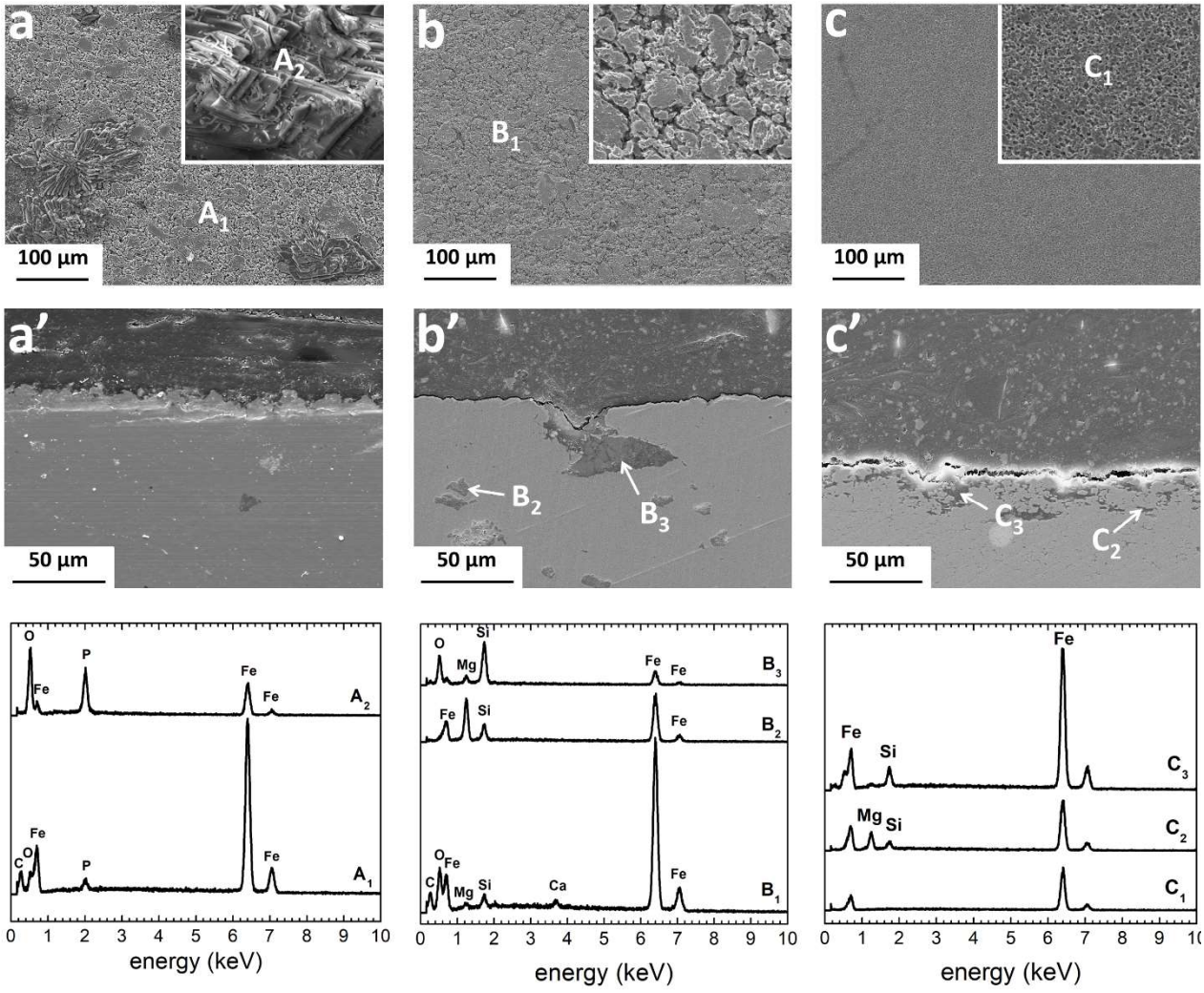

Figure 4.6. *Degraded surfaces after 240 h of immersion test a) PF, b) MX, c) MM samples, and corresponding cross sections (a_2-c_2) with EDS analyses of specified points*

The addition of Mg_2Si noticeably altered MX and MM corrosion pattern. The corroded morphology of MX samples after 240h of static immersion test was non-homogenous accompanied by the formation of deep pits between metal matrix and reinforcement (Fig. 4.6b-b'). EDS analyses confirmed the presence of silicon and oxygen in the pits, suggesting the dealloying of reinforcement and a possible formation of SiO_2. The size and distribution of reinforcement particles in the composite matrix are one of the most important microstructural features affecting corrosion properties. Generally, the micro-galvanic corrosion between Fe matrix

and Mg_2Si led to a more aggressive dissolution of the composite surface compared to PF. More uniform distribution of submicron in size Mg_2Si particles resulted in homogenous corrosion mode and the formation of shallow pits in case of MM samples (as seen in Fig. 4.6c'). With progressing immersion time, the pits grew and became interconnected, evolving into the uniformly degraded surface as it is evident after SEM observation (Fig. 4.5c and Fig. 4.6c).

XRD patterns obtained after 240 hours of immersion test (Fig. 4.7) showed the diffraction lines of α-Fe and $FeCO_3$ (siderite*, JCPDS #29-0696) for* MX and MM samples. XRD analysis of corroded PF samples revealed only α-Fe peaks. Despite the presence of corrosion precipitates, as demonstrated by SEM-EDS analyses, no peaks related to phosphate-based corrosion products were observed, suggesting that these precipitates might be nanocrystalline or amorphous [77].

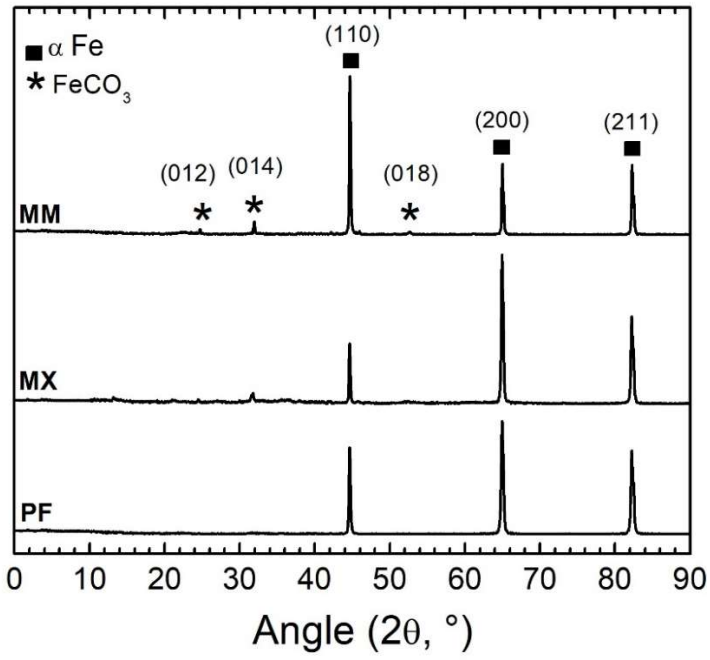

Figure 4.7*. XRD patterns on the corroded surfaces after 240 hours of immersion in modified Hanks' solution for Fe and Fe/Mg_2Si composites*

AES analysis of exhausted solutions after immersion of Fe and its composites showed that Mg concentration was higher compared to Fe. It is important to notice that a low amount of Mg ions, that is ~14 mg/L is present in a modified Hanks' solution (as listed in Table 4.5). AES results confirm explicitly the selective leaching of Mg ions from Mg_2Si particles. Further, according to

Mg Pourbaix diagram, $Mg(OH)_2$ does not precipitate in solutions exhibiting pH values lower than 10, thus dissolved divalent Mg^{2+} ions do not precipitate as stable Mg hydroxide [183].

Table 4.5. *Corrosion rates and ion release calculated on the base of 24 and 240 hours static immersion tests for pure Fe and Fe/Mg_2Si composites*

Material	Corrosion rate (mm·year^{-1})		Ion release (mg/L) *		
	1 day	10 days	Ion	1 day	10 days
PF	0.11±0.02	0.19±0.01	Fe	0.09±0.05	0.20±0.06
			Mg	13.75±0.21	13.92±0.12
MX	0.17±0.08	0.31±0.04	Fe	0.24±0.08	0.48±0.08
			Mg	16.51±0.90	20.44±0.42
MM	0.12±0.04	0.27±0.01	Fe	0.21±0.04	0.44±0.05
			Mg	15.91±0.54	19.51±0.55

*pure modified Hanks' solution contains 14 mg/L of Mg^{2+} ion (as seen in Table 4.2)

The addition of Mg_2Si reinforcement induced a rapid increase in the ion release for periods considered in this study and corrosion rates of composites were always higher compared to PF samples.

4.6. Discussion

The high reactivity of Mg leads to dealloying of Mg_2Si reinforcement accompanied with the enrichment of Si. The size of Mg_2Si reinforcement is very small (~0.1-10μm), thus it is not possible to isolate the Mg_2Si particles from Fe matrix and accurately determine their electrochemical features (such as galvanic current). Mg_2Si bulk material and pure Fe prepared by PM were used to measure the galvanic current between matrix and reinforcement. The results of the galvanic coupling experiment show that electrochemical characteristics of Mg_2Si phase considerably change with progressing corrosion time (Fig. 4.4). The study reveals that Mg_2Si dissolves readily in near neutral pH (~7.4) in modified Hanks' solution. These findings agree with those reported by Li at al. [199]. At the initial stage, the anodic activity of Mg_2Si phase is very high. The main anodic reaction occurring on Mg_2Si is a dissolution of Mg:

$$Mg \rightarrow Mg^{2+} + 2e \qquad \text{(Eq. 4.3)}$$

The oxygen reduction (cathodic reaction) at the matrix surface might occur at the same time with the local pH increase promoting surface passivation:

$$O_2 + 2H_2O + 4e \rightarrow 4OH^- \qquad \text{(Eq. 4.4)}$$

The active dissolution of Mg leads to the enrichment of Si, which has been demonstrated by EDS analyses (Fig. 4.4e, Fig. 4.8):

$$Mg_2Si + 2H_2O \rightarrow Mg^{2+} + SiO_2 + 4H^+ + 8e \qquad \text{(Eq. 4.5)}$$

Concurrently, the pitting corrosion of the matrix in the formed crevices can be accelerated once the Mg_2Si reinforcement is dissolved because of increasing pH on the sample surface. A mechanism related to the composite dissolution in physiological medium might be presented as follows [77]: (i) corrosion attack confined to Mg_2Si particles which had begun the process of dealloying, (ii) corrosion of Fe matrix at the matrix-reinforcement interface, (iii) Fe matrix dissolution by uniform corrosion and interconnection of pits, as it is depicted in Fig. 4.8.

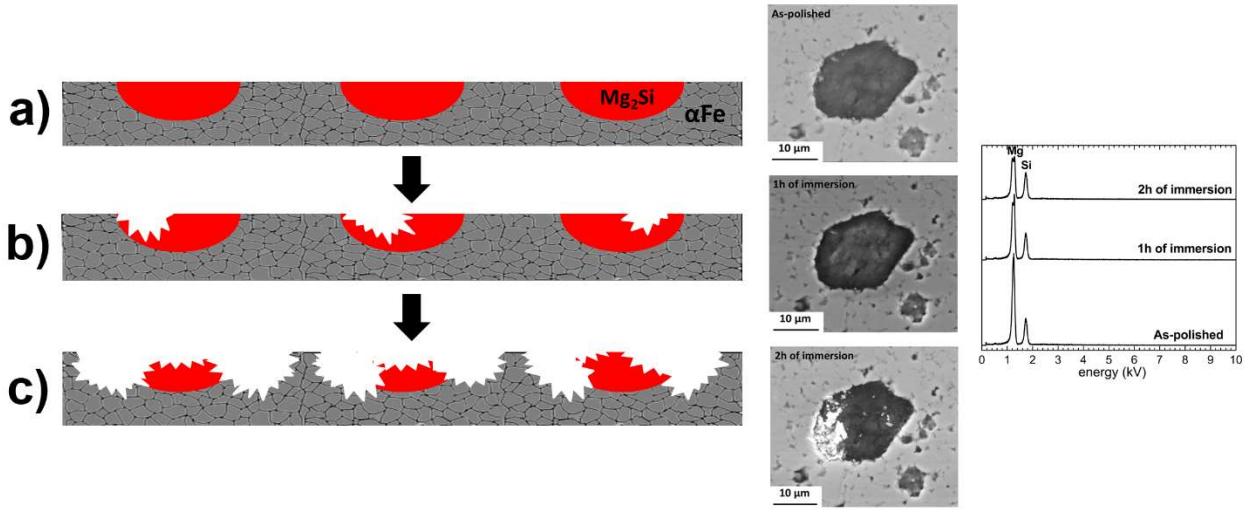

Figure 4.8. *Schematic of Mg_2Si phase dealloying within an iron matrix due to anodic polarization of the particle resulting in preferential loss of Mg: a) Mg_2Si particles embedded into Fe matrix; b) corrosion initiation on the Mg_2Si surface at the beginning of the corrosion process; c) subsequent corrosion of Fe matrix around the corroded Mg_2Si particles; and corrosion morphologies of MX sample i) freshly polished, and after immersion in modified Hanks' solution for ii) 1h, iii) 2h with corresponding EDS spectra*

At initial stages of corrosion (such as 1h or 2h of immersion, Fig. 4.8), there is an evidence of etching encircling Mg_2Si particle. It is clear from SEM observations, that the corrosion has initiated on the Mg_2Si/Fe interface, indicating greater electrochemical activity of this part of the particle. After 2 h of immersion, the localized attack appears around the reinforcement particle.

With the ongoing selective depletion of Mg from Mg_2Si, the anodic activity of this phase considerably decreases and its E_{corr} increases (Fig. 4.4d). Mg_2Si changes into electrochemically inert SiO_2 while being immersed in modified Hanks' solution as it is evidence by EDS studies (Fig.4.4e). The presented mechanism is consistent with the obtained results and with the localized corrosion mechanisms for metallic materials in a Cl^-containing solution previously reported in the literature [6,93,113].

In the nearly neutral physiological environment, the corrosion reactions for pure Fe involve the anodic dissolution and the cathodic reaction which is oxygen reduction (Eq. 4.4). The interaction between local cathodes, anodes, and the matrix leads to several forms of corrosion in Fe-based BMs including pitting corrosion or intergranular attack [78,128].

From corrosion point of view, the key features of the microstructure of Fe-based BMs are the grain structure and the distribution of second phases including impurity or reinforcement particles and precipitates [200,201]. For example, corrosion attack is observed around Mg_2Si particles having electrochemical characteristics that differ from the behavior of the surrounding Fe-based matrix, which is the cause of localized forms of corrosion. Therefore, the corrosion products found on the composites' surfaces vary significantly compared to those on pure Fe. $FeCO_3$ forms on the surfaces of MX and MM composites due to increasing concentration of hydroxides coming from the dissolution of finely distributed reinforcement (as shown in Fig. 4.7). The local pH near to the surface raises followed by the formation of the iron carbonate layer [77]. It was already found that pH is a dominant factor controlling the $FeCO_3$ saturation state [202,203]. In contrast, on the corroded surfaces of PF samples, number of phosphate-based crystals is observed (Fig 4.5a). These precipitates are not present on the surfaces of MX or MM composites. It could be concluded that Mg_2Si presence impedes the formation of phosphate-based nuclei. A possible explanation is that the initial P deposition stage is hindered by the galvanic coupling between Mg_2Si and Fe phases, followed by pH rise, which is in favor for $FeCO_3$ formation. Inhomogeneity of the substrate as well the presence of Si remarkably alters phosphor-based compounds deposition [204,205].
A shift of the corrosion regime from localized to a more uniform is observed in case of the MM samples, mainly due to reinforcement refinement. Further, MM reveals the smallest grain size among the three investigated materials. It was reported that materials with smaller grain size have a higher density of nucleation sites for protective film, which led to a higher fraction of corrosion

deposit, and to a lower passive current density [85,206]. Accordingly, MM samples reveal a lower mass loss compared to MX as seen in Table 4.4.

4.7. Conclusions

Powder metallurgy Fe and Fe/Mg_2Si composites, aimed for use as metallic degradable biomaterial with accelerated corrosion rate and homogenous degradation mode were successfully prepared by mixing or mechanical milling of powders followed by hot rolling. The initial *in vitro* corrosion behavior of these materials was investigated by 24 and 240 h static immersion tests and electrochemical measurements. Based on the obtained results, the main conclusions are listed as follows:

- As the Mg_2Si is coupled with Fe in modified Hanks' solution, its potential increases until a potential shift occurs between the electrodes. This corrosion mechanism is caused by preferential anodic dissolution of Mg in Mg_2Si particle.
- The addition of 1 wt. % of Mg_2Si particles successfully increased corrosion of pure Fe. The lowest corrosion rate was recorded for PF (0.19±0.01 mm·year^{-1}), while the highest one was obtained for MX samples (0.31±0.04 mm·year^{-1}).
- A rapid increase in Fe ion release for periods considered in this study was induced after the addition of Mg_2Si reinforcement (i.e. PF = 0.20 mg/L vs MX = 0.48 mg/L after 240 hours of immersion test).
- The size and distribution of Mg_2Si reinforcement are one of the most important microstructural features altering corrosion properties. A shift of a corrosion regime from localized to a more uniform was observed in case of the mechanically milled composite, mainly due to reinforcement refinement and its uniform distribution.
- The ability to tune corrosion behavior of the composites as a function of reinforcement properties and manufacturing method was experimentally verified and the microstructure-corrosion properties relationship was highlighted.

4.8. Acknowledgements

MSJ was awarded a doctoral scholarship from the Italian Ministry of Education, Universities and Research (Ministero dell'Istruzione, dell'Università e della Ricerca, MIUR). The research involved in this work was partially supported by the Natural Science and Engineering Research Council (NSERC) of Canada. MSJ, CP, DM and MV were recipients of Linkage Grant from Quebec/Italy sub-commission of Quebec. The authors would like to acknowledge V. Dodier, N. Moisan, J. Frenette from the Dept of Min-Met-Materials Eng at Laval University for a kind help and guidance during experimental activities.

5. Long-term *in vitro* degradation behaviour of Fe and Fe/Mg_2Si composites for biodegradable implant applications

****

This paper reports on the results of long-term static immersion tests of Fe and Fe-Mg_2Si composites prepared by different powder metallurgy techniques. Predicting degradation behavior of biodegradable metals is crucial for the clinical success of these medical devices. Thus far, this is the only research work that systematically investigates their long-term in vitro corrosion behavior and explores their corrosion mechanism.

****

Long-term *in vitro* degradation behaviour of Fe and Fe/Mg_2Si composites for biodegradable implant applications

M. Sikora-Jasinska[1,2], P Chevallier[2], S Turgeon[2], C Paternoster[2], E Mostaed[1], M Vedani[1], D Mantovani[1]

[1] *Department of Mechanical Engineering, Politecnico di Milano, Milan, Italy.*

[2] *Lab. for Biomaterials & Bioengineering (CRC-I), Dept. Min-Met-Materials Engineering & Research Center CHU de Québec, Laval University, Québec City, Canada.*

This chapter was accepted with minor revision,

Journal: *RSC Advances*

5.1. Résumé

L'inconvénient majeur des matériaux à base de Fe pour les applications d'implants biodégradables est un taux de dégradation lent. L'ajout de particules de deuxième phase dans la matrice de Fe peut augmenter le taux de dégradation au début du processus de corrosion. Cependant, jusqu'à présent, il n'existe pas de données quantitatives sur la dégradation in vitro ni de preuves expérimentales directes de la dissolution à long terme de composites biodégradables à base de fer.

Ici, une série de tests d'immersion à différents intervalles d'exposition (20, 50 et 100 jours) à la solution modifiée de Hanks a été réalisée à fin d'évaluer le comportement de dégradation des composites Fe/Mg_2Si et Fe pur préparés par différentes techniques de métallurgie des poudres.

Les résultats ont révélé l'importance du Mg_2Si dans la composition et la stabilité des films protecteurs formés lors des expériences de corrosion statique. Les composites Fe/Mg_2Si présentaient des taux de dégradation plus élevés que le Fe pur à toutes les étapes du test d'immersion. Les taux de dégradation à des intervalles d'exposition distincts dépendaient fortement de la composition et de la stabilité des films protecteurs d'oxyde, d'hydroxyde, de carbonate et de phosphate formés sur les surfaces dégradées. La libération d'ions Fe dans la solution aux stades ultérieurs de l'expérience était limitée en raison de l'effet de barrière dû au dépôt insoluble. Cette étude fondamentale a servi de base aux processus de formation de film protecteur dans la solution de Hanks modifiée, permettant une identification détaillée de leurs caractéristiques.

5.2. Abstract

The major disadvantage of Fe-based materials for biodegradable implant applications is a slow degradation rate. Addition of second phase particles into Fe matrix can increase the degradation rate at the beginning of the corrosion process. However, so far, there is neither quantitative data on *in vitro* degradation nor direct experimental evidence for long-term dissolution of Fe-based biodegradable composites.

Here, a series of immersion tests at different exposure intervals (20, 50 and 100 days) to modified Hanks' solution was performed to study the degradation behavior of Fe and Fe/Mg_2Si composites prepared by different powder metallurgy techniques.

The results revealed the Mg_2Si role in the composition and stability of the protective films formed during static corrosion experiments. Fe/Mg_2Si composites showed higher degradation rates compared to pure Fe at all stages of the immersion test. Degradation rates at distinct exposure intervals strongly depended on the composition and stability of formed oxide, hydroxide, carbonate and phosphate protective films on the degraded surfaces. The release of Fe ions into the solution at later stages of the experiment was limited due to the barrier effect of the insoluble deposit. This fundamental study provided a basis for the processes of protective film formation in modified Hanks' solution, enabling detailed identification of their characteristic features.

5.3. Introduction

Over the last two decades, many studies on the development of Fe-based degradable implants have been performed [77,80,94,102,207]. From a mechanical point of view, Fe and its alloys and composites are very attractive for cardiovascular stent applications, due to a good combination of high ultimate tensile strength and acceptable ductility [94]. Such implants should degrade at a proper degradation rate and disappear entirely after total repair of the surrounding tissues. Unfortunately, challenges related to the extremely slow degradation rate of currently available Fe-based materials remain unsolved [208].

Recently, researchers have focused on the increase in the degradation rate of Fe-based biodegradable metals (BMs) by modifying their chemical composition, microstructure and surface property [94]. It was proved, that the presence of phases with a difference in corrosion potential from that of the Fe matrix can increase the degradation rate by promoting micro-galvanic corrosion [209]. The amount, distribution and size of the reinforcement phase might alter the corrosion properties of Fe-based metal matrix composites (MMCs) [77].

To date, corrosion studies have been focused mainly on the calculation of the degradation rates [99,105,113,210,211]. A detailed investigation on the corrosion initiation, its progression, formation, development, and growth of corrosion products and their precise identification still remains largely unexplored. In most cases, an addition of reinforcement or alloying element could increase the degradation rate of Fe during initial stages of static immersion tests [80,113,119,126]. However, the effect of long-term exposure to the physiological solution on the degradation of Fe-based alloys remains poorly understood. More importantly, the lack of data on the formation and composition of the degradation products over time unable considerations on their biosafety. Degradation precipitates generated by the progressively dissolving metal may disturb the physiological equilibrium, thus they should be identified and evaluated. Further, it is obvious that degradation product formation generates volume increase. It can limit material application especially in terms of mechanical properties, causing corrosion induced-failure [212]. However, the effect of expanding volume of degradation products over time seems to be dismissed in the literature. The latest efforts have brought the development of several testing strategies, that predict the evolution of Fe corrosion and release [82,135,213]. A variety of parameters affect the Fe ion release and there is no agreement regarding the quantitative extent that each factor contributes. As

a result, a direct comparison between the reported in the literature degradation rates for Fe and Fe-based BMs remains impossible. Although each model might be beneficial for simulating certain mechanisms Fe dissolution, thus far, no single model has been developed, providing a comprehensive depiction of Fe release phenomena.

Previously, the corrosion initiation mechanism for Fe and Fe/Mg_2Si composites was discussed in detail [77]. Here, the research is focused on their long-term degradation behavior. A series of immersion tests at different exposure intervals (20, 50 and 100 days) was performed. This fundamental study provides a basis for the sequence of protective film formation in physiological media. Further, the influence of the Mg_2Si addition on the corrosion of Fe and corresponding mechanism of degradation is explored. Samples' surfaces after immersion at different exposure intervals were thoroughly characterized by X-ray diffraction (XRD). As shown in the previous study [77], XRD is not suitable for the detection of the phosphate-based products at shorter exposures to the corrosive environment. Consequently, Fourier transform infrared spectroscopy (FTIR) was used as a complementary characterization method, which is in contrast very sensitive to even nanocrystalline or amorphous phosphate-based degradation products. The combined use of XRD and FTIR allows identifying all the solid phases forming protective films on the top of investigated biomaterials. In this work, details about the degradation behavior at long-term exposure times to the physiological environment are highlighted adding a crucial knowledge on the degradation mechanism of degradable implant materials.

5.4. Materials and methods

5.4.1. Synthesis of composites

Fe and Fe/Mg_2Si composites were fabricated via powder metallurgy process as described in [77]. Table 5.1. summarizes the detailed description of the investigated powder conditions and the corresponding denotation of the investigated specimens.

Table 5.1. *Samples investigated in the present study and their denotation*

Sample denotation	Composition		Starting powders	Powder preparation	Sample name after X days (X=20, 50 or 100) of immersion in modified Hanks' solution		
					20	50	100
PF	Fe	100 wt.%	as received		PF20	PF50	PF100
MX	Fe	99 wt.%	as received	24h mixed	MX20	MX50	MX100
	Mg_2Si	1 wt.%	32 h mechanically milled				
MM	Fe	99 wt.%	as received	24h mechanically milled	MM20	MM50	MM100
	Mg_2Si	1 wt.%	32 h mechanically milled				

PF samples were made only of pure Fe powders (99.9% purity supplied by Alfa Aesar) and used as reference materials (Table 5.1). In case of composites, corresponding to MX and MM conditions, samples were composed by Fe and 1%wt Mg_2Si powders (99.5% purity, supplied by Sigma Aldrich). Beforehand, the as-received, coarse Mg_2Si powders were mechanically milled. For MX condition, the powders were mixed in a horizontal cylindrical mixer for 24 hours, while for MM conditions, the powders were mechanically milled in a planetary ball mill (PM 400 Retsch®), in an argon atmosphere for 24 hours with a milling speed of 240 rpm. Afterwards, powders were compacted by multi-step hot rolling to a total nominal reduction in thickness of 60%. Before each rolling step, samples were preheated to 700 °C in a resistance furnace for 20 min.

5.4.2. Metallographic examination

Samples for microstructural observation were cut, ground and polished according to the standard metallographic procedure. A FEI Quanta 250 scanning electron microscopy (SEM) with a tungsten filament equipped with an electron dispersive X-ray spectrometry (EDS) was used to investigate the microstructure and morphology of the samples and to analyze the chemical

composition of the phases with an acceleration voltage in the range of 10-30kV. In order to evaluate the reinforcement size distribution, SEM micrographs were analyzed using Microstructure Characterizer software. Feret's equivalent diameter was chosen to estimate the size of the reinforcement. Diffraction patterns of as-received and degraded sample surfaces and degradation products were obtained by X-ray diffractometry (XRD). The Siemens D5000 diffractometer with a curved graphite crystal monochromator operated with a Cu anode ($\lambda_{Cu\ K\alpha}$ = 1.54184 nm), an acceleration voltage of 40 kV and a current of 30 mA.

5.4.3. Degradation behavior

The degradation behavior of Fe and Fe/Mg_2Si composites was studied in Hanks' modified solution. The solution composition and its preparation are reported by Lévesque et al. [70]. The solution pH was adjusted to 7.4, by the addition of 1M HCl or 1M NaOH, where appropriate. Prior to corrosion tests, the samples surfaces were polished according to the standard metallographic procedure. Static immersion tests were performed to investigate the long-term degradation behavior of the Fe and Fe/Mg_2Si composites, according to ASTM G31-72 standards. 18 mm × 9 mm × 1 mm samples were immersed for 20, 50 and 100 days in 80 mL of Hanks' modified solution [70]. The containers were stored in a controlled environment (T = 37±1°C), with a CO_2 atmosphere content of 5 vol. % and a relative humidity of 90%. The solution was changed every10 days. Subsequently, the samples were washed with 70% ethanol in an ultrasonic bath for 5 minutes in order to remove the degradation products on the surface before measuring the final weight. The corrosion rates of the composites were calculated using the weight loss method according to the following equation:

$$CR = 8.74 \cdot 10^4 \frac{W}{A \cdot t \cdot \rho} \qquad \text{(Eq. 5.1)}$$

In this equation, *CR* is the corrosion rate (mm·year^{-1}), *W* is the weight loss (g), *A* is the exposed area (cm^2), *t* is exposure time (h) and ρ is the material density (g·cm^{-3}). Four specimens were tested for each condition and the average values and relative standard deviations were calculated.

Additionally, insoluble degradation precipitates gathered after ethanol ultrasound cleaning of experimental specimens were centrifuged. The degradation products were then added to a solution of 50% ethanol and 50% nanopure water and vortexed, again centrifuged, dried and characterized by SEM-EDS and FTIR and XRD.

5.4.4. Degradation characterization

The surface morphology, chemical compositions and phase composition of the degraded samples were examined by SEM, EDS, and XRD. The protective films formed on the samples were compared on the basis of their composition and average thickness. Additionally, sample surfaces were also analyzed by attenuated total reflectance Fourier transform infrared spectroscopy (ATR-FTIR, Agilent Cary 660 FTIR, Agilent Technologies, MN, USA) equipped with a deuterated L-alanine doped triglycine sulfate (DLa-TGS) detector and a Ge coated KBr beam splitter; the acquisition was performed in the wavelength range 4000–400 cm^{-1}, with a resolution of 4 cm^{-1}. Further, atomic emission spectroscopy (AES) was performed (model 4200 MP-AES, Agilent Technologies) to assess the release of Fe and Mg ions. A 10% nitric acid solution in deionized water was used to clean glassware for the digestion procedure, to avoid any kind of contamination.

5.5. Results

5.5.1. Microstructure of as-received specimens

The distribution of reinforcement varies with powder processing methods. In case of MM samples, Mg_2Si particles were considerably refined and homogenously spread within the Fe matrix. As expected, this behavior was not seen in the sample prepared by conventional mixing.

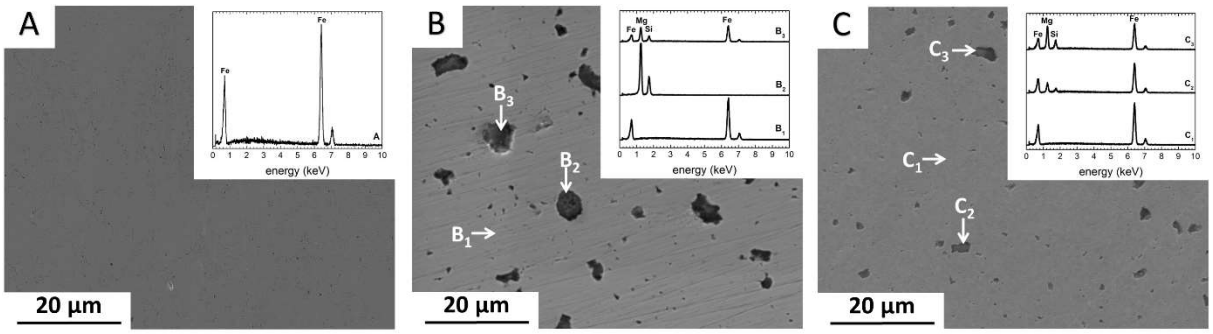

Figure 5.1. *SEM micrographs of as-polished powder metallurgy Fe, Fe/Mg2Si composites and corresponding EDS spectra a) PF, b) MX, c) MM*

The size distribution of Mg_2Si was calculated using image analysis. The results showed the presence of coarse (~12% in the range of 5-10 µm) and small (~50% in the range of 1-4.9 µm and

~38% in the range 0.3-0.99 μm) Mg_2Si particles for MX samples. In contrast, high energy ball milling resulted in significantly decreased reinforcement size down to the sub-micrometer regime (Fig. 5.1c). For MM samples, ~83% of reinforcement particles were in a range of 0.1-0.99 μm) and 17% particles exhibited size between 1-3 μm).

5.5.2. XRD and FTIR analysis of degraded samples

As the structure, chemical composition and mechanical properties of Mg_2Si are different from those of pure Fe, the addition of reinforcement to the latter had an influence on the chemical composition and morphology of degradation products. Considering the degradation products on the surface samples, those formed on PF were different from those formed on composites.
XRD patterns of as-received and degraded Fe and Fe/Mg_2Si composites are presented in Fig. 5.2.

In case of PF20, XRD analysis showed only the presence of α-Fe *(JCPDS #06-0696)*, as evidenced by the presence of (100), (200) and (211) peaks. Despite the formation of degradation products on the Fe surface, as evidenced by SEM-EDS studies (Fig. 5.4a-a"), no reflections corresponding to phosphate compounds or iron oxides, hydroxides or carbonates were found. The presence of O and P, highlighted by EDS and FTIR (Fig. 5.3a, Fig. 5.4a) analyses, was due to the formation of insoluble phosphates so that this degradation layer could be amorphous or nanocrystalline, thus not detectable by XRD.

XRD spectra for PF50 revealed the presence of siderite ($FeCO_3$-*JCPDS #29-0696)* and goethite (α-FeOOH-JCPDS #29-0713). The $FeCO_3$ peaks corresponding to (012) and (014) planes were the most intense reflections. Other low-intensity siderite peaks corresponding to (113), (133), (022), (018) and (116) planes were identified. The presence of minor intensity peaks of goethite corresponding to the (020), (130), (021), (121) and (221) was also confirmed. α-Fe (110), (200) and (211) reflections exhibited reduced intensity compared to FP20; this fact can be attributed to the thickening of the protective film on the samples' surface with increasing exposure time.

PF100 XRD pattern showed the corresponding peaks to vivianite ($Fe^{2+}_3(PO_4)_2 \cdot 8H_2O$, JCPDS #30-0662) related peaks. The most intense reflections belonged to (020), (131) and (150) planes. Other lower intensity peaks such as (110), (130) and (121) are also present. In addition, peaks of $FeCO_3$ were observed with the most intense reflections coherent with (012), (014) and (018) planes.

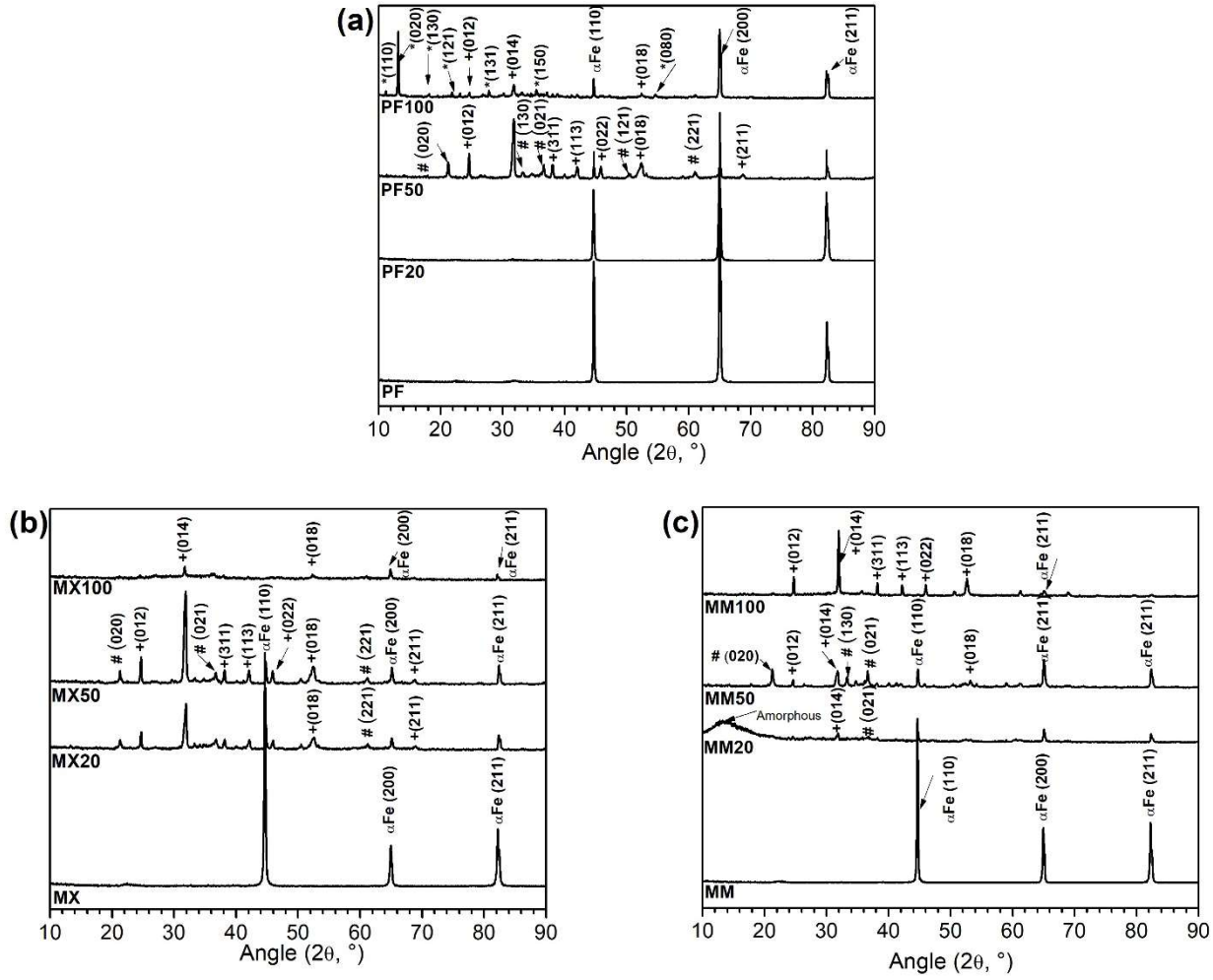

Figure 5.2. *XRD patterns of a) PF, b) MX, c) MM, in as received condition and after immersion test in modified Hanks' solution at different exposure intervals (20, 50 and 100 days, respectively). The identified phases are following:* # *α-FeOOH (JCPDS #29-0713);* + $FeCO_3$ (JCPDS #29-0696), * $Fe^{2+}{}_3(PO_4)_2{\cdot}8H_2O$ *(JCPDS #30-0662)*

MX20 and MM20 XRD patterns (Fig. 5.2b and c) showed diffraction lines of Fe(III) oxy-hydroxides and $FeCO_3$. These peaks were more numerous and diffraction lines were more intense in case of MX type samples. MM showed only one peak of siderite (021), one peak of goethite (014) and α-Fe peaks corresponding to (100), (200) and (211) planes. Additionally, a poorly crystalline pattern showing an angle reflection around 10-15° has been observed for the composite prepared by mechanical milling, which could be attributed to the degradation layer of amorphous ferrous phosphates (Fig. 5.2c) [135]. Similarly, after 50 days of an experiment, the degraded surfaces of composites consist of siderite and goethite (Fig. 5.2 b and c). The peaks of carbonate and hydroxide phases are more intense in case of Fe/Mg_2Si prepared by mixing.

The αFe peak intensity appears to decrease with increasing immersion time. It could be due to the growing protective layer formed on the surface, as it was further proved by SEM analyses (Fig. 5.5 and 5.6).

After 100 days immersion test, the diffraction pattern changed in a relevant way, suggesting the formation of a multilayered protective film on the surface of MX and MM samples. Fe(II) carbonate peaks were found also for MX100 and MM100. In case of MX samples, only iron carbonate low-intensity peaks corresponding respectively to (104) and (018) planes were observed. MM showed several high-intensity peaks of $FeCO_3$ belonging to (012), (014), (311), (113), (022), (018) planes. MX samples revealed two low-intensity peaks of α-Fe corresponding to (200) and (211) planes. For MM only one α-Fe peak was observed, coherent to (211) plane.

To determine the functional groups among different alloys after immersion testing, FTIR analysis was employed. Fig. 5.3 shows the sequential FTIR spectra of the surface of Fe and $FeMg_2Si$, which were exposed to the modified Hanks' solution at different intervals.

For pure Fe, the PO_4^{3-} band is observed at 1026 cm^{-1}, which is related to the asymmetric stretching of the ν3 group [214]. Absorption intensity of this group increases with prolonged immersion time, which may indicate an improvement of the properties of the phosphate-based compound, making this phase more stable. This result is in good agreement with XRD (Fig. 5.2a) and SEM-EDS (Fig. 5.4) investigations, where at the end of the experiment crystalline vivianite was identified. Additionally, low-intensity CO_3^{2-} absorption peaks vibration at around 1402, 875 and 825 cm^{-1} are visible. Further, the CO_3^{2-} band at 1580-1620 cm^{-1} was detected on the Fe surface only after 100 days of experiment [215].

The FTIR spectra of composites are similar, presenting the same pattern. They are dominated by a broad peak centered at around 1400 cm^{-1} and two sharp vibration peaks at around 860 and 725 cm^{-1}, [216,217]. Furthermore, the results of FTIR indicate the formation of the phosphate functional group on the surface of the investigated composites only at the final stages of the corrosion experiment. The low-intensity absorption band in the range 1040-1140 cm^{-1} was observed on their surfaces after 50 and 100 days of the experiment. Furthermore, at the final stages of the corrosion experiment, the formation of the phosphate functional group on the surface of the Fe/Mg_2Si composites was revealed by FTIR analysis. In particular, the low-intensity absorption

band in the range 1040-1140 cm^{-1} was observed on their surfaces after 50 and 100 days of the experiment. The broad peak at 3150 cm^{-1} with a shoulder at 3550 cm^{-1} can be assigned to OH^- stretching vibrations [218].

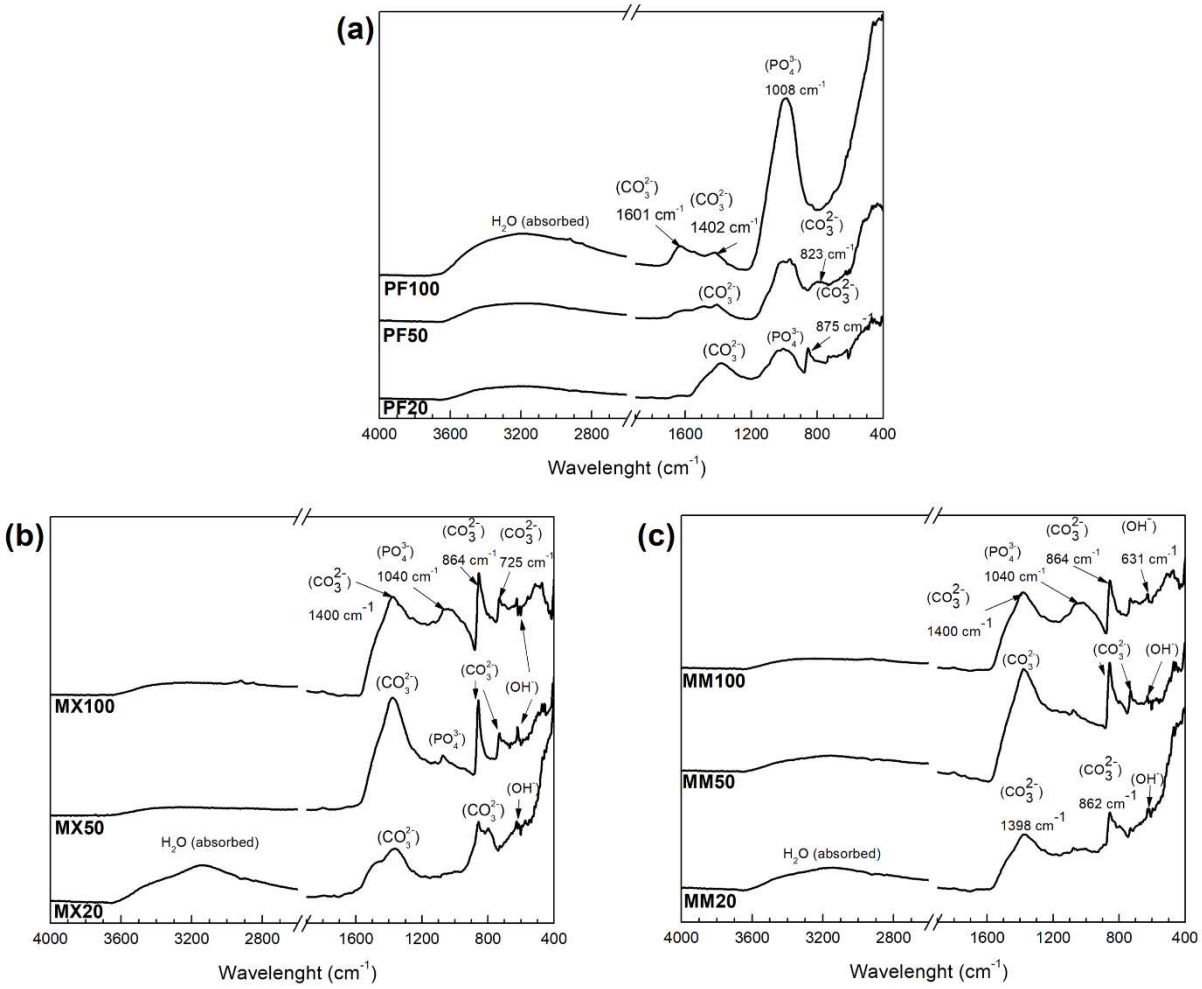

Figure 5.3. *FTIR patterns of a) PF, b) MX, c) MM samples after immersion test in modified Hanks' solution at different exposure intervals (20, 50 and 100 days, respectively)*

5.5.3. Degradation morphologies of Fe and its composites after 20, 50 and 100 days of immersion in modified Hanks' solution

Figures 5.4-6. show typical surface morphologies and corresponding cross sections for PF, and its composites (MM and MX) at 20, 50 and 100 days exposure intervals in modified Hanks' solution. For PF20, the surface was covered with amorphous products containing Fe, O, P

(Fig. 4 a). Cross section revealed uniformly degraded surface with ~15µm thick deposit on the top.

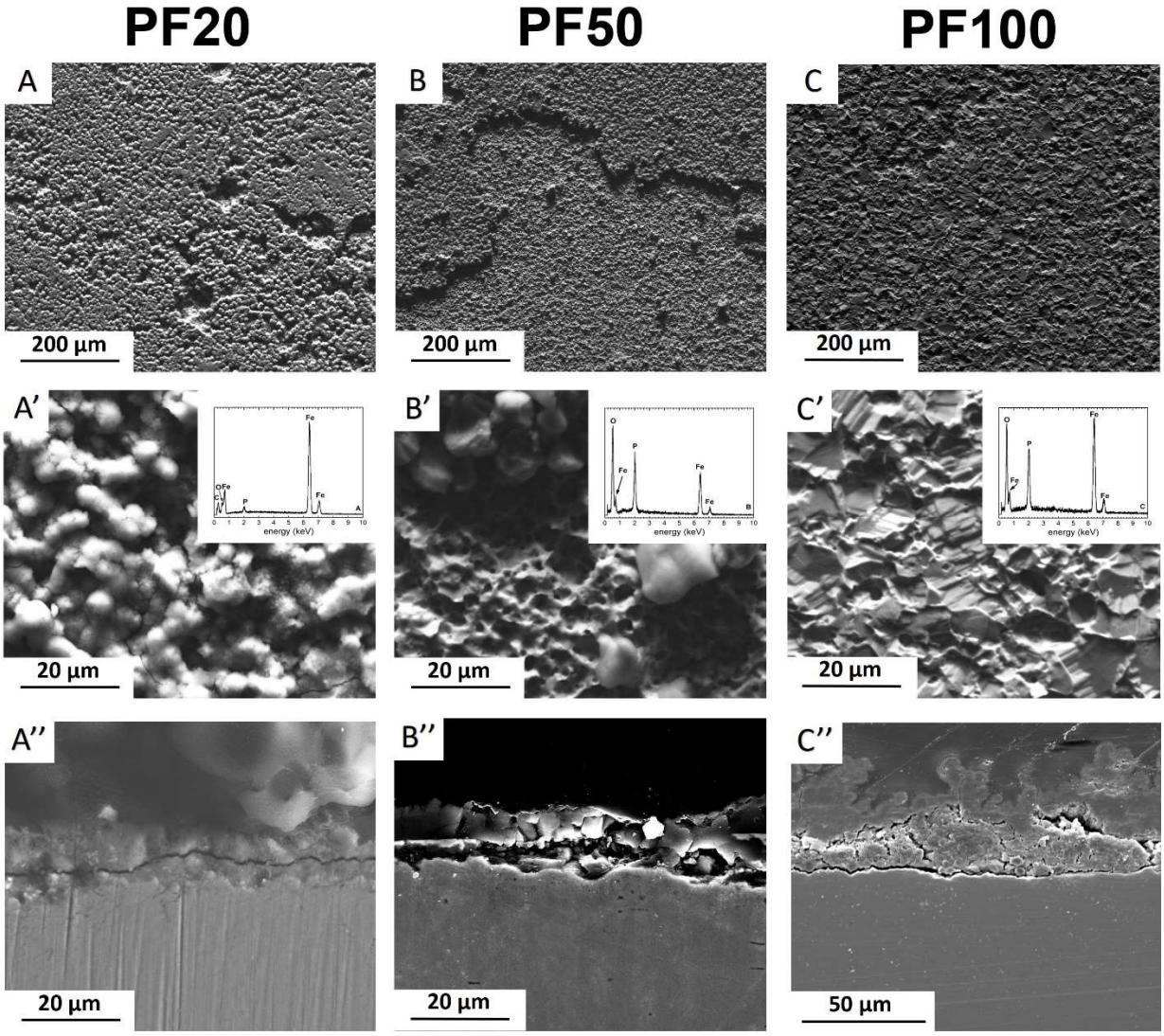

Figure 5.4. *Typical degradation morphologies of PF samples at different exposure intervals to modified Hanks' solution: (a-a') 20 days, (b-b') 50 days and (c-c') 100 days, and (a"-c") corresponding cross-sections*

As depicted in Fig. 4b, PF50 days revealed the surface covered by degradation products in the form of spherical particles adhering to the amorphous areas in the background, containing a high amount of P and O. The cross-sectional observation revealed a formation of a film with a uniform thickness of around 20 µm.

PF100 samples were covered entirely by phosphate. The cross-sectional analysis showed a characteristic double protective layer. This comprises the outer layer, mainly consisting of iron

phosphate based compound alongside the inner layer mainly made of siderite and goethite (Fig. 5.4c). The total thickness varies from around 20 µm to 60 µm where the inner core uniformly covers the substrate and no pits are observed. The thickness of the outer layer varies significantly and can rise to 40 µm, while the thickness of the inner film varies from 10 to 20 µm.

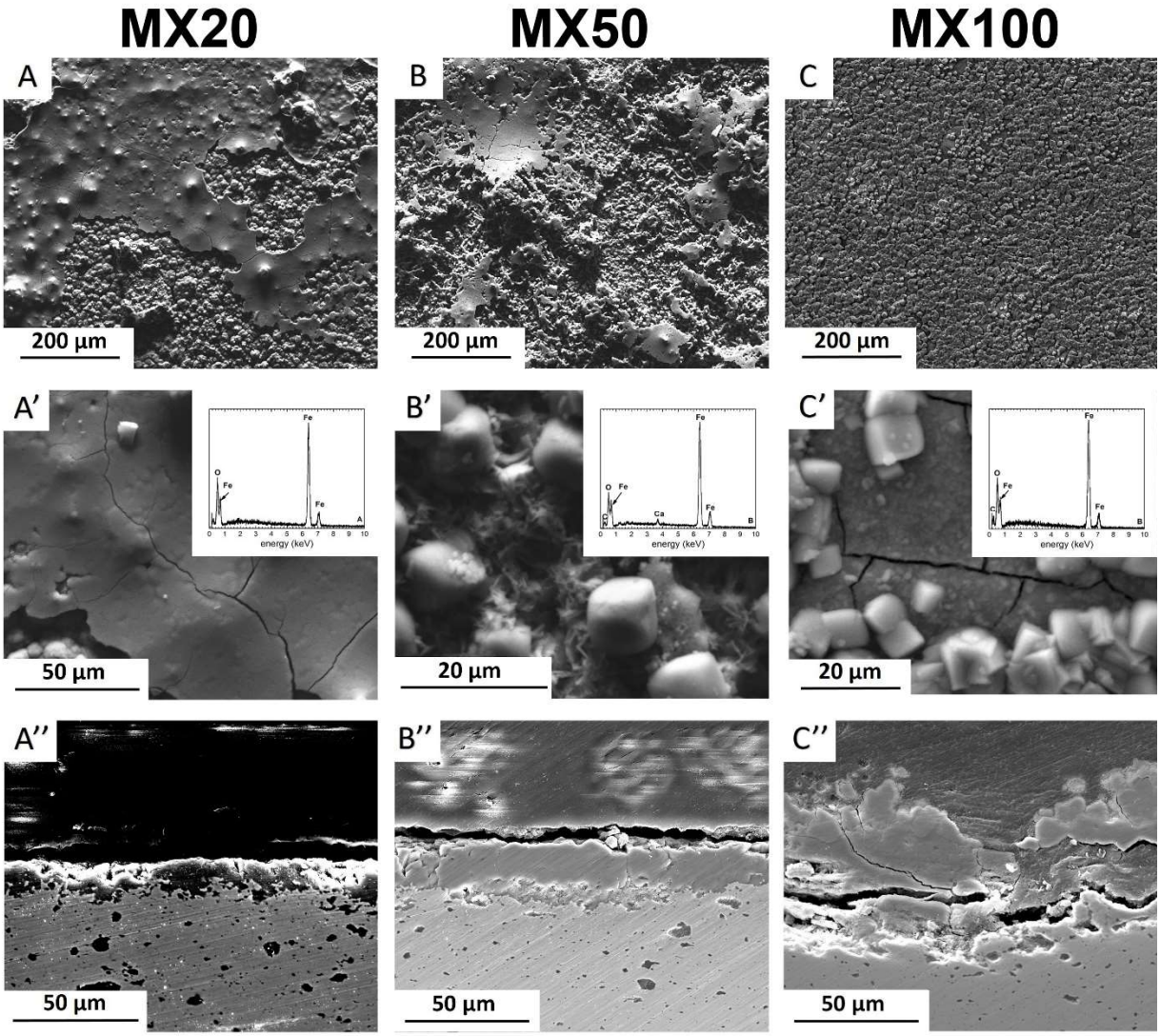

Figure 5.5. *Typical degradation morphologies of MX samples at different exposure intervals to modified Hanks' solution: (a-a') 20 days, (b-b') 50 days and (c-c') 100 days, and (a"-c") corresponding cross-sections*

MX and MM samples' surfaces (Fig. 5.5 and 5.6) showed the formation of a degradation layer with different features from PF samples. Nevertheless, both composites, prepared by mixing or mechanical milling exhibited similar surface features. The surface of MX20 (Fig. 5.5a) was

covered by a compact and shell-like structure containing Fe and O. Despite similar, Fe and O containing compounds found on the surface of MM20, their irregular and cotton balls morphology differs compared to those of composite prepared by mixing.

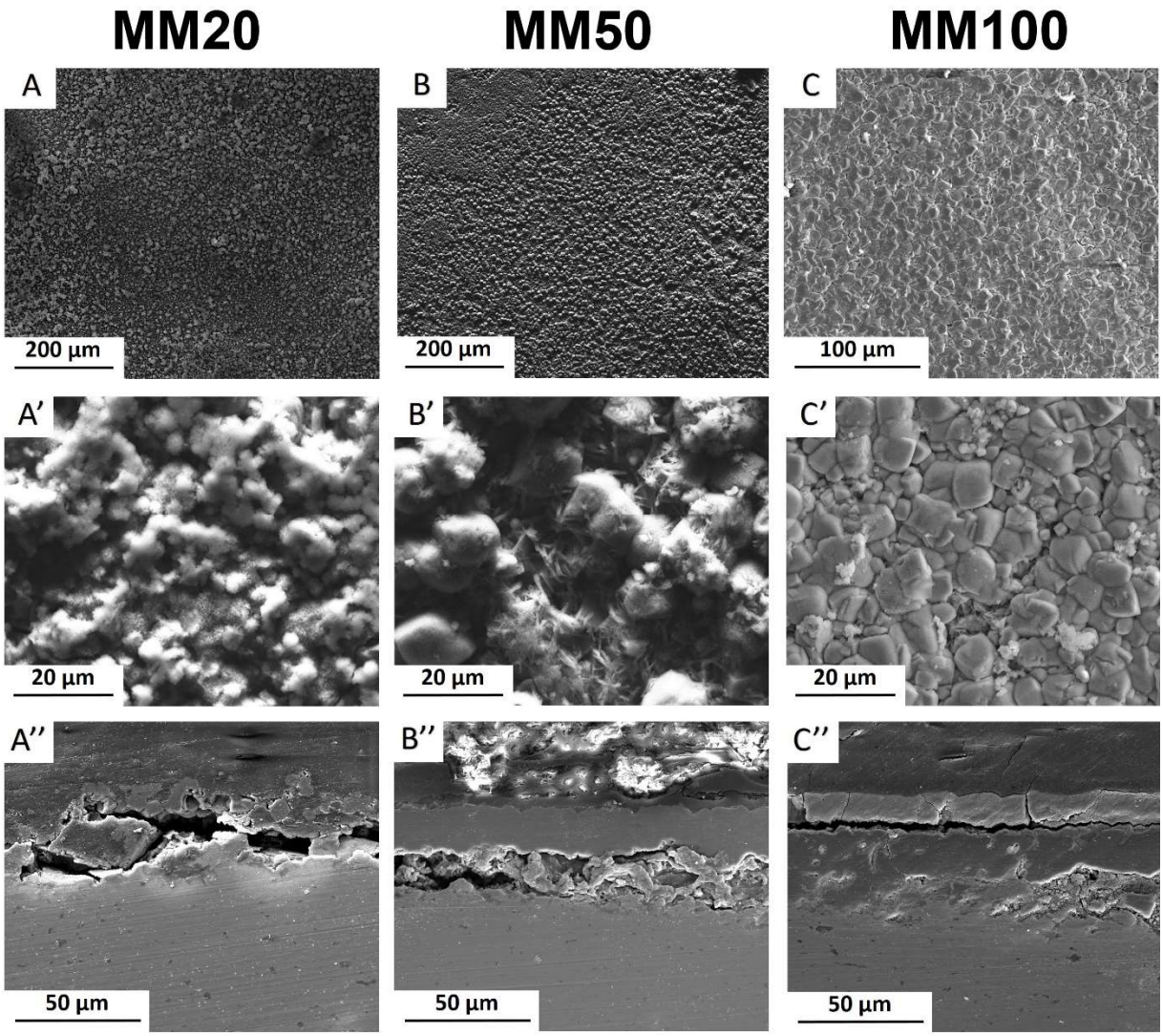

Figure 5.6. *Typical degradation morphologies of MM samples at different exposure intervals to modified Hanks' solution: (a-a') 20 days, (b-b') 50 days and (c-c') 100 days, and (a"-c") corresponding cross-sections*

50 days of experiment resulted in nearly identical surface morphologies for both composites: sharp edges crystals were distributed uniformly on the areas visible in the background. The background surface contained mainly Fe, O, and traces of Ca. After cross-sectional observations, the protective layer on composites appears more robust than that of the pure Fe. Moreover, as seen in Fig 5.5a''-c'', dissolution of the composite substrate is deeper compared to Fe with visible pits.

The protective layer thickness for all kinds of investigated specimens increased with exposure time. In case of the composites, the thickness of the deposit is greater than that measured for PF. Nevertheless, the solubility of final degradation products formed on the surface after 100 days of immersion differed significantly. PF was covered entirely by vivianite, while on the surface of Fe/Mg_2Si composites siderite was detected. The degradation of Fe-based materials can develop homogenously on the surface or can be confined to specific sites featuring a pitting corrosion. More homogenous corrosion of PF and MM results in the development of uniform protective films (as seen in Fig. 5.4a''-c'' and Fig. 5.6a''-c''). Localized corrosion of MX produces mounds of degradation products (Fig 5.5a''-c''). The higher layer thickness for MM and MX is due to the occurrence of nonuniform galvanic corrosion between coarse reinforcement particles and Fe matrix. The increase in film thickness within 20 days of immersion in case of composites is greater than that of pure Fe and may be related to the susceptibility to the localized corrosion. The thinner film on the surface of Fe was related to the passivating property of the degraded sample surface.

5.5.4. Degradation precipitates

The degradation precipitates were collected after ultrasound sample rinsing in ethanol solution. The representative morphology of the precipitates removed from the degraded MX sample after 50 days of immersion test is shown in Fig. 5.7a. The degradation products of PF and MX were essentially composed of a high amount of Fe, O, P, Ca. C and traces of Na, measured by EDS (Fig. 5.7b). This layer is in contact with the solution and is affected by its composition. As seen in XRD pattern (Fig. 5.7c) no crystalline phases associated with Fe compounds were detected. XRD showed only a presence of the broad maxima, which could be attributed to amorphous ferrous phosphate degradation layer. Fe oxide phases as lepidocrocite and goethite may be present here in addition to the other precipitates (such as phosphates and carbonates). FTIR (Fig. 5.7 d) confirmed the presence of phosphates among the degradation products.

5.5.5. Degradation rates and ion release

Degradation rates of investigated materials were initially high, especially for low immersion durations and decreased rapidly as the protective film grew and provided increasing resistance to the corrosion reaction.

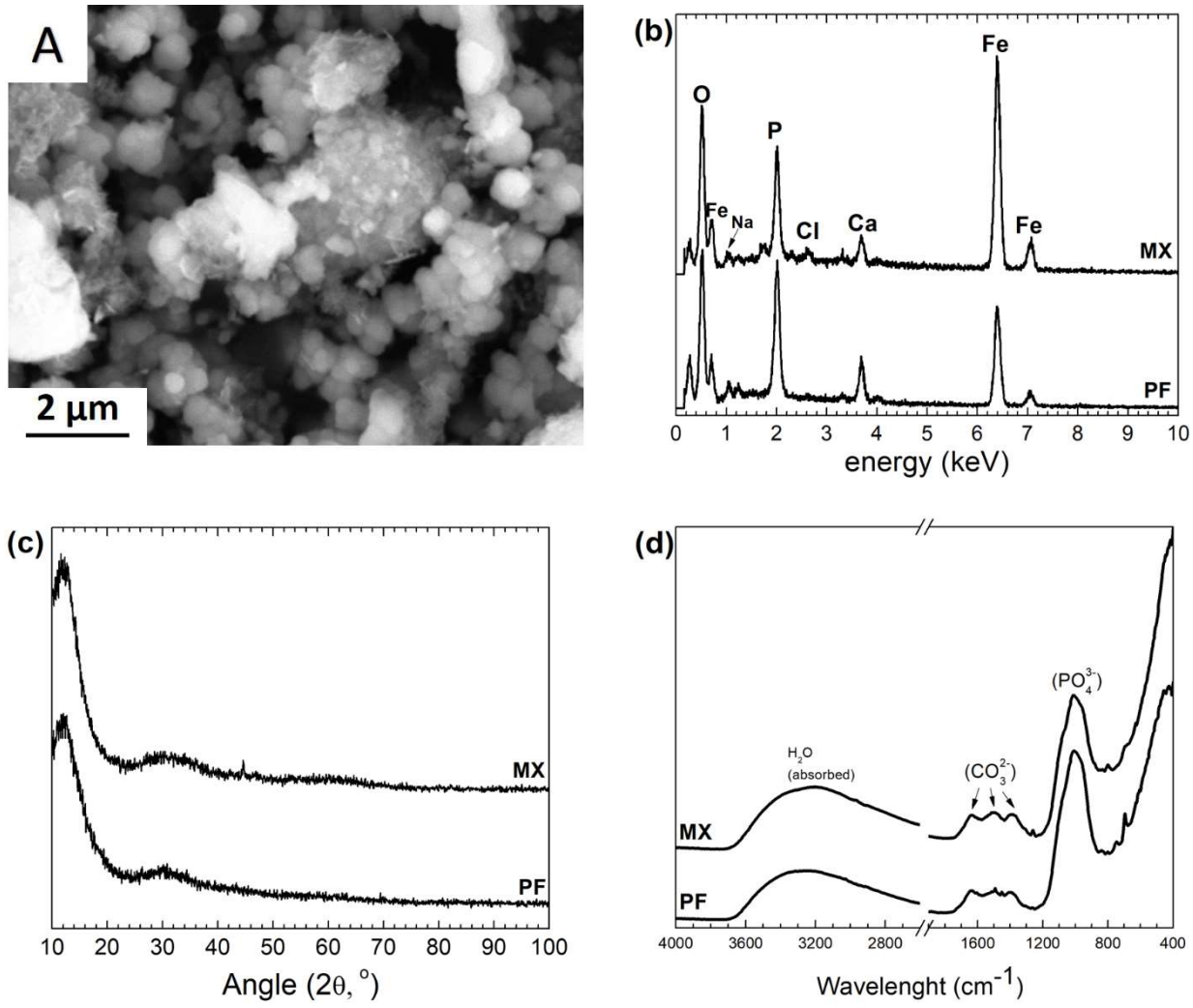

Figure 5.7. *a) representative image of degradation products after 50 days of immersion of MX sample, b) EDS, c) XRD and d) FTIR on degradation precipitates after 50 days of immersion*

AES analysis of exhausted solutions after immersion of Fe and its composites showed that Mg concentration was higher than Fe ions. It is important to notice that a low amount of Mg (~14 mg/L) is present in modified Hanks' solution. The amount of Mg ions in the exhausted solution after immersion test at longer intervals of exposure (50 and 100 days) revealed the decreasing concentration of Fe and Mg ions. Nevertheless, ion release in case of composites was always higher than that of PF. These results confirm explicitly the efficiency of Mg_2Si in the increasing degradation rate of degradable Fe biomaterials, even at long-term exposures. During

the corrosion process of metallic biomaterials in physiological solutions active and passive surfaces exist concurrently in contact with electrolyte [219].

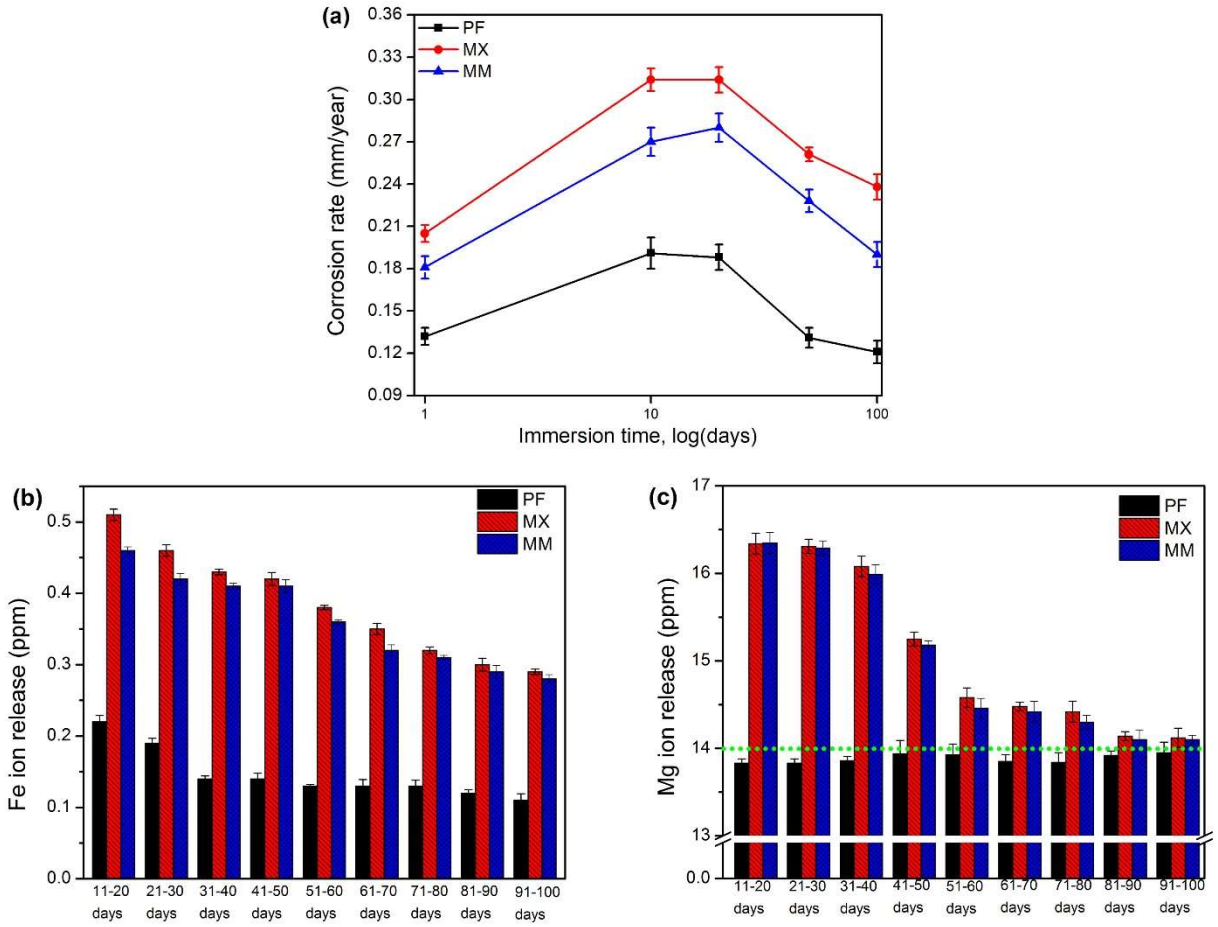

Figure 5.8. *a) Degradation rates of PF, MX, and MM after 1, 10, 20, 50 and 100 days of immersion (logarithmic scale), and ion release of b) Fe and c) Mg, after 20 to 100 days of static immersion test, *dotted line in Fig. (c) indicates the amount of Mg ions included in modified Hanks' solution ~14mg/L*

Therefore, the surface oxide/ hydroxide/ phosphate/carbonate film on the Fe and Fe/Mg_2Si continuously pursues a process of partial dissolution and reprecipitation in modified Hanks' solution. When the dissolution rate is larger than that of reprecipitation, Fe and Mg ions are gradually released. When the metallic surfaces are covered with a thick and compact film, the ion release and degradation rates show a decreasing tendency. The composition of this protective film might change even though these precipitates are macroscopically stable.

5.6. Discussion

Body fluids are aqueous solutions consisting of inorganic and organic compounds and ions. Their combined effect is a key factor affecting the degradation of Fe-based alloys and composites [134]. Hanks' modified solution is one of the most common simulated body fluids to perform *in vitro* degradation tests [77,94,135]. The corrosion pattern of Fe and Fe/Mg_2Si composites in this solution can be used to predict their *in vivo* behavior because its ionic concentration is similar to that in blood plasma [70] . The degradation of Fe is a phenomenon triggered by surface conditions and it depends on the chemical composition of the corrosive medium, pH, temperature, and solubility of metallic ions released from the substrate [135].

When Fe is immersed in a solution, it is oxidized to Fe^{2+} based on the following reaction [78]:

$$Fe \rightarrow Fe^{2+} + 2e \qquad \text{(Eq. 5.3)}$$

Some of Fe^{2+} can be transformed to Fe^{3+} because of alkaline pH and the presence of oxygen in Hanks' solution; $Fe(OH)_3$ is produced according to the following reactions:

$$^1/_2O_2 + H_2O + 2e^- \rightarrow 2OH^- \qquad \text{(Eq. 5.4)}$$

$$Fe^{2+} + 2OH^- \rightarrow Fe(OH)_2 \qquad \text{(Eq. 5.5)}$$

$$Fe^{2+} \rightarrow Fe^{3+} + e^- \qquad \text{(Eq. 5.6)}$$

$$Fe^{3+} + 3OH^- \rightarrow Fe(OH)_3 \qquad \text{(Eq. 5.7)}$$

Because of the presence of chloride ions, $Fe(OH)_3$ is hydrolyzed and goethite (α-FeOOH) is formed. According to the Pourbaix diagram with increasing pH, the local H^+ concentration at the metal-solution interface decreases, resulting in a formation of Fe oxides and hydroxides on the iron surface [136]. $Fe(OH)_2$ and $Fe(OH)_3$ are solid phases with a low solubility (respectively K_{sp} ($Fe(OH)_2$) = 8×10^{-16} , K_{sp} ($Fe(OH)_3$) = 4×10^{-38}) [137]. The stability of these compounds is limited by the presence of carbonates/bicarbonates and phosphates, chloride ions and changes in the concentration of the degradation products[138,139]. Subsequently, after immersion, apart from the contact with Cl^-, HCO_3^-, HPO_4^{2-}, Fe and Fe/Mg_2Si were also exposed to an environment rich in cations (such as Ca^{2+}, Mg^{2+}, Na^+, K^+ *etc.*), dissolved oxygen and CO_2. Therefore, in addition to the deposition of a Fe hydroxide layer, the presence of HCO_3^- , Cl^- and HPO_4^{2-} in modified Hanks' solution also promotes thermodynamically the precipitation of other phases. The corrosion

deposit is thus reconstructed into layers of oxides, hydroxides, Fe and Ca carbonates and phosphates, as illustrated in the scheme in Fig. 5.9. Chloride, carbonate and sulfate anions, present in the body fluid are responsible for the formation of intermediate phases in the iron oxidation process. $Fe_6(OH)_{12}CO_3$, $Fe_4(OH)_8Cl$ and $Fe_6(OH)_{12}SO_4$ complexes, known as green rust (GR), might be formed during Fe biodegradation [140]. GR rust forms on the substrate surface in a pH range of 7 to 9 and has a substantial contribution to the degradation of Fe based biomaterials [140]. The nature of the protective film (chemical composition and thickness) depends not only on the environmental parameters such as the buffer solution, pH, and temperature. Microstructural features (such as grain size, uniformity) and chemical composition of the substrate have a significant contribution to the corrosion susceptibility of Fe-based BMs.

The film formed on pure Fe in a slightly alkaline buffer solution containing phosphate species was reported to be composed of an inner layer of iron oxides and an outer part of iron phosphates [220]. Other researchers reported that the presence of phosphates in the solution promotes Fe passivation, resulting in the formation of phosphates in either amorphous or crystalline form [135,139,221]. It was reported by Refait at al. [221] that the amorphous deposit created on the Fe surface was made of nanoparticles revealing a similar structure to that of carbonate-based green rust. The adsorption of phosphate species on these nanoparticles hindered their growth and transformation into a fully ripened Fe carbonates. It is well accepted that phosphate species show high affinity to Fe oxides and hydroxides [137]. They can adsorb on their surfaces and then precipitate with dissolved Fe^{2+} species, therefore acting as an important precursor phase for vivianite formation. As evidenced by SEM-EDS analyses the formation of phosphate-based chaotically distributed compounds on the surface of Fe is observed at all stages of the corrosion experiment for PF samples. At the initial stages of immersion, Fe^{2+} ions react with phosphates present in Hanks' modified solution, resulting in amorphous phosphate precipitation. During the following stages of the degradation these compounds grew, forming finally protective, crystalline vivianite layer after 100 days (Fig. 5.2, Fig. 5.4c). FTIR and XRD results confirmed coexistence of crystalline vivianite and siderite on PF samples surface after 100 days of immersion test. It was suggested that siderite having a higher solubility ($K_{sp} = 5\times10^{-9}$) protects growing vivianite from being attacked by corrosion. Higher concentration of Fe^{2+} ions, coming from siderite decomposition might favor the phosphate-based species formation [222]. Further, the production of vivianite might be limited by lack of P ions in the solution and/or the amount of available Fe^{2+} ions [222].

Degradation products found on the composites' surface vary compared to PF. As shown in Fig. 5.2, $FeCO_3$ is formed on MX and MM surfaces more readily. Indeed, this could be due to increasing concentration of hydroxides coming from the dissolution of finely distributed reinforcement and thus, the local pH near to the surface raises followed by the formation of the iron carbonate layer [77]. It was already found that pH is a dominant factor controlling the saturation state for siderite [202,203]. Further, the deposition of iron carbonate can be promoted by environmental factors during an experiment. The 5% vol. CO_2 atmosphere at pH = 7.4 leads to the formation of H_2CO_3. This dissociates and forms bicarbonate and hydrogen carbonate ions, contributing to the $FeCO_3$ deposition. Additionally, modified Hanks' solution is a buffer of high capacity, which is in favor of $FeCO_3$ formation [223].

The degraded surfaces of MM50 samples are characterized by a denser and more homogeneous distribution of $FeCO_3$ crystals (Fig. 5.6a', b') compared to MX50 samples (Fig. 5.5a', b'). Finally, MM100 samples are entirely covered by a dense layer of siderite (Fig. 5.6c'). This difference can be ascribed to the initial microstructure of considered specimens. Markedly refined Mg_2Si reinforcement particles were distributed homogenously through the Fe matrix (Fig. 5.1b, c). Reinforcement particles for MM samples might be responsible for a uniform rise of the local pH near the surface and therefore the formation of more homogenous and compact $FeCO_3$ deposit. The proposed mechanism was supported by experimental investigation of corrosion initiation for Fe/Mg_2Si composites prepared by different powder metallurgy methods [77].

5.6.1. Protective film structure and formation

Stages of protective film formation involve the initiation of corrosion on the polished metallic surface. During this stage, oxidants existing in modified Hanks' solution reach a metal – solution interface and initiate corrosion process. Further, a growth of the protective deposit results in continued dissolution followed by a combination of degradation products oxidation and precipitation. With increasing thickness of the degradation layer, it becomes progressively difficult for the corrosive medium to diffuse to the metal-physiological solution interface. Different morphological features of the degradation layers start forming on the surfaces of PF, MX and MM samples at distinct stages of corrosion experiment as evidenced by SEM observations (Fig 5.4-6). The change in the ratio of the inner and outer layer, as can be seen in Fig. 5.4-6a''-b'', indicates

changes in the transport of ionic species. This depends on the composition of the substrate as well as the size and distribution of reinforcement in case of MM and MX composites. We observed that uniform corrosion results in the development of more uniform films (PF, MM in Fig. 5.4a"-c" and Fig. 5.6 a"-c", respectively), while localized corrosion can produce mounds of corrosion products (as in case of MX samples – Fig. 5.5 a"-c").

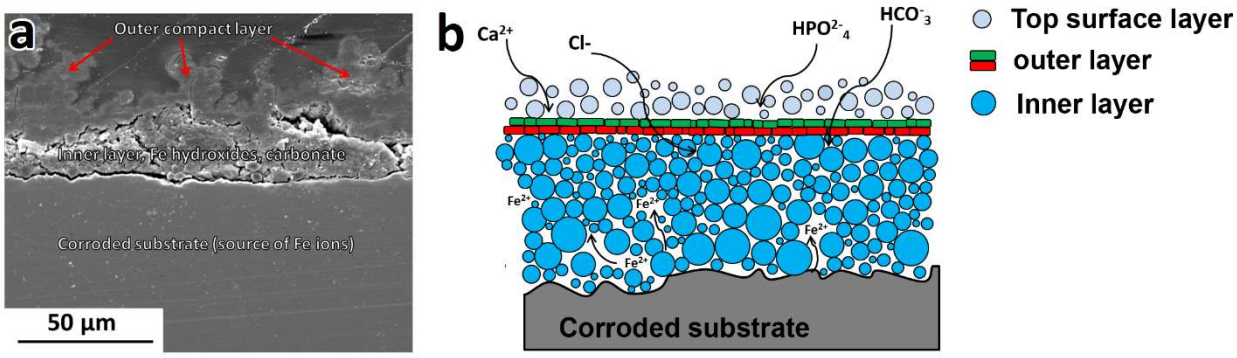

Figure 5.9. *a) SEM micrograph of PF100 cross-section showing the layered structure of protective films formed during degradation b) schematic showing characteristic features of the degradation deposit*

With increasing exposure time the reaction mechanism for carbonates/phosphates and hydroxides is significantly slower and mutual diffusion of the elements from the substrate and Hanks' modified solution is reduced Principal diffusion pathways are provided by the capillaries in the porous corrosion layers where Fe ions diffuse from the bulk material toward the solution/surface interface, whereas ions present in the body fluid diffuse in the opposite direction (as depicted in Fig. 5.9b). Thus, the degradation rates are reduced with degradation deposit thickening and its densification. For example, the compact outer phosphate-based layer (on the surface of PF100) could hinder ion diffusion and further oxidation at the metal–layer interface. Fe-based phosphates are in fact characterized by very low solubility [224].

The chemical composition, the stability, and the sequence of protective film formation on the surface depend on the microstructure and composition of the substrate as well as the fabrication method. The characteristic features of these deposits proposed based on the detailed investigations of degraded samples included: (i) degraded substrate (PF, MX or MM sample surface), (ii) inner layer, (iii) outer layer, and (iv) top surface layer as seen in Fig. 5.9.

The degraded metal surface underneath a protective film is a main source of the Fe ions. After the protective film has formed, further substrate dissolution proceeds at a slower rate, resulting in the continued growth of the degradation products film.

The inner protective film. Siderite, goethite, and lepidocrocite were identified by XRD as components of the inner layer. This region localized closer to the metal surface is expected to contain a higher amount of Fe. EDS analyses showed increased Fe and O concentration in this part of the deposit.

The outer layer covers the inner one. SEM images (Fig. 5.4-6 a''-b'') of the cross-section of PF, MX and MM show the compact layer of varying thickness (20 to 80 μm), depending on immersion time and composition of the substrate. This layer acts as a barrier between modified Hanks' solution, Fe ions and solids present inside of the inner layer.

The top surface layer consists of loosely held particles on the top of the outer layer made of Fe oxides, hydroxides in addition to the precipitates of carbonates and phosphates (as seen in Fig. 5.7).

5.7. Conclusions

In this article, the *in vitro* degradation properties of pure Fe and Fe/Mg_2Si composites prepared by different PM techniques were investigated to evaluate their potential as a biodegradable implant material. Their degradation performance was investigated via static immersion test in modified Hanks' solution at different exposure intervals up to 100 days. The degradation mechanism in physiological solution was proposed, and degradation rates (obtained from the immersion tests) were discussed. At subsequent stages of degradation, the structure and chemical composition of the formed protective layers had an important impact on the dissolution of the experimental specimens. Further, the results revealed the role of Mg_2Si in the composition and stability of the protective films formed during the static corrosion experiment.

Fe/Mg_2Si showed higher degradation rates compared to that of pure iron at all stages of the degradation experiment (i.e. 0.12 vs 0.24 mm/year for PF100 and MX100 samples, respectively). Whereas the degradation of pure Fe relates more to the properties of Fe itself, in Fe/Mg_2Si composites relates to the distribution and size of the reinforcement particles. Thus, the features of the degradation products obtained after 100 days of the experiment varied with the substrate

chemical composition and its microstructure. In case of pure Fe - low solubility vivianite covered entire surface, while Fe/Mg_2Si composites exhibited the presence of carbonates at the latest stages of the test. A shift of the corrosion regime from localized to a more uniform was observed in case of the mechanically milled composite, mainly due to reinforcement refinement.

This study provided a basis for the processes of protective film formation in modified Hanks' solution, enabling detailed identification of their characteristic features. In particular, the ability to tune long-term degradation behavior of the composites as a function of reinforcement properties and manufacturing method was experimentally verified.

5.8. Acknowledgements

MSJ was awarded a doctoral scholarship from the Italian Ministry of Education, Universities and Research (Ministero dell'Istruzione, dell'Università e della Ricerca, MIUR). The research involved in this work was partially supported by the Natural Science and Engineering Research Council (NSERC) of Canada. MSJ, CP, DM and MV were recipients of the Linkage Grant from Quebec/Italy sub-commission of the Quebec. The authors would like to acknowledge V. Dodier, N. Moisan, J. Frenette from the Dept of Min-Met-Materials Eng at Laval University for kind help and guidance during experimental activities.

6. General discussion

Over the last two decades, biodegradable metallic implants for cardiovascular and orthopedic applications have gained substantial interest, as they can avoid the negative effects related to the use of permanent implants, such as inflammation and stress shielding [4,5,7]. In recent years, iron and its alloys have been proposed as potential biomaterial candidates, especially for the applications where strong mechanical support during the healing process is needed [128,147]. However, thus far, developed iron-based materials have shown a number of deficiencies in biomedical performances. One of the deficiencies, which is considered the major one is the low degradation rate [7,128]. It is obvious that further research efforts are needed to accelerate the degradation of iron-based biomaterials and in the meantime to enhance their bioactivity [120,121,144]. To date, most of the research on the subject has been focused on accelerating the degradation of iron-based biomaterials by means of alloying [94,95,225]. It has been found that alloying iron with elements such as manganese, palladium or silver can indeed enhance its degradation rate [208]. However, to achieve effective increases in degradation rate, these alloying elements have to be added in very large weight percentages, e.g., greater than 15% Mn, which may lead to uncertainties about the biocompatibility of alloys. Moreover, alloying with these elements is unlikely to improve the bioactivity of iron [97].

6.1. Development of MMCs for BM applications

In recent years, the development of metal matrix composites (MMCs) has been recognized as an alternative approach aimed at developing iron-based biomaterials with accelerated degradation rates [77,113,119,211]. Ulum et al., for example, developed a series of biocomposites by incorporating hydroxyapatite (HA), β-tricalcium phosphate (TCP) or HA-TCP mixtures into pure iron [120]. The degradation rates of the biocomposites were found to be slightly higher than that measured for pure iron [120]. This was attributed to the presence of these bioceramics in the composite structure. Although the research in this field has yet been quite scarce, the feasibility of improving the degradation rate by incorporating ceramic particles has been well acknowledged. Nevertheless, more research efforts are needed to optimize the compositions of iron-matrix composites in order to achieve more effective improvements in corrosion rates and uniformity. For

example, one hypothesis is that the use of a reinforcement having a higher reactivity rate than HA and TCP can lead to the attainment of the desired improvements.
Another approach is to enlarge the weight percentages or volume fractions of reinforcement particles added to the iron matrix [112].

Here, a new class of Fe-matrix composites was designed by optimizing both the selection and the content of the second phase particles. In this study, Mg_2Si intermetallic was chosen as the reinforcement phase to the iron matrix. Among several types of ceramics Mg_2Si presents the simplest chemical composition. Several studies have already confirmed its inferior corrosion resistance and reactivity in a corrosive medium, as compared with other ceramics including HA and TCP [192,193,199]. These characteristic properties make Mg_2Si an interesting reinforcement material for pure iron, when enhanced biomedical properties are desired.

Fe and Fe-based composites are promising candidates for BMs applications considering their excellent mechanical properties and biodegradability. Nowadays, the majority of metallic implants is fabricated by casting followed by cold or hot working (to tailor microstructure and mechanical properties) and finally mechanical machining [2,8]. PM is an appealing fabrication method enabling the direct production of relatively complex parts i.e. stent precursors or orthopedic implants (such as screws or foams) thus eliminating laser micro cutting and machining. Materials with finely tailored properties can be obtained by PM techniques, through the control and modulation of several manufacturing parameters in a wide range (for example, the reinforcement particle size and its amount). Moreover, metal–reinforcement interface reactivity can be controlled by using solid-state processing methods, controlling process temperature [169,170]. Furthermore, PM allows flexibility of Fe-based BMs design by mixing pure Fe powder with different elemental alloy powders or reinforcements. In addition, PM techniques allow to introduce functional porosity by adjusting process parameters (such as sintering time or temperature) and by initial conditions control (such as particle size of staring powders) [160,162].

The progress in the development of PM Fe-based biodegradable alloys and composites is described in detail in section 1.5. In this work different methods of powder processing were applied such as mixing or mechanical milling followed by hot rolling for powder consolidation. High-energy mechanical milling of Fe and Mg_2Si is a very efficacious and powerful process to synthesize metal–ceramic composite powders, which enables incorporation of the metal and the

ceramic phases into each powder particle [158,159], as seen in Fig. 6.1. The starting powders particles are micrometer in size. With progressing milling time, the metal, ductile phase is deformed, while the ceramic, brittle phase is mainly fractured. During repeated welding, fracturing and rewelding of metal matrix composite powder, the size of ceramic particles decreases continuously until the particle fracture strength is equal to or higher than the stress caused by the collision.

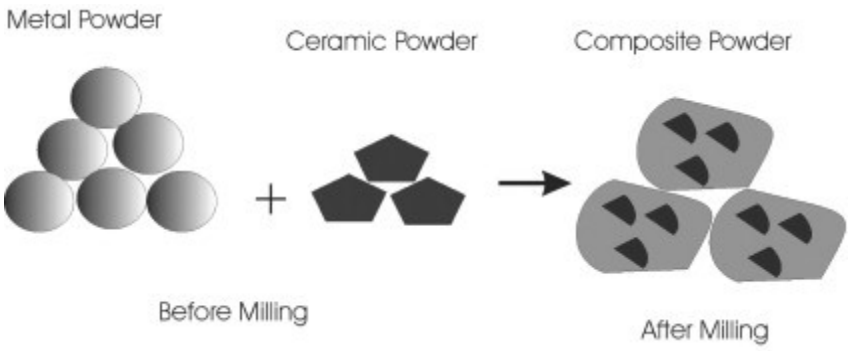

Figure 6.1. *Scheme of the composite powder formation after high-energy ball milling [189]*

Metal matrix nanocomposites can be produced during longer milling times. Since the microstructure of each powder particle develops through number of fracturing and cold-welding cycles, after a certain period of milling, particle uniform distribution through the matrix can be achieved [158,188,189].

Mechanical milling of the initial powders used in this study (Fe and Mg_2Si) resulted in a smaller reinforcement uniformly distributed throughout the Fe matrix compared to the samples prepared by mixing process. The outstanding strength of mechanically milled composites was at the expense of its fracture elongation. The small reinforcement size produced not only a relevant grain refinement, but also had an effect of higher amount of dislocations. Moreover, the particle shape of the powders used for MM samples was irregular, and the matrix milled powders were subjected to a heavy work hardening. These features are supposed to affect the recrystallization behavior during powder consolidation and the final microstructure of the material.

6.2. Determination of corrosion rate and identification of corrosion products

The corrosion rate of degradable Fe-based biomaterials can be evaluated gravimetrically, electrochemically, and by ion release [208]. Several *in vitro* and *in vivo* studies were performed to determine their specific degradation rate. Since corrosion mode is considerably altered by experimental parameters (e.g. temperature, constancy of pH, composition of the testing solution, duration of tests, etc.), a direct comparison between the reported results can in some cases become uncertain [39]. Accordingly to the method employed to calculate the degradation rate *in vitro* (i.e. electrochemical measurements, volume/mass loss after static corrosion test, etc.), a wide range of results can be obtained in case of the same material. The methods of corrosion rates evaluation used for BMs *in vitro* testing are summarized in Table 6.2.

Main purpose of electrochemical measurements is to enable identification and understanding reactions, rate determining processes, and the stability of the passive film. Electrochemical measurements do not provide accurate estimates of long-term progression of degradation. Even if the technique could produce very accurate rate measurements, it would only be good for the pristine surface immersed into the solution (with precise chemistry, temperature and aeration) for a relatively short-time. Electrochemical tests are suitable for qualitative corrosion investigations. Potentiodynamic polarization is the most frequently used electrochemical test for studying *in vitro* corrosion of Fe alloys. PTD measurements allow to better understand why and how corrosion takes place. However, during this test the samples surface is damaged, and the accurate estimation of the corrosion rates becomes impossible. Further, the investigation of the corrosion layers that form during rapid dissolution of Fe is not possible. Electrochemical impedance spectroscopy (EIS) is another technique that has been largely applied to study the corrosion of Fe-based BMs. This method highlights the behaviour of corrosion films that form during experiment. The time-dependent formation and dissolution of protective layer on Fe-surface can be determined by EIS. In addition, EIS has an ability to detect individual layers formed on the surface of Fe-based alloys during its corrosion. EIS results might be affected by constant dissolution of Fe substrate thus the choice of the electrical circuit can be uncertain. Therefore, EIS requires deep understanding of the degradation processes occurring on the surface of experimental specimens. Mass loss experiments allow to determine the actual amount of cumulative corrosion. It is most appropriate for determine

the corrosivity of physiological solution and the degradability of BMs in *in vitro* conditions. All aforementioned techniques are complementary to each other. Single testing strategy does not provide all information necessary to fully understand the corrosion behaviour in a complex physiological environment.

A detailed investigation on the corrosion mechanism and the formation of *in vitro* corrosion products for this biodegradable metal candidate remains largely unexplored. Commercial Hanks', modified Hanks' balanced salts, simulated body fluids, Dulbecco's phosphate buffered saline (DPBS), Earle's Balanced Salt Solution (EBSS), and commonly used cell culture medium such as Dulbecco's Modified Eagle's Medium (DMEM) are among the most common solutions adopted to conduct *in vitro* tests on recently elaborated Fe-based alloys [67]. Their ionic composition is listed in Table 6.1. The degradation patterns of metals in simulated body environment can be extended to a certain degree to predict the *in vivo* behavior of BMs because the ion concentration of the media is similar to that of physiological body fluids. These solutions represent different ionic compositions and concentrations of buffering agents.

Table 6.1. *Composition of commonly used solutions for BMs degradation testing compared to blood plasma [135]*

	Element	Blood plasma (mM)	Saline (NaCl) (mM)	Commercial Hanks' (mM)	Modified Hanks' (mM)	SBF (mM)	EBSS (mM)	DPBS (mM)	MEM (mM)
Inorganic ions	Na	142.0	236	142.0	122	142.0	144.0	153	143.0
	K	5.0	−	5.8	4.4	5.8	5.4	4.15	5.4
	Mg	1.5	−	0.8	1.2	1.5	0.4		0.4
	Cl	103.0	100	145.0	101	147.8	125.0	141	125.0
	Ca	2.5	−	2.5	1.75	2.5	1.8		1.8
	HPO_4	1.0	−	0.4	0.5	1.0	1.0	9.48	0.9
	SO_4	0.5	−	0.8	1.6	0.5	0.4		0.4
	HCO_3	27.0	−	4.2	27	27.0	26.0		26.0
Organic components	Glucose	3.6–5.2	−	1	0.72	−	5.60	−	5.60
	*Albumin ($g\ l^{-1}$)	35–50	−	−	−	−	−	−	−
	*Amino acids ($g\ l^{-}$	Variable	−	−	−	−	−	−	0.95
	*Vitamins ($g\ l^{-1}$)	Variable	−	−	−	−	−	−	8.10

*$g \cdot l^{-1}$

Variations in their composition alter degradation process. The general opinion is that the composition of the solution used for in vitro BMs degradation testing should be as close as possible to physiological conditions. Tolouei et al. [135] performed fundamental study on a degradation of pure Fe in five different physiological solutions. These studies revealed an inhomogeneous corrosion layer growth which is associated with different local dissolution-passivation behavior on the Fe surface. The influence of particular ions on the corrosion behavior of pure Fe was demonstrated. Their results revealed that chloride ions in a CO_2-rich atmosphere may induce pitting corrosion, promoting a porous surface formation. Bicarbonate ions stimulated the corrosion of Fe at early immersion stage. Phosphates hindered further degradation, and the formation of pitting corrosion was considerably delayed due to precipitation of insoluble phosphate-based compounds. Finally, the presence of proteins promoted to the formation of an amorphous protective layer. Another study investigated the influence of physiological solution on the degradation mechanism of Fe-20Mn-1C austenitic alloy [226]. It was established that CO_3^{2-} and HCO_3^- rich solutions, such as modified Hanks' solution, promoted the formation of $MnCO_3$ crystals on the surface and insoluble iron hydro-oxides in the solution. Furthermore, the amount of iron and manganese ion released were strongly dependent on the chemical composition of the solution. In DPBS solution, no corrosion precipitations were present in the exhausted solution but sample surface was entirely covered by $Fe_x(PO_4)_y$ corrosion deposit. It was suggested that the amount of carbonate and dihydrogen carbonate ions plays a key role in the formation of an insoluble layer of $MnCO_3$ that can hinder the further dissolution of the substrate material. For this reason, the degradation in modified Hanks' solution was lower compared to commercial one. The same group studied the influence of CO_2 presence on the corrosion behavior of an austenitic Fe-21Mn-1C alloy. The *in vitro* static degradation tests were carried out under two different atmospheres, one with high 5%CO_2 concentration and the second one with low CO_2 concentration. Modified Hanks' solution used in this study, features the same carbonate content as blood plasma and a very similar amount of other inorganic ions (as seen in Fig. 6.2 and Table 1). After 14 days of immersion test a dense and compact degradation layer, hindering further dissolution of the substrate was formed on samples under a 5%CO_2 atmosphere. Corrosion morphologies under CO_2-low atmosphere revealed uneven protective film with several uncovered areas. Under 5%CO_2 atmosphere, rhodochrosite particles were identified, while under CO_2-low atmosphere an

amorphous iron phosphate compound was detected and higher Mn^{2+} ions release in the solution was observed.

Above mentioned studies improved our understanding of the degradation mechanism of Fe-based biomaterials in the complex physiological environment. *In vitro* degradation of pure iron is a function of following factors (i) composition of the electrolyte solution, (ii) quality of degradation layer, pore and defect densities and (iii) local dissolution and pH which could be explained by the formation and dissolution of salt film coupled to changes in local pH. Mainly because the degradation behavior of Fe-based biodegradable alloys depends on multiple factors, the overall results of the studies of Tolouei [135] and Mouzou [226] emphasize the importance of conducting *in vitro* static immersion test under several conditions (i.e. multiple physiological solutions, various samples' surface finishing etc.). This approach represents a reliable testing procedure for performance assessment of developing metallic resorbable medical devices.

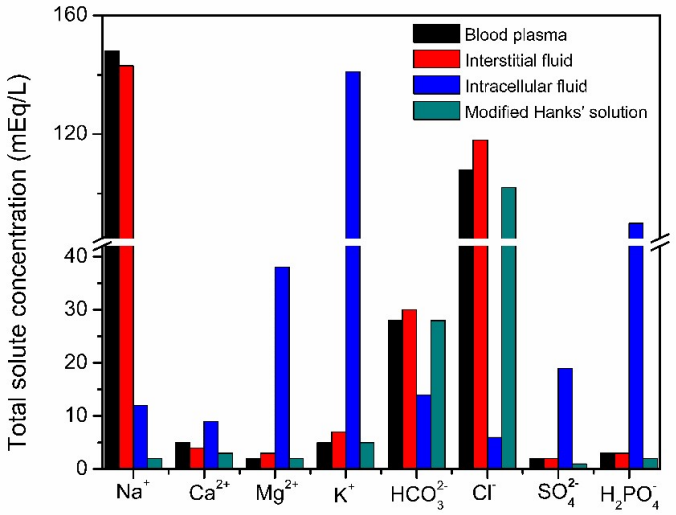

Figure 6.2. *Ionic composition in mammalian organisms compared to Hanks' modified solution*

Addition of alloying elements/reinforcement gives an opportunity to further modulate the corrosion properties of Fe-based bioabsorbable metals in terms the rate/uniformity of corrosion and mechanical integrity of the implant during serving period. The corrosion of pure Fe depends more on the properties of Fe itself, while in Fe-based alloys corrosion is mainly related to the size/distribution and fraction of the second phases. The differences in corrosion rates of the investigated Fe-based composites are depicted in Fig. 6.3 are ascribed to the presence, size and distribution of the reinforcement. Even minor changes in the Fe-matrix chemistry could

significantly alter the degradation mode compared to that of pure Fe. Addition of Mg_2Si increases corrosion kinetics to different extents. From the corrosion point of view, each phase has its individual electrochemical properties. Due to the galvanic coupling between second phases and surrounding matrix, the former are the initiation sites for localized corrosion. Subsequent alloy processing, such as thermal and/or thermomechanical treatments result in a tailored microstructure with homogenously distributed second phases, promoting uniform corrosion which is the desirable mode in biomaterials applications. In brief, understanding the metallurgy of the specific material can help to achieve final microstructures designed to achieve optimal mechanical properties and to provide safe and long-term controlled corrosion.

6.3. Periods considered to measure the corrosion rates *in vitro*

As mentioned earlier, the duration of the corrosion experiment upon which degradation rates are evaluated is essential. Most of the researches have considered degradation rates as a constant value. However, they show the decreasing tendency with progressing corrosion. More detailed time-dependent evaluation of corrosion rates might reveal their non-linearity over time due to the formation of a protective corrosion deposit on their surfaces.

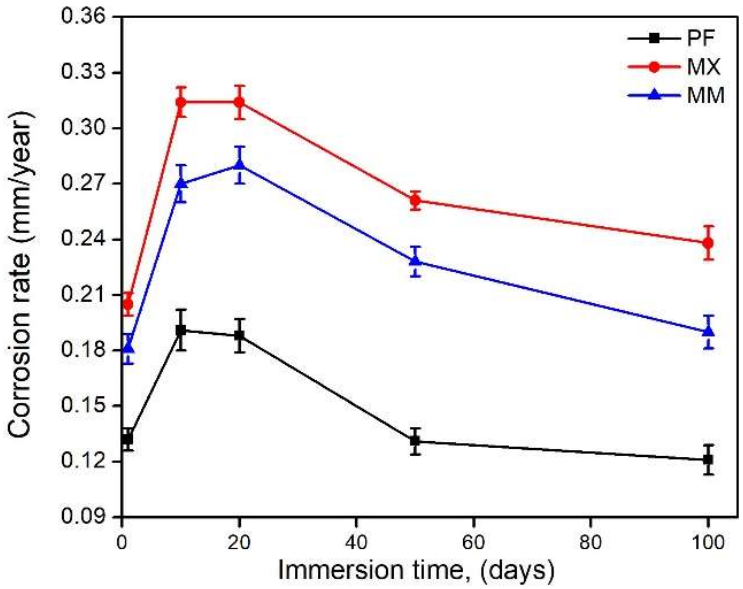

Figure 6.3. *Corrosion rate over the time measured for Fe and Fe-Mg_2Si composites prepared by mixing (MX) or mechanical milling (MM) in modified Hanks' solution*

Most of the studies reported corrosion rates of Fe-based BMs up to 14 days. Furthermore, addition of alloying elements or reinforcement increase the complexity of the time-dependent corrosion behavior. Time points from 1 day to 100 days are reported in our study. BMs exhibit a high initial degradation rates that decreases with ongoing immersion time due to the progressive deposition of a protective film. The chemical composition, the stability, and the sequence of protective film formation on the surface that can only be evaluated when considering several time point measurements. Protective film formation and the precipitation of other insoluble salts on the metallic surface has an important impact on the dissolution of the substrate, reducing its corrosion speed which is a non-linear process that decreases in velocity over time (Fig. 6.3.). Thus, the period during which degradation rates are evaluated is essential. The results of corrosion experiment performed considering several time points is consistent with certain in vivo biocorrosion studies on biodegradable metals. The behavior of metallic surfaces in long term *in vivo* (such as 1 year or longer) studies, revealed similar structures to those found in our study. In particular, the sequences of passive films formed on the surfaces as described in our work such as an inner layer rich in substrate metal containing high amount of metal oxides/hydroxides and also carbonates alongside outer layer made of phosphate rich compounds [49,81,227]. Lin at al. [81] investigated biocorrosion of Fe scaffold up to 53 months after implantation and explored its bioresorption mechanism. The struts of Fe were surrounded by a layer of corrosion products such as Fe oxides, hydroxides and carbonates, whereas the middle layer was made of Fe phosphates. The outermost layer contained Ca and P.

Table 6.2. *Methodology for evaluating the corrosion rate in vitro and in vivo [20,195]*

Immersion test		Electrochemical test		μCT	X-ray spectroscopy
Mass loss	Ion release	Potentiodynamic polarization	Electrochemical impedance spectroscopy	Volume loss	
$CR = 8.76 \times 10^4 \Delta W/Atp$	$CR = cV/St$	$CR = K(I_{corr}/\rho)m_e$		$CR = 8.76 \times 10^4 \Delta V/At$	
ΔW: weight loss A: original surface area t: exposure time ρ: standard density of the material	c: ion release concentration V: volume of immersion solution S: original surface area exposed to corrosive media t: exposure time	K: 3.273 × 10^{-3} mm g/(μA cm a) I_{corr}: current density m_e: equivalent mass.		ΔV: differences in volume before-after immersion A: original surface area t: exposure time	

7. Conclusions & Perspectives

7.1. Conclusions

In this study, a series of Fe/Mg_2Si composites was prepared by different routes, such as mixing and/or mechanical milling of powders. Specimens were fabricated by powder metallurgy, using hot rolling as a consolidation method. The addition of Mg_2Si particles was selected to obtain a faster corrosion rate of Fe-based composites through a micro-galvanic coupling mechanism.

- The introduction of a second phase was found to significantly modify the mechanical properties of pure Fe. In fact, the addition of coarse Mg_2Si particles by simple mixing leads to an evident decrease in the tensile properties of YS, UTS and A from 400 MPa, 416 MPa and 21% for pure Fe to 290 MPa, 321 MPa and 5% for coarse particulate reinforced Fe-1.5%Mg_2Si composite.

- The composites made by small size reinforcement showed a general increase of tensile properties. Samples prepared by mechanical milling presented the highest tensile strength (YS = 523 MPa, UTS = 630 MPa) while exhibiting the lowest ductility compared to that of pure Fe (4% vs 20%).

- Concerning potentiodynamic and static immersion tests in modified Hanks' solution, a higher corrosion rate was obtained when 1.5 wt.% of Mg_2Si particles were added to the pure Fe matrix; both tests showed the same trend for the different studied conditions. For example, the lowest corrosion rates were obtained for pure Fe, CR_p = 0.25±0.01 mm/year and CR_s = 0.14±0.01 mm/year and the highest for fine-particulate reinforced composite prepared by mixing CR_p = 0.28±0.04 mm/year and CR_s = 0.31±0.04 mm/year.

- The size and uniform distribution of reinforcement particles in the matrix of a composite is one of the most important microstructural features altering corrosion

properties. A shift of a corrosion regime from localized to a more uniform was observed in case of the mechanically milled composite, mainly due to reinforcement refinement.

- The ability to tune corrosion behavior of the composites as a function of reinforcement properties and manufacturing method was experimentally verified and the microstructure-corrosion properties relationship was highlighted.

- The degradation rate at distinct stages of the immersion test strongly depends on the composition and stability of the formed oxide, hydroxide, carbonate and phosphate films.

- A rapid increase in Fe ion release for periods considered in this study was induced after the addition of Mg_2Si reinforcement (i.e. PF = 0.20 mg/L vs MX = 0.48 mg/L after 240 hours of immersion test). However, at subsequent stages of degradation, metals were covered by protective films which had an important impact on the substrate dissolution. Even if the metal surface was completely covered by the protective deposit, corrosion still occurred at slower rates.

- The results revealed the Mg_2Si role in the composition and stability of the protective films formed during static corrosion experiment. The addition of Mg_2Si plays a key role in the degradation passivation process as well as in the degradation mechanism. Fe/Mg_2Si showed higher corrosion rates compared to that of pure iron at all stages of the degradation experiment (i.e. CR_s = 0.12 vs CR_s = 0.24 mm/year for PF100 and MX100 samples, respectively).

- Whereas the degradation of pure Fe relates more to the properties of Fe itself, in Fe/Mg_2Si composites relates to the distribution and size of the reinforcement particles. Thus, the features of the degradation products obtained after 100 days of the experiment varied with the substrate chemical composition and its microstructure. In case of pure Fe - low solubility vivianite covered entire surface, while Fe/Mg_2Si composites exhibited the presence of carbonates at the latest stages of the test.

- Our fundamental study on the long-term corrosion behaviour of powder metallurgy pure Fe and Fe/Mg_2Si composites provided a basis about the processes of protective films formation in physiological media, enabling detailed identification of their characteristic features. Additionally, the long-term *in vitro* influence of Mg_2Si was highlighted. The details about the corrosion behavior at longer exposure times to physiological environment highlighted in this work provide a new knowledge on corrosion mechanism of degradable implant materials.

7.2. Perspectives

The mechanical properties and degradation behavior of the Fe/Mg_2Si composites can be further enhanced. Their present conditions are still far away from their limit. Future works for the continuation of this doctoral project are proposed as follows:

- Optimizing structure (i.e. finer grain size) and mechanical properties (i.e. higher ductility) of Fe/Mg_2Si composites by further modifying process parameters and by adding other alloying elements. The ductility can be further increased, i.e. by modifying the parameters of initial powder preparations (i.e. time and speed of mechanical milling, ball to powder ratio etc.). In addition, the ductility of the produced composites can be significantly enhanced by modifying the size and content of the reinforcement, alloying, and by using severe plastic deformation techniques e.g. accumulative roll bonding or equal channel angular pressing as consolidation or thermomechanical processing routes.

- To finally translate these composites into clinical applications, the biological activity of the released alloying elements in terms of cytotoxicity and *in vivo* inflammatory response, as well as the long-term effects induced by the possible deposition of alloying elements in the organism, must be fully understood.

- Considering the increasing interest in biodegradable metals more representative corrosion studies of Fe and its composites in the presence of microorganisms (such as bacteria) are also required.

- Conducting *in vitro* degradation study in a presence of proteins in physiological solution to understand the formation and dissolution of the degradation layer and to better mimic *in vivo* environment. The addition of organic components in simulated solutions is the next step towards a simulation of *in vivo* conditions. Protein adsorption on Fe surface alters the formation of the degradation layer during immersion (its composition, compactness, and thickness). Deep understanding of the interactions on the Fe – physiological solution interface leads to a design of smart, biocompatible surface responsive biomaterials.

- Another modified method of more representative corrosion evaluation of Fe/Mg_2Si composites is applying the electrochemical impedance spectroscopy (EIS) measurement to study and analyze the influence of cells on the metallic implant. A custom-made electrochemical testing system can be developed for these particular measurements.

8. Bibliography

[1] M.B. Nasab, M.R. Hassan, B.B. Sahari, Metallic Biomaterials of Knee and Hip - A Review, Trends Biomater. Artif. Organs. 24 (2010). http://www.biomaterials.org, (accessed December 24, 2015).

[2] Q. Chen, G.A. Thouas, Metallic implant biomaterials, Mater. Sci. Eng. R Rep. 87 (2015) 1–57. doi:10.1016/j.mser.2014.10.001.

[3] M. Niinomi, Metals for Biomedical Devices, Elsevier, 2010.

[4] Y.F. Zheng, X.N. Gu, F. Witte, Biodegradable metals, Mater. Sci. Eng. R Rep. 77 (2014) 1–34. doi:10.1016/j.mser.2014.01.001.

[5] R. Zeng, W. Dietzel, F. Witte, N. Hort, C. Blawert, Progress and Challenge for Magnesium Alloys as Biomaterials, Adv. Eng. Mater. 10 (2008) B3–B14. doi:10.1002/adem.200800035.

[6] A. Francis, Y. Yang, S. Virtanen, A.R. Boccaccini, Iron and iron-based alloys for temporary cardiovascular applications, J. Mater. Sci. Mater. Med. 26 (2015) 1–16. doi:10.1007/s10856-015-5473-8.

[7] H. Li, Y. Zheng, L. Qin, Progress of biodegradable metals, Prog. Nat. Sci. Mater. Int. 24 (2014) 414–422. doi:10.1016/j.pnsc.2014.08.014.

[8] J.B. Park, J.D. Bronzino, Biomaterials: Principles and Applications, CRC Press, 2002.

[9] B.C. Syrett, A. Acharya, Corrosion and Degradation of Implant Materials, ASTM International, 1979.

[10] H.A. Luckey, Titanium Alloys in Surgical Implants, ASTM International, 1983.

[11] G.L. Winters, M.J. Nutt, Stainless Steels for Medical and Surgical Applications, ASTM International, 2003.

[12] B. O'Brien, W. Carroll, The evolution of cardiovascular stent materials and surfaces in response to clinical drivers: A review, Acta Biomater. 5 (2009) 945–958. doi:10.1016/j.actbio.2008.11.012.

[13] A. Colombo, E. Karvouni, Biodegradable Stents "Fulfilling the Mission and Stepping Away," Circulation. 102 (2000) 371–373. doi:10.1161/01.CIR.102.4.371.

[14] Virmani, Renu, A. Farb, G. Giulio, Drug-eluting stents: caution and concerns for long-term outcome, 313-318. 15 (2004).

[15] A.T.L. Ong, E.P. McFadden, E. Regar, P.P.T. de Jaegere, R.T. van Domburg, P.W. Serruys, Late angiographic stent thrombosis (LAST) events with drug-eluting stents, J. Am. Coll. Cardiol. 45 (2005) 2088–2092. doi:10.1016/j.jacc.2005.02.086.

[16] H.L. Vingan, Stents: State of the Art, Future Developments, J. Vasc. Interv. Radiol. 7 (1996) 98. doi:10.1016/S1051-0443(96)70742-X.

[17] S.E. Kimmel, A.R. Localio, R.J. Krone, W.K. Laskey, The effects of contemporary use of coronary stents on in-hospital mortality, J. Am. Coll. Cardiol. 37 (2001) 499–504. doi:10.1016/S0735-1097(00)01115-3.

[18] R. Mitchell, AO Principles of Fracture Management in the Dog and Cat, Aust. Vet. J. 84 (2006) 316–316. doi:10.1111/j.1751-0813.2006.00007.x.

[19] N.C. Andrews, Disorders of Iron Metabolism, N. Engl. J. Med. 341 (1999) 1986–1995. doi:10.1056/NEJM199912233412607.

[20] F. Witte, N. Hort, C. Vogt, S. Cohen, K.U. Kainer, R. Willumeit, F. Feyerabend, Degradable biomaterials based on magnesium corrosion, Curr. Opin. Solid State Mater. Sci. 12 (2008) 63–72. doi:10.1016/j.cossms.2009.04.001.
[21] A. Hartwig, Role of magnesium in genomic stability, Mutat. Res. Mol. Mech. Mutagen. 475 (2001) 113–121. doi:10.1016/S0027-5107(01)00074-4.
[22] M.P. Staiger, A.M. Pietak, J. Huadmai, G. Dias, Magnesium and its alloys as orthopedic biomaterials: A review, Biomaterials. 27 (2006) 1728–1734. doi:10.1016/j.biomaterials.2005.10.003.
[23] Wiley: Alloys: Preparation, Properties, Applications - Fathi Habashi, (n.d.). http://eu.wiley.com/WileyCDA/WileyTitle/productCd-3527611924.html (accessed November 16, 2015).
[24] M. Bamberger, G. Dehm, Trends in the Development of New Mg Alloys, Annu. Rev. Mater. Res. 38 (2008) 505–533. doi:10.1146/annurev.matsci.020408.133717.
[25] Y. Chen, Z. Xu, C. Smith, J. Sankar, Recent advances on the development of magnesium alloys for biodegradable implants, Acta Biomater. 10 (2014) 4561–4573. doi:10.1016/j.actbio.2014.07.005.
[26] Z.G. Huan, M.A. Leeflang, J. Zhou, L.E. Fratila-Apachitei, J. Duszczyk, In vitro degradation behavior and cytocompatibility of Mg–Zn–Zr alloys, J. Mater. Sci. Mater. Med. 21 (2010) 2623–2635. doi:10.1007/s10856-010-4111-8.
[27] S.K. Lu, H.I. Yeh, T.Y. Tian, W.H. Lee, Degradation of Magnesium Alloys in Biological Solutions and Reduced Phenotypic Expression of Endothelial Cell Grown on These Alloys, in: F. Ibrahim, N.A.A. Osman, J. Usman, N.A. Kadri (Eds.), 3rd Kuala Lumpur Int. Conf. Biomed. Eng. 2006, Springer Berlin Heidelberg, 2007: pp. 98–101. http://link.springer.com/chapter/10.1007/978-3-540-68017-8_25 (accessed December 1, 2015).
[28] F. Witte, V. Kaese, H. Haferkamp, E. Switzer, A. Meyer-Lindenberg, C.J. Wirth, H. Windhagen, In vivo corrosion of four magnesium alloys and the associated bone response, Biomaterials. 26 (2005) 3557–3563. doi:10.1016/j.biomaterials.2004.09.049.
[29] Z. Li, X. Gu, S. Lou, Y. Zheng, The development of binary Mg–Ca alloys for use as biodegradable materials within bone, Biomaterials. 29 (2008) 1329–1344. doi:10.1016/j.biomaterials.2007.12.021.
[30] S. Zhang, X. Zhang, C. Zhao, J. Li, Y. Song, C. Xie, H. Tao, Y. Zhang, Y. He, Y. Jiang, Y. Bian, Research on an Mg–Zn alloy as a degradable biomaterial, Acta Biomater. 6 (2010) 626–640. doi:10.1016/j.actbio.2009.06.028.
[31] X.N. Gu, X.H. Xie, N. Li, Y.F. Zheng, L. Qin, In vitro and in vivo studies on a Mg–Sr binary alloy system developed as a new kind of biodegradable metal, Acta Biomater. 8 (2012) 2360–2374. doi:10.1016/j.actbio.2012.02.018.
[32] E. Zhang, L. Yang, J. Xu, H. Chen, Microstructure, mechanical properties and bio-corrosion properties of Mg–Si(–Ca, Zn) alloy for biomedical application, Acta Biomater. 6 (2010) 1756–1762. doi:10.1016/j.actbio.2009.11.024.
[33] X. Zhang, G. Yuan, J. Niu, P. Fu, W. Ding, Microstructure, mechanical properties, biocorrosion behavior, and cytotoxicity of as-extruded Mg-Nd-Zn-Zr alloy with different extrusion ratios, J. Mech. Behav. Biomed. Mater. 9 (2012) 153–162. doi:10.1016/j.jmbbm.2012.02.002.
[34] K. Pichler, S. Fischerauer, P. Ferlic, E. Martinelli, H.-P. Brezinsek, P.J. Uggowitzer, J.F. Löffler, A.-M. Weinberg, Immunological Response to Biodegradable Magnesium Implants, JOM. 66 (2014) 573–579. doi:10.1007/s11837-014-0874-6.
[35] C.M. Serre, M. Papillard, P. Chavassieux, J.C. Voegel, G. Boivin, Influence of magnesium substitution on a collagen–apatite biomaterial on the production of a calcifying matrix by

human osteoblasts, J. Biomed. Mater. Res. 42 (1998) 626–633. doi:10.1002/(SICI)1097-4636(19981215)42:4<626::AID-JBM20>3.0.CO;2-S.
[36] G. Song, Control of biodegradation of biocompatable magnesium alloys, Corros. Sci. 49 (2007) 1696–1701. doi:10.1016/j.corsci.2007.01.001.
[37] C. Janning, E. Willbold, C. Vogt, J. Nellesen, A. Meyer-Lindenberg, H. Windhagen, F. Thorey, F. Witte, Magnesium hydroxide temporarily enhancing osteoblast activity and decreasing the osteoclast number in peri-implant bone remodelling, Acta Biomater. 6 (2010) 1861–1868. doi:10.1016/j.actbio.2009.12.037.
[38] H.G. Seiler, H. Sigel, A. Sigel, Handbook on toxicity of inorganic compounds, (1988). http://inis.iaea.org/Search/search.aspx?orig_q=RN:20015779 (accessed December 10, 2015).
[39] D. Zhao, T. Wang, J. Kuhlmann, Z. Dong, S. Chen, M. Joshi, P. Salunke, V.N. Shanov, D. Hong, P.N. Kumta, W.R. Heineman, In vivo monitoring the biodegradation of magnesium alloys with an electrochemical H2 sensor, Acta Biomater. 36 (2016) 361–368. doi:10.1016/j.actbio.2016.03.039.
[40] A. Chaya, S. Yoshizawa, K. Verdelis, N. Myers, B.J. Costello, D.-T. Chou, S. Pal, S. Maiti, P.N. Kumta, C. Sfeir, In vivo study of magnesium plate and screw degradation and bone fracture healing, Acta Biomater. 18 (2015) 262–269. doi:10.1016/j.actbio.2015.02.010.
[41] S. Yoshizawa, A. Chaya, K. Verdelis, E.A. Bilodeau, C. Sfeir, An in vivo model to assess magnesium alloys and their biological effect on human bone marrow stromal cells, Acta Biomater. 28 (2015) 234–239. doi:10.1016/j.actbio.2015.08.037.
[42] D. Zhao, F. Witte, F. Lu, J. Wang, J. Li, L. Qin, Current status on clinical applications of magnesium-based orthopaedic implants: A review from clinical translational perspective, Biomaterials. 112 (2017) 287–302. doi:10.1016/j.biomaterials.2016.10.017.
[43] D. Tousoulis, Coronary Artery Disease: From Biology to Clinical Practice, Academic Press, 2017.
[44] H. Tapiero, K.D. Tew, Trace elements in human physiology and pathology: zinc and metallothioneins, Biomed. Pharmacother. 57 (2003) 399–411. doi:10.1016/S0753-3322(03)00081-7.
[45] M. Hambidge, Human Zinc Deficiency, J. Nutr. 130 (2000) 1344S–1349S.
[46] P.K. Bowen, J. Drelich, J. Goldman, Zinc Exhibits Ideal Physiological Corrosion Behavior for Bioabsorbable Stents, Adv. Mater. 25 (2013) 2577–2582. doi:10.1002/adma.201300226.
[47] D. Vojtěch, J. Kubásek, J. Šerák, P. Novák, Mechanical and corrosion properties of newly developed biodegradable Zn-based alloys for bone fixation, Acta Biomater. 7 (2011) 3515–3522. doi:10.1016/j.actbio.2011.05.008.
[48] E. Mostaed, M. Sikora-Jasinska, A. Mostaed, S. Loffredo, A.G. Demir, B. Previtali, D. Mantovani, R. Beanland, M. Vedani, Novel Zn-based alloys for biodegradable stent applications: Design, development and in vitro degradation, J. Mech. Behav. Biomed. Mater. 60 (2016) 581–602. doi:10.1016/j.jmbbm.2016.03.018.
[49] S. Zhao, J.-M. Seitz, R. Eifler, H.J. Maier, R.J. Guillory II, E.J. Earley, A. Drelich, J. Goldman, J.W. Drelich, Zn-Li alloy after extrusion and drawing: Structural, mechanical characterization, and biodegradation in abdominal aorta of rat, Mater. Sci. Eng. C. 76 (2017) 301–312. doi:10.1016/j.msec.2017.02.167.
[50] H.F. Li, X.H. Xie, Y.F. Zheng, Y. Cong, F.Y. Zhou, K.J. Qiu, X. Wang, S.H. Chen, L. Huang, L. Tian, L. Qin, Development of biodegradable Zn-1X binary alloys with nutrient alloying elements Mg, Ca and Sr, Sci. Rep. 5 (2015) 10719. doi:10.1038/srep10719.
[51] P.K. Bowen, J.-M. Seitz, R.J. Guillory, J.P. Braykovich, S. Zhao, J. Goldman, J.W. Drelich, Evaluation of wrought Zn–Al alloys (1, 3, and 5 wt % Al) through mechanical and in vivo

testing for stent applications, J. Biomed. Mater. Res. B Appl. Biomater. (2017) n/a-n/a. doi:10.1002/jbm.b.33850.
[52] J. Niu, Z. Tang, H. Huang, J. Pei, H. Zhang, G. Yuan, W. Ding, Research on a Zn-Cu alloy as a biodegradable material for potential vascular stents application, Mater. Sci. Eng. C. 69 (2016) 407–413. doi:10.1016/j.msec.2016.06.082.
[53] M. Sikora-Jasinska, E. Mostaed, A. Mostaed, R. Beanland, D. Mantovani, M. Vedani, Fabrication, mechanical properties and in vitro degradation behavior of newly developed ZnAg alloys for degradable implant applications, Mater. Sci. Eng. C. 77 (2017) 1170–1181. doi:10.1016/j.msec.2017.04.023.
[54] X. Liu, J. Sun, F. Zhou, Y. Yang, R. Chang, K. Qiu, Z. Pu, L. Li, Y. Zheng, Micro-alloying with Mn in Zn–Mg alloy for future biodegradable metals application, Mater. Des. 94 (2016) 95–104. doi:10.1016/j.matdes.2015.12.128.
[55] H.R. Bakhsheshi-Rad, E. Hamzah, H.T. Low, M. Kasiri-Asgarani, S. Farahany, E. Akbari, M.H. Cho, Fabrication of biodegradable Zn-Al-Mg alloy: Mechanical properties, corrosion behavior, cytotoxicity and antibacterial activities, Mater. Sci. Eng. C. 73 (2017) 215–219. doi:10.1016/j.msec.2016.11.138.
[56] X. Liu, J. Sun, Y. Yang, Z. Pu, Y. Zheng, In vitro investigation of ultra-pure Zn and its mini-tube as potential bioabsorbable stent material, Mater. Lett. 161 (2015) 53–56. doi:10.1016/j.matlet.2015.06.107.
[57] X. Liu, J. Sun, K. Qiu, Y. Yang, Z. Pu, L. Li, Y. Zheng, Effects of alloying elements (Ca and Sr) on microstructure, mechanical property and in vitro corrosion behavior of biodegradable Zn–1.5Mg alloy, J. Alloys Compd. Complete (2016) 444–452. doi:10.1016/j.jallcom.2015.10.116.
[58] H. Li, H. Yang, Y. Zheng, F. Zhou, K. Qiu, X. Wang, Design and characterizations of novel biodegradable ternary Zn-based alloys with IIA nutrient alloying elements Mg, Ca and Sr, Mater. Des. 83 (2015) 95–102. doi:10.1016/j.matdes.2015.05.089.
[59] Z. Tang, H. Huang, J. Niu, L. Zhang, H. Zhang, J. Pei, J. Tan, G. Yuan, Design and characterizations of novel biodegradable Zn-Cu-Mg alloys for potential biodegradable implants, Mater. Des. 117 (2017) 84–94. doi:10.1016/j.matdes.2016.12.075.
[60] S. Zhao, C.T. McNamara, P.K. Bowen, N. Verhun, J.P. Braykovich, J. Goldman, J.W. Drelich, Structural Characteristics and In Vitro Biodegradation of a Novel Zn-Li Alloy Prepared by Induction Melting and Hot Rolling, Metall. Mater. Trans. A. 48 (2017) 1204–1215. doi:10.1007/s11661-016-3901-0.
[61] J. Kubásek, D. Vojtěch, E. Jablonská, I. Pospíšilová, J. Lipov, T. Ruml, Structure, mechanical characteristics and in vitro degradation, cytotoxicity, genotoxicity and mutagenicity of novel biodegradable Zn–Mg alloys, Mater. Sci. Eng. C. 58 (2016) 24–35. doi:10.1016/j.msec.2015.08.015.
[62] X. Liu, J. Sun, Y. Yang, F. Zhou, Z. Pu, L. Li, Y. Zheng, Microstructure, mechanical properties, in vitro degradation behavior and hemocompatibility of novel Zn–Mg–Sr alloys as biodegradable metals, Mater. Lett. 162 (2016) 242–245. doi:10.1016/j.matlet.2015.07.151.
[63] C. Shen, X. Liu, B. Fan, P. Lan, F. Zhou, X. Li, H. Wang, X. Xiao, L. Li, S. Zhao, Z. Guo, Z. Pu, Y. Zheng, Mechanical properties, in vitro degradation behavior, hemocompatibility and cytotoxicity evaluation of Zn–1.2Mg alloy for biodegradable implants, RSC Adv. 6 (2016) 86410–86419. doi:10.1039/C6RA14300H.
[64] E. Mostaed, M. Vedani, M. Hashempour, M. Bestetti, Influence of ECAP process on mechanical and corrosion properties of pure Mg and ZK60 magnesium alloy for biodegradable stent applications, Biomatter. 4 (2014) e28283. doi:10.4161/biom.28283.

[65] E. Mostaed, M. Hashempour, A. Fabrizi, D. Dellasega, M. Bestetti, F. Bonollo, M. Vedani, Microstructure, texture evolution, mechanical properties and corrosion behavior of ECAP processed ZK60 magnesium alloy for biodegradable applications, J. Mech. Behav. Biomed. Mater. 37 (2014) 307–322. doi:10.1016/j.jmbbm.2014.05.024.
[66] H.R. Bakhsheshi-Rad, E. Hamzah, H.T. Low, M.H. Cho, M. Kasiri-Asgarani, S. Farahany, A. Mostafa, M. Medraj, Thermal Characteristics, Mechanical Properties, In Vitro Degradation and Cytotoxicity of Novel Biodegradable Zn–Al–Mg and Zn–Al–Mg–xBi Alloys, Acta Metall. Sin. Engl. Lett. 30 (2017) 201–211. doi:10.1007/s40195-017-0534-2.
[67] K. Törne, M. Larsson, A. Norlin, J. Weissenrieder, Degradation of zinc in saline solutions, plasma, and whole blood, J. Biomed. Mater. Res. B Appl. Biomater. 104 (2016) 1141–1151. doi:10.1002/jbm.b.33458.
[68] X.G. Zhang, Corrosion and Electrochemistry of Zinc, Springer Science & Business Media, 2013.
[69] E. Jablonská, D. Vojtěch, M. Fousová, J. Kubásek, J. Lipov, J. Fojt, T. Ruml, Influence of surface pre-treatment on the cytocompatibility of a novel biodegradable ZnMg alloy, Mater. Sci. Eng. C. 68 (2016) 198–204. doi:10.1016/j.msec.2016.05.114.
[70] J. Lévesque, H. Hermawan, D. Dubé, D. Mantovani, Design of a pseudo-physiological test bench specific to the development of biodegradable metallic biomaterials, Acta Biomater. 4 (2008) 284–295. doi:10.1016/j.actbio.2007.09.012.
[71] T. Falk, J.-E. Svensson, L.-G. Johansson, The Influence of CO 2 and NaCl on the Atmospheric Corrosion of Zinc A Laboratory Study, J. Electrochem. Soc. 145 (1998) 2993–2999. doi:10.1149/1.1838753.
[72] Iron substitution in the treatment of chronic heart failure, (n.d.). https://smw.ch/article/doi/smw.2017.14453/ (accessed October 6, 2017).
[73] P. Trumbo, S. Schlicker, A.A. Yates, M. Poos, Dietary reference intakes for energy, carbohydrate, fiber, fat, fatty acids, cholesterol, protein and amino acids, J. Am. Diet. Assoc. 102 (2002) 1621–1630. doi:10.1016/S0002-8223(02)90346-9.
[74] M. Peuster, P. Wohlsein, M. Brügmann, M. Ehlerding, K. Seidler, C. Fink, H. Brauer, A. Fischer, G. Hausdorf, A novel approach to temporary stenting: degradable cardiovascular stents produced from corrodible metal—results 6–18 months after implantation into New Zealand white rabbits, Heart. 86 (2001) 563–569. doi:10.1136/heart.86.5.563.
[75] P. Ohlmann, G.S. Mintz, S.-W. Kim, A.D. Pichard, L.F. Satler, K.M. Kent, W.O. Suddath, R. Waksman, N.J. Weissman, Intravascular ultrasound findings in patients with restenosis of sirolimus- and paclitaxel-eluting stents, Int. J. Cardiol. 125 (2008) 11–15. doi:10.1016/j.ijcard.2007.02.021.
[76] D. Pierson, J. Edick, A. Tauscher, E. Pokorney, P. Bowen, J. Gelbaugh, J. Stinson, H. Getty, C.H. Lee, J. Drelich, J. Goldman, A simplified in vivo approach for evaluating the bioabsorbable behavior of candidate stent materials, J. Biomed. Mater. Res. B Appl. Biomater. 100B (2012) 58–67. doi:10.1002/jbm.b.31922.
[77] M. Sikora-Jasinska, C. Paternoster, E. Mostaed, R. Tolouei, R. Casati, M. Vedani, D. Mantovani, Synthesis, mechanical properties and corrosion behavior of powder metallurgy processed Fe/Mg2Si composites for biodegradable implant applications, Mater. Sci. Eng. C. 81 (2017) 511–521. doi:10.1016/j.msec.2017.07.049.
[78] M. Moravej, A. Purnama, M. Fiset, J. Couet, D. Mantovani, Electroformed pure iron as a new biomaterial for degradable stents: In vitro degradation and preliminary cell viability studies, Acta Biomater. 6 (2010) 1843–1851. doi:10.1016/j.actbio.2010.01.008.
[79] C.S. Obayi, R. Tolouei, C. Paternoster, S. Turgeon, B.A. Okorie, D.O. Obikwelu, G. Cassar, J. Buhagiar, D. Mantovani, Influence of cross-rolling on the micro-texture and

biodegradation of pure iron as biodegradable material for medical implants, Acta Biomater. 17 (2015) 68–77. doi:10.1016/j.actbio.2015.01.024.
[80] B. Liu, Y.F. Zheng, Effects of alloying elements (Mn, Co, Al, W, Sn, B, C and S) on biodegradability and in vitro biocompatibility of pure iron, Acta Biomater. 7 (2011) 1407–1420. doi:10.1016/j.actbio.2010.11.001.
[81] W. Lin, L. Qin, H. Qi, D. Zhang, G. Zhang, R. Gao, H. Qiu, Y. Xia, P. Cao, X. Wang, W. Zheng, Long-term in vivo corrosion behavior, biocompatibility and bioresorption mechanism of a bioresorbable nitrided iron scaffold, Acta Biomater. 54 (2017) 454–468. doi:10.1016/j.actbio.2017.03.020.
[82] Q. Feng, D. Zhang, C. Xin, X. Liu, W. Lin, W. Zhang, S. Chen, K. Sun, Characterization and in vivo evaluation of a bio-corrodible nitrided iron stent, J. Mater. Sci. Mater. Med. 24 (2013) 713–724. doi:10.1007/s10856-012-4823-z.
[83] F. Moszner, A.S. Sologubenko, M. Schinhammer, C. Lerchbacher, A.C. Hänzi, H. Leitner, P.J. Uggowitzer, J.F. Löffler, Precipitation hardening of biodegradable Fe–Mn–Pd alloys, Acta Mater. 59 (2011) 981–991. doi:10.1016/j.actamat.2010.10.025.
[84] Y. Mine, Z. Horita, Y. Murakami, Effect of high-pressure torsion on hydrogen trapping in Fe–0.01mass% C and type 310S austenitic stainless steel, Acta Mater. 58 (2010) 649–657. doi:10.1016/j.actamat.2009.09.043.
[85] F.L. Nie, Y.F. Zheng, S.C. Wei, C. Hu, G. Yang, In vitro corrosion, cytotoxicity and hemocompatibility of bulk nanocrystalline pure iron, Biomed. Mater. 5 (2010) 65015. doi:10.1088/1748-6041/5/6/065015.
[86] V.C. Nardone, K.M. Prewo, On the strength of discontinuous silicon carbide reinforced aluminum composites, Scr. Metall. 20 (1986) 43–48. doi:http://dx.doi.org/10.1016/0036-9748(86)90210-3.
[87] R. Casati, M. Vedani, Metal Matrix Composites Reinforced by Nano-Particles: A Review, Metals. 4 (2014) 65. doi:10.3390/met4010065.
[88] K.U. Kainer, Metallische Verbundwerkstoffe, John Wiley & Sons, 2003.
[89] A. Sanaty-Zadeh, Comparison between current models for the strength of particulate-reinforced metal matrix nanocomposites with emphasis on consideration of Hall-Petch effect, Mater. Sci. Eng. A. 531 (2012) 112–118. doi:http://dx.doi.org/10.1016/j.msea.2011.10.043.
[90] P. Mariot, M.A. Leeflang, L. Schaeffer, J. Zhou, An investigation on the properties of injection-molded pure iron potentially for biodegradable stent application, Powder Technol. 294 (2016) 226–235. doi:10.1016/j.powtec.2016.02.042.
[91] M. Moravej, F. Prima, M. Fiset, D. Mantovani, Electroformed iron as new biomaterial for degradable stents: Development process and structure–properties relationship, Acta Biomater. 6 (2010) 1726–1735. doi:10.1016/j.actbio.2010.01.010.
[92] M. Moravej, S. Amira, F. Prima, A. Rahem, M. Fiset, D. Mantovani, Effect of electrodeposition current density on the microstructure and the degradation of electroformed iron for degradable stents, Mater. Sci. Eng. B. 176 (2011) 1812–1822. doi:10.1016/j.mseb.2011.02.031.
[93] J. Cheng, Y. f. Zheng, In vitro study on newly designed biodegradable Fe-X composites (X = W, CNT) prepared by spark plasma sintering, J. Biomed. Mater. Res. B Appl. Biomater. 101B (2013) 485–497. doi:10.1002/jbm.b.32783.
[94] M. Schinhammer, A.C. Hänzi, J.F. Löffler, P.J. Uggowitzer, Design strategy for biodegradable Fe-based alloys for medical applications, Acta Biomater. 6 (2010) 1705–1713. doi:10.1016/j.actbio.2009.07.039.

[95] H. Hermawan, D. Dubé, D. Mantovani, Degradable metallic biomaterials: Design and development of Fe–Mn alloys for stents, J. Biomed. Mater. Res. A. 93A (2010) 1–11. doi:10.1002/jbm.a.32224.
[96] H. Hermawan, H. Alamdari, D. Mantovani, D. Dubé, Iron–manganese: new class of metallic degradable biomaterials prepared by powder metallurgy, Powder Metall. 51 (2008) 38–45. doi:10.1179/174329008X284868.
[97] H. Hermawan, A. Purnama, D. Dube, J. Couet, D. Mantovani, Fe–Mn alloys for metallic biodegradable stents: Degradation and cell viability studies, Acta Biomater. 6 (2010) 1852–1860. doi:10.1016/j.actbio.2009.11.025.
[98] N.B. Sing, A. Mostavan, E. Hamzah, D. Mantovani, H. Hermawan, Degradation behavior of biodegradable Fe35Mn alloy stents, J. Biomed. Mater. Res. B Appl. Biomater. 103 (2015) 572–577. doi:10.1002/jbm.b.33242.
[99] M. Heiden, A. Kustas, K. Chaput, E. Nauman, D. Johnson, L. Stanciu, Effect of microstructure and strain on the degradation behavior of novel bioresorbable iron–manganese alloy implants, J. Biomed. Mater. Res. A. 103 (2015) 738–745. doi:10.1002/jbm.a.35220.
[100] M. Heiden, E. Walker, E. Nauman, L. Stanciu, Evolution of novel bioresorbable iron–manganese implant surfaces and their degradation behaviors in vitro, J. Biomed. Mater. Res. A. 103 (2015) 185–193. doi:10.1002/jbm.a.35155.
[101] A. Drynda, T. Hassel, F.W. Bach, M. Peuster, In vitro and in vivo corrosion properties of new iron–manganese alloys designed for cardiovascular applications, J. Biomed. Mater. Res. B Appl. Biomater. 103 (2015) 649–660. doi:10.1002/jbm.b.33234.
[102] M. Schinhammer, P. Steiger, F. Moszner, J.F. Löffler, P.J. Uggowitzer, Degradation performance of biodegradable FeMnC(Pd) alloys, Mater. Sci. Eng. C. 33 (2013) 1882–1893. doi:10.1016/j.msec.2012.10.013.
[103] M. Schinhammer, C.M. Pecnik, F. Rechberger, A.C. Hänzi, J.F. Löffler, P.J. Uggowitzer, Recrystallization behavior, microstructure evolution and mechanical properties of biodegradable Fe–Mn–C(–Pd) TWIP alloys, Acta Mater. 60 (2012) 2746–2756. doi:10.1016/j.actamat.2012.01.041.
[104] B. Liu, Y.F. Zheng, L. Ruan, In vitro investigation of Fe30Mn6Si shape memory alloy as potential biodegradable metallic material, Mater. Lett. 65 (2011) 540–543. doi:10.1016/j.matlet.2010.10.068.
[105] D.-T. Chou, D. Wells, D. Hong, B. Lee, H. Kuhn, P.N. Kumta, Novel processing of iron–manganese alloy-based biomaterials by inkjet 3-D printing, Acta Biomater. 9 (2013) 8593–8603. doi:10.1016/j.actbio.2013.04.016.
[106] Q. Zhang, P. Cao, Degradable porous Fe-35wt.%Mn produced via powder sintering from NH4HCO3 porogen, Mater. Chem. Phys. 163 (2015) 394–401. doi:10.1016/j.matchemphys.2015.07.056.
[107] Microstructural, mechanical, corrosion and cytotoxicity characterization of the hot forged FeMn30(wt.%) alloy - ScienceDirect, (n.d.). http://www.sciencedirect.com/science/article/pii/S0928493115303751 (accessed November 27, 2017).
[108] X.W.L.X.T.L.Y. Ke, X.W.L.X.T.L.Y. Ke, STUDY ON PROPERTIES OF A NOVEL BIODEGRADABLE Fe–30Mn–1C ALLOY, STUDY ON PROPERTIES OF A NOVEL BIODEGRADABLE Fe–30Mn–1C ALLOY, Acta Met. Sin. 47 (2011) 1342–1347. doi:10.3724/SP.J.1037.2011.00258.
[109] H. Wang, Y. Zheng, J. Liu, C. Jiang, Y. Li, In vitro corrosion properties and cytocompatibility of Fe-Ga alloys as potential biodegradable metallic materials, Mater. Sci. Eng. C. 71 (2017) 60–66. doi:10.1016/j.msec.2016.09.086.

[110] J. Čapek, K. Stehlíková, A. Michalcová, Š. Msallamová, D. Vojtěch, Microstructure, mechanical and corrosion properties of biodegradable powder metallurgical Fe-2 wt% X (X = Pd, Ag and C) alloys, Mater. Chem. Phys. 181 (2016) 501–511. doi:10.1016/j.matchemphys.2016.06.087.
[111] B. Wegener, B. Sievers, S. Utzschneider, P. Müller, V. Jansson, S. Rößler, B. Nies, G. Stephani, B. Kieback, P. Quadbeck, Microstructure, cytotoxicity and corrosion of powder-metallurgical iron alloys for biodegradable bone replacement materials, Mater. Sci. Eng. B. 20 (2011) 1789–1796. doi:10.1016/j.mseb.2011.04.017.
[112] M. Dehestani, E. Adolfsson, L.A. Stanciu, Mechanical properties and corrosion behavior of powder metallurgy iron-hydroxyapatite composites for biodegradable implant applications, Mater. Des. 109 (2016) 556–569. doi:10.1016/j.matdes.2016.07.092.
[113] T. Huang, J. Cheng, D. Bian, Y. Zheng, Fe–Au and Fe–Ag composites as candidates for biodegradable stent materials, J. Biomed. Mater. Res. B Appl. Biomater. 104 (2016) 225–240. doi:10.1002/jbm.b.33389.
[114] Hrubov&#x10d, &#xe1, kov&#xe1, Monika, Kupkov&#xe1, Miriam, D&#x17e, M. Upon, Fe and Fe-P Foam for Biodegradable Bone Replacement Material: Morphology, Corrosion Behaviour, and Mechanical Properties, Adv. Mater. Sci. Eng. (2016). https://www.hindawi.com/journals/amse/2016/6257368/cta/ (accessed October 17, 2017).
[115] G. Xie, H. Takada, H. Kanetaka, Development of high performance MgFe alloy as potential biodegradable materials, Mater. Sci. Eng. A. 671 (2016) 48–53. doi:10.1016/j.msea.2016.06.051.
[116] J. He, F.-L. He, D.-W. Li, Y.-L. Liu, D.-C. Yin, A novel porous Fe/Fe-W alloy scaffold with a double-layer structured skeleton: Preparation, in vitro degradability and biocompatibility, Colloids Surf. B Biointerfaces. 142 (2016) 325–333. doi:10.1016/j.colsurfb.2016.03.002.
[117] W.Q. Wang, J. Wang, M. Qi, Microstructure and In Vitro Biodegradable Properties of Fe-Zn Alloys Prepared by Electroforming, Adv. Mater. Res. 1033–1034 (2014) 1200–1206. doi:10.4028/www.scientific.net/AMR.1033-1034.1200.
[118] J. Cheng, T. Huang, Y.F. Zheng, Microstructure, mechanical property, biodegradation behavior, and biocompatibility of biodegradable Fe–Fe2O3 composites, J. Biomed. Mater. Res. A. 102 (2014) 2277–2287. doi:10.1002/jbm.a.34882.
[119] T. Huang, J. Cheng, Y.F. Zheng, In vitro degradation and biocompatibility of Fe–Pd and Fe–Pt composites fabricated by spark plasma sintering, Mater. Sci. Eng. C. 35 (2014) 43–53. doi:10.1016/j.msec.2013.10.023.
[120] M.F. Ulum, A. Arafat, D. Noviana, A.H. Yusop, A.K. Nasution, M.R. Abdul Kadir, H. Hermawan, In vitro and in vivo degradation evaluation of novel iron-bioceramic composites for bone implant applications, Mater. Sci. Eng. C. 36 (2014) 336–344. doi:10.1016/j.msec.2013.12.022.
[121] S. Wang, Y. Xu, J. Zhou, H. Li, J. Chang, Z. Huan, In vitro degradation and surface bioactivity of iron-matrix composites containing silicate-based bioceramic, Bioact. Mater. 2 (2017) 10–18. doi:10.1016/j.bioactmat.2016.12.001.
[122] T. Huang, Y. Cheng, Y. Zheng, In vitro studies on silver implanted pure iron by metal vapor vacuum arc technique, Colloids Surf. B Biointerfaces. 142 (2016) 20–29. doi:10.1016/j.colsurfb.2016.01.065.
[123] T. Huang, Y. Zheng, Y. Han, Accelerating degradation rate of pure iron by zinc ion implantation, Regen. Biomater. 3 (2016) 205–215. doi:10.1093/rb/rbw020.
[124] T. Jurgeleit, E. Quandt, C. Zamponi, Magnetron Sputtering a New Fabrication Method of Iron Based Biodegradable Implant Materials, Adv. Mater. Sci. Eng. (2015). https://www.hindawi.com/journals/amse/2015/294686/ (accessed October 17, 2017).

[125] T. Jurgeleit, E. Quandt, C. Zamponi, Mechanical Properties and In Vitro Degradation of Sputtered Biodegradable Fe-Au Foils, Mater. Basel Switz. 9 (2016). doi:10.3390/ma9110928.
[126] T. Huang, Y. Zheng, Uniform and accelerated degradation of pure iron patterned by Pt disc arrays, Sci. Rep. 6 (2016). doi:10.1038/srep23627.
[127] A.H.M. Yusop, N.M. Daud, H. Nur, M.R.A. Kadir, H. Hermawan, Controlling the degradation kinetics of porous iron by poly(lactic-co-glycolic acid) infiltration for use as temporary medical implants, Sci. Rep. 5 (2015). doi:10.1038/srep11194.
[128] M. Moravej, D. Mantovani, Biodegradable Metals for Cardiovascular Stent Application: Interests and New Opportunities, Int. J. Mol. Sci. 12 (2011) 4250–4270. doi:10.3390/ijms12074250.
[129] M. Furukawa, Z. Horita, M. Nemoto, T.G. Langdon, Review: Processing of metals by equal-channel angular pressing, J. Mater. Sci. 36 (2001) 2835–2843. doi:10.1023/A:1017932417043.
[130] L. Yuanyuan, Z. Datong, C. Weiping, L. Ying, G. Guowen, Microstructure evolution of AZ31 magnesium alloy during equal channel angular extrusion, J. Mater. Sci. 39 (2004) 3759–3761. doi:10.1023/B:JMSC.0000030731.04301.5f.
[131] K. Xia, J.T. Wang, X. Wu, G. Chen, M. Gurvan, Equal channel angular pressing of magnesium alloy AZ31, Mater. Sci. Eng. A. 410–411 (2005) 324–327. doi:10.1016/j.msea.2005.08.123.
[132] A. Yamashita, Z. Horita, T.G. Langdon, Improving the mechanical properties of magnesium and a magnesium alloy through severe plastic deformation, Mater. Sci. Eng. A. 300 (2001) 142–147. doi:10.1016/S0921-5093(00)01660-9.
[133] J. Frattolin, R. Barua, H. Aydin, S. Rajagopalan, L. Gottellini, R. Leask, S. Yue, D. Frost, O.F. Bertrand, R. Mongrain, Development of a Novel Biodegradable Metallic Stent Based on Microgalvanic Effect, Ann. Biomed. Eng. 44 (2016) 404–418. doi:10.1007/s10439-015-1458-5.
[134] X.N. Gu, Y.F. Zheng, L.J. Chen, Influence of artificial biological fluid composition on the biocorrosion of potential orthopedic Mg–Ca, AZ31, AZ91 alloys, Biomed. Mater. 4 (2009) 65011. doi:10.1088/1748-6041/4/6/065011.
[135] R. Tolouei, J. Harrison, C. Paternoster, S. Turgeon, P. Chevallier, D. Mantovani, The use of multiple pseudo-physiological solutions to simulate the degradation behavior of pure iron as a metallic resorbable implant: a surface-characterization study, Phys. Chem. Chem. Phys. 18 (2016) 19637–19646. doi:10.1039/C6CP02451C.
[136] B. Beverskog, I. Puigdomenech, Revised pourbaix diagrams for iron at 25–300 °C, Corros. Sci. 38 (1996) 2121–2135. doi:10.1016/S0010-938X(96)00067-4.
[137] M. Reffass, R. Sabot, M. Jeannin, C. Berziou, P. Refait, Effects of phosphate species on localised corrosion of steel in NaHCO3+NaCl electrolytes, Electrochimica Acta. 54 (2009) 4389–4396. doi:10.1016/j.electacta.2009.03.014.
[138] S.H. Drissi, P. Refait, M. Abdelmoula, J.M.R. Génin, The preparation and thermodynamic properties of Fe(II)□Fe(III) hydroxide-carbonate (green rust 1); Pourbaix diagram of iron in carbonate-containing aqueous media, Corros. Sci. 37 (1995) 2025–2041. doi:10.1016/0010-938X(95)00096-3.
[139] P. Refait, J.-M.R. Génin, The oxidation of ferrous hydroxide in chloride-containing aqueous media and pourbaix diagrams of green rust one, Corros. Sci. 34 (1993) 797–819. doi:10.1016/0010-938X(93)90101-L.
[140] J.-M.R. Génin, C. Ruby, A. Géhin, P. Refait, Synthesis of green rusts by oxidation of Fe(OH)2, their products of oxidation and reduction of ferric oxyhydroxides; Eh–pH

Pourbaix diagrams, Comptes Rendus Geosci. 338 (2006) 433–446. doi:10.1016/j.crte.2006.04.004.
[141] M. Peuster, C. Hesse, T. Schloo, C. Fink, P. Beerbaum, C. von Schnakenburg, Long-term biocompatibility of a corrodible peripheral iron stent in the porcine descending aorta, Biomaterials. 27 (2006) 4955–4962. doi:10.1016/j.biomaterials.2006.05.029.
[142] R. Waksman, R. Pakala, R. Baffour, R. Seabron, D. Hellinga, F.O. Tio, Short-Term Effects of Biocorrodible Iron Stents in Porcine Coronary Arteries, J. Intervent. Cardiol. 21 (2008) 15–20. doi:10.1111/j.1540-8183.2007.00319.x.
[143] T. Kraus, F. Moszner, S. Fischerauer, M. Fiedler, E. Martinelli, J. Eichler, F. Witte, E. Willbold, M. Schinhammer, M. Meischel, P.J. Uggowitzer, J.F. Löffler, A. Weinberg, Biodegradable Fe-based alloys for use in osteosynthesis: Outcome of an in vivo study after 52weeks, Acta Biomater. 10 (2014) 3346–3353. doi:10.1016/j.actbio.2014.04.007.
[144] M.F. Ulum, A.K. Nasution, A.H. Yusop, A. Arafat, M.R.A. Kadir, V. Juniantito, D. Noviana, H. Hermawan, Evidences of in vivo bioactivity of Fe-bioceramic composites for temporary bone implants, J. Biomed. Mater. Res. B Appl. Biomater. 103 (2015) 1354–1365. doi:10.1002/jbm.b.33315.
[145] M. Fântânariu, L.C. Trincă, C. Solcan, A. Trofin, Ş. Strungaru, E.V. Şindilar, G. Plăvan, S. Stanciu, A new Fe–Mn–Si alloplastic biomaterial as bone grafting material: In vivo study, Appl. Surf. Sci. 352 (2015) 129–139. doi:10.1016/j.apsusc.2015.04.197.
[146] Biomaterials Market by Type of Materials & Application - 2021 | MarketsandMarkets, (n.d.). http://www.marketsandmarkets.com/Market-Reports/biomaterials-393.html (accessed October 15, 2017).
[147] H. Hermawan, D. Dubé, D. Mantovani, Developments in metallic biodegradable stents, Acta Biomater. 6 (2010) 1693–1697. doi:10.1016/j.actbio.2009.10.006.
[148] Y. Tian, H. Cao, Y. Qiao, F. Meng, X. Liu, Antibacterial activity and cytocompatibility of titanium oxide coating modified by iron ion implantation, Acta Biomater. 10 (2014) 4505–4517. doi:10.1016/j.actbio.2014.06.002.
[149] S. Zhu, N. Huang, L. Xu, Y. Zhang, H. Liu, Y. Lei, H. Sun, Y. Yao, Biocompatibility of Fe–O films synthesized by plasma immersion ion implantation and deposition, Surf. Coat. Technol. 203 (2009) 1523–1529. doi:10.1016/j.surfcoat.2008.11.033.
[150] I. Bertini, A. Sigel, Handbook on Metalloproteins, CRC Press, 2001.
[151] H. Seiler, A. Sigel, H. Sigel, Handbook on Metals in Clinical and Analytical Chemistry, CRC Press, 1994.
[152] H.G. Seiler, H. Sigel, A. (eds) Sigel, Handbook on toxicity of inorganic compounds, (1988). https://www.osti.gov/scitech/biblio/6744464 (accessed October 15, 2017).
[153] E. Pagounis, M. Talvitie, V.K. Lindroos, Influence of the metal/ceramic interface on the microstructure and mechanical properties of HIPed iron-based composites, Compos. Sci. Technol. 56 (1996) 1329–1337. doi:10.1016/S0266-3538(96)00101-7.
[154] E. Pagounis, V.K. Lindroos, Processing and properties of particulate reinforced steel matrix composites, Mater. Sci. Eng. A. 246 (1998) 221–234. doi:10.1016/S0921-5093(97)00710-
[155] Nanostructuring of metals by severe plastic deformation for advanced properties - ProQuest, (n.d.). https://search.proquest.com/openview/c002603bdde1e5d527eded27e982e757/1?pq-origsite=gscholar&cbl=27576 (accessed October 15, 2017).
[156] Li, Y.-H., et al., The influence of porosity on corrosion characteristics of porous NiTi alloy in simulated body fluid. Materials Letters, 2002. 57(2): p. 448-451., (n.d.).
[157] H. Abdizadeh, R. Ebrahimifard, M.A. Baghchesara, Investigation of microstructure and mechanical properties of nano MgO reinforced Al composites manufactured by stir casting and powder metallurgy methods: A comparative study, Compos. Part B Eng. 56 (2014) 217–221. doi:10.1016/j.compositesb.2013.08.023.

[158] C.C. Koch, Synthesis of nanostructured materials by mechanical milling: problems and opportunities, Nanostructured Mater. 9 (1997) 13–22. doi:10.1016/S0965-9773(97)00014-
[159] C. Suryanarayana, Mechanical alloying and milling / C. Suryanarayana, SERBIULA Sist. Libr. 20. (2007).
[160] H. Kuhn, Powder Metallurgy Processing: The Techniques and Analyses, Elsevier, 2012.
[161] G.S. Upadhyaya, Powder Metallurgy Technology, Cambridge Int Science Publishing, 1997.
[162] E. Klar, Powder metallurgy: Applications, advantages, and limitations, (1983). https://www.osti.gov/scitech/biblio/5532586 (accessed October 15, 2017).
[163] G. Qiang, E. Mostaed, C. Zanella, Y. Zhentao, M. Vedani, Ultra-Fine Grained Degradable Magnesium for Biomedical Applications, Rare Met. Mater. Eng. 43 (2014) 2561–2566. doi:10.1016/S1875-5372(15)60001-7.
[164] S. Virtanen, Biodegradable Mg and Mg alloys: Corrosion and biocompatibility, Mater. Sci. Eng. B. 176 (2011) 1600–1608. doi:10.1016/j.mseb.2011.05.028.
[165] Marco Montani, Ali Gökhan Demir, Ehsan Mostaed, Maurizio Vedani, Barbara Previtali, Processability of pure Zn and pure Fe by SLM for biodegradable metallic implant manufacturing, Rapid Prototyp. J. (2017). doi:10.1108/RPJ-08-2015-0100.
[166] M. Peuster, P. Wohlsein, M. Brugmann, M. Ehlerding, K. Seidler, C. Fink, H. Brauer, A. Fischer, G. Hausdorf, A novel approach to temporary stenting: degradable cardiovascular stents produced from corrodible metal—results 6-18 months after implantation into New Zealand white rabbits, Heart. 86 (2001) 563–569. doi:10.1136/heart.86.5.563.
[167] Y. Ding, C. Wen, P. Hodgson, Y. Li, Effects of alloying elements on the corrosion behavior and biocompatibility of biodegradable magnesium alloys: a review, J. Mater. Chem. B. 2 (2014) 1912. doi:10.1039/c3tb21746a.
[168] G.-B.R. Yong-Hua Li, The influence of porosity on corrosion characteristics of porous NiTi alloy in simulated body fluid, Mater. Lett. 57 (2002) 448–451. doi:10.1016/S0167-577X(02)00809-1.
[169] W.C. Harrigan Jr., Commercial processing of metal matrix composites, Mater. Sci. Eng. A. 244 (1998) 75–79. doi:10.1016/S0921-5093(97)00828-9.
[170] J.W. Kaczmar, K. Pietrzak, W. Włosiński, The production and application of metal matrix composite materials, J. Mater. Process. Technol. 106 (2000) 58–67. doi:10.1016/S0924-0136(00)00639-7.
[171] F. Rosalbino, S.D. Negri, A. Saccone, E. Angelini, S. Delfino, Bio-corrosion characterization of Mg–Zn–X (X = Ca, Mn, Si) alloys for biomedical applications, J. Mater. Sci. Mater. Med. 21 (2009) 1091–1098. doi:10.1007/s10856-009-3956-1.
[172] E. Zhang, L. Yang, J. Xu, H. Chen, Microstructure, mechanical properties and bio-corrosion properties of Mg–Si(–Ca, Zn) alloy for biomedical application, Acta Biomater. 6 (2010) 1756–1762. doi:10.1016/j.actbio.2009.11.024.
[173] R. Jugdaohsingh, K. Kessler, B. Messner, M. Stoiber, L.D. Pedro, H. Schima, G. Laufer, J.J. Powell, D. Bernhard, Dietary Silicon Deficiency Does Not Exacerbate Diet-Induced Fatty Lesions in Female ApoE Knockout Mice, J. Nutr. 145 (2015) 1498–1506. doi:10.3945/jn.114.206193.
[174] ASTM E112-13: Standard Test Methods for Determining Average Grain Size, (2013).
[175] M. Yu, C. George, Y. Cao, D. Wootton, J. Zhou, Microstructure, corrosion, and mechanical properties of compression-molded zinc-nanodiamond composites, J. Mater. Sci. 49 (2014) 3629–3641. doi:10.1007/s10853-014-8066-x.
[176] ASTM E8/E8M-13: Standard Test Methods for Tension Testing of Metallic Materials, (2013).
[177] ASTM E92-16: Standard Test Methods for Vickers Hardness and Knoop Hardness of Metallic Materials, (2016).

[178] ASTM G59-14: Standard Test Method for Conducting Potentiodynamic Polarization Resistance Measurements, (2014).
[179] ASTM G31-72: Standard Practice for Laboratory Immersion Corrosion Testing of Metals, (2004).
[180] S.F. Corbin, D.S. Wilkinson, Influence of matrix strength and damage accumulation on the mechanical response of a particulate metal matrix composite, Acta Metall. Mater. 42 (1994) 1329–1335. doi:10.1016/0956-7151(94)90149-X.
[181] P.M. Singh, J.J. Lewandowski, Effects of heat treatment and reinforcement size, Metall. Trans. A. 24 (1993) 2531–2543. doi:10.1007/BF02646532.
[182] T. Mitchell, S. Diplas, P. Tsakiropoulos, Characterisation of corrosion products formed on PVD in situ mechanically worked Mg–Ti alloys, J. Alloys Compd. 392 (2005) 127–141. doi:10.1016/j.jallcom.2004.08.086.
[183] S. Shetty, J. Nayak, A.N. Shetty, Influence of sulfate ion concentration and pH on the corrosion of Mg-Al-Zn-Mn (GA9) magnesium alloy, J. Magnes. Alloys. 3 (2015) 258–270. doi:10.1016/j.jma.2015.07.004.
[184] Fran Cverna, Thermal Properties of Metals, in: Materials Park, Ohio 44073-0002, Fran Cverna, 2002.
[185] K. Kondoh, H. Oginuma, R. Tuzuki, T. Aizawa, Magnesium Matrix Composite with Solid-state Synthesized Mg₂Si Dispersoids, Mater. Trans. 44 (2003) 611–618. doi:10.2320/matertrans.44.611.
[186] W.S. Miller, F.J. Humphreys, Strengthening mechanisms in particulate metal matrix composites, Scr. Metall. Mater. 25 (1991) 33–38. doi:10.1016/0956-716X(91)90349-6.
[187] I.A. Ibrahim, F.A. Mohamed, E.J. Lavernia, Particulate reinforced metal matrix composites — a review, J. Mater. Sci. 26 (1991) 1137–1156. doi:10.1007/BF00544448.
[188] C. Suryanarayana, Mechanical alloying and milling, Prog. Mater. Sci. 46 (2001) 1–184. doi:10.1016/S0079-6425(99)00010-9.
[189] D.L. Zhang, Processing of advanced materials using high-energy mechanical milling, Prog. Mater. Sci. 49 (2004) 537–560. doi:10.1016/S0079-6425(03)00034-3.
[190] D. Postma, Formation of siderite and vivianite and the pore-water composition of a Recent bog sediment in Denmark, Chem. Geol. 31 (1980) 225–244. doi:10.1016/0009-2541(80)90088-1.
[191] A. Pfennig, A. Kranzmann, Effect of CO2 and pressure on the stability of steels with different amounts of chromium in saline water, Corros. Sci. 65 (2012) 441–452. doi:10.1016/j.corsci.2012.08.041.
[192] F. ZENG, Z. WEI, J. LI, C. LI, X. TAN, Z. ZHANG, Z. ZHENG, Corrosion mechanism associated with Mg2Si and Si particles in Al–Mg–Si alloys, Trans. Nonferrous Met. Soc. China. 21 (2011) 2559–2567. doi:10.1016/S1003-6326(11)61092-3.
[193] R.K. Gupta, N.L. Sukiman, K.M. Fleming, M.A. Gibson, N. Birbilis, Electrochemical Behavior and Localized Corrosion Associated with Mg2Si Particles in Al and Mg Alloys, ECS Electrochem. Lett. 1 (2012) C1–C3. doi:10.1149/2.002201eel.
[194] P. Volovitch, J.E. Masse, A. Fabre, L. Barrallier, W. Saikaly, Microstructure and corrosion resistance of magnesium alloy ZE41 with laser surface cladding by Al–Si powder, Surf. Coat. Technol. 202 (2008) 4901–4914. doi:10.1016/j.surfcoat.2008.04.052.
[195] J. Walker, S. Shadanbaz, N.T. Kirkland, E. Stace, T. Woodfield, M.P. Staiger, G.J. Dias, Magnesium alloys: Predicting in vivo corrosion with in vitro immersion testing, J. Biomed. Mater. Res. B Appl. Biomater. 100B (2012) 1134–1141. doi:10.1002/jbm.b.32680.
[196] A. Purnama, H. Hermawan, D. Mantovani, Biodegradable Metal Stents: A Focused Review on Materials and Clinical Studies, J. Biomater. Tissue Eng. 4 (2014) 868–874. doi:10.1166/jbt.2014.1263.

[197] S. Barui, S. Mandal, B. Basu, Thermal inkjet 3D powder printing of metals and alloys: Current status and challenges, Curr. Opin. Biomed. Eng. 2 (2017) 116–123. doi:10.1016/j.cobme.2017.05.010.
[198] R.D. Guminski, P.G. Sheasby, H.J. Lamb, Reaction Rates of Second-Phase Constituents in Aluminium During Etching, Brightening and Oxalic Acid Anodizing Processes, Trans. IMF. 46 (1968) 44–48. doi:10.1080/00202967.1968.11870048.
[199] L.L. Li, B. Zhang, B. Tian, Y. Zhou, J.Q. Wang, E.H. Han, W. Ke, SVET Study of Galvanic Corrosion of Al/Mg2Si Couple in Aqueous Solutions at Different pH, J. Electrochem. Soc. 164 (2017) C240–C249. doi:10.1149/2.0671706jes.
[200] P. Marcus, Corrosion Mechanisms in Theory and Practice, Third Edition, CRC Press, 2011.
[201] G.S. Frankel, N. Sridhar, Understanding localized corrosion, Mater. Today. 11 (2008) 38–44. doi:10.1016/S1369-7021(08)70206-2.
[202] A. Pfennig, P. Zastrow, A. Kranzmann, Influence of heat treatment on the corrosion behaviour of stainless steels during CO2-sequestration into saline aquifer, Int. J. Greenh. Gas Control. 15 (2013) 213–224. doi:10.1016/j.ijggc.2013.02.016.
[203] A. Pfennig, R. Bäßler, Effect of CO2 on the stability of steels with 1% and 13% Cr in saline water, Corros. Sci. 51 (2009) 931–940. doi:10.1016/j.corsci.2009.01.025.
[204] A.S. Akhtar, P.C. Wong, K.C. Wong, K.A.R. Mitchell, Microstructural effects on the formation and degradation of zinc phosphate coatings on 2024-Al alloy, Appl. Surf. Sci. 254 (2008) 4813–4819. doi:10.1016/j.apsusc.2008.01.113.
[205] D. Susac, X. Sun, R.Y. Li, K.C. Wong, P.C. Wong, K.A.R. Mitchell, R. Champaneria, Microstructural effects on the initiation of zinc phosphate coatings on 2024-T3 aluminum alloy, Appl. Surf. Sci. 239 (2004) 45–59. doi:10.1016/j.apsusc.2004.04.038.
[206] L. Wang, J. Zhang, Y. Gao, Q. Xue, L. Hu, T. Xu, Grain size effect in corrosion behavior of electrodeposited nanocrystalline Ni coatings in alkaline solution, Scr. Mater. 55 (2006) 657–660. doi:10.1016/j.scriptamat.2006.04.009.
[207] D. Hong, D.-T. Chou, O.I. Velikokhatnyi, A. Roy, B. Lee, I. Swink, I. Issaev, H.A. Kuhn, P.N. Kumta, Binder-jetting 3D printing and alloy development of new biodegradable Fe-Mn-Ca/Mg alloys, Acta Biomater. 45 (2016) 375–386. doi:10.1016/j.actbio.2016.08.032.
[208] J. He, F.-L. He, D.-W. Li, Y.-L. Liu, Y.-Y. Liu, Y.-J. Ye, D.-C. Yin, Advances in Fe-based biodegradable metallic materials, RSC Adv. 6 (2016) 112819–112838. doi:10.1039/C6RA20594A.
[209] L.H. Hihara, R.M. Latanision, Corrosion of metal matrix composites, Int. Mater. Rev. 39 (1994) 245–264. doi:10.1179/imr.1994.39.6.245.
[210] J. Cheng, B. Liu, Y.H. Wu, Y.F. Zheng, Comparative in vitro Study on Pure Metals (Fe, Mn, Mg, Zn and W) as Biodegradable Metals, J. Mater. Sci. Technol. 29 (2013) 619–627. doi:10.1016/j.jmst.2013.03.019.
[211] A. Reindl, R. Borowsky, S.B. Hein, J. Geis-Gerstorfer, P. Imgrund, F. Petzoldt, Degradation behavior of novel Fe/ß-TCP composites produced by powder injection molding for cortical bone replacement, J. Mater. Sci. 49 (2014) 8234–8243. doi:10.1007/s10853-014-8532-5.
[212] Wiley: Uhlig's Corrosion Handbook, 3rd Edition - R. Winston Revie, (n.d.). http://www.wiley.com/WileyCDA/WileyTitle/productCd-0470080329.html (accessed November 14, 2017).
[213] M. Schinhammer, J. Hofstetter, C. Wegmann, F. Moszner, J.F. Löffler, P.J. Uggowitzer, On the Immersion Testing of Degradable Implant Materials in Simulated Body Fluid: Active pH Regulation Using CO2, Adv. Eng. Mater. 15 (2013) 434–441. doi:10.1002/adem.201200218.

[214] R.L. Frost, W. Martens, P.A. Williams, J.T. Kloprogge, Raman and infrared spectroscopic study of the vivianite-group phosphates vivianite, baricite and bobierrite, Mineral. Mag. 66 (2016) 1063–1074. doi:10.1180/0026461026660077.
[215] J.R. Bargar, J.D. Kubicki, R. Reitmeyer, J.A. Davis, ATR-FTIR spectroscopic characterization of coexisting carbonate surface complexes on hematite, Geochim. Cosmochim. Acta. 69 (2005) 1527–1542. doi:10.1016/j.gca.2004.08.002.
[216] S. Meejoo, W. Maneeprakorn, P. Winotai, Phase and thermal stability of nanocrystalline hydroxyapatite prepared via microwave heating, Thermochim. Acta. 447 (2006) 115–120. doi:10.1016/j.tca.2006.04.013.
[217] I.R. Gibson, W. Bonfield, Preparation and characterization of magnesium/carbonate co-substituted hydroxyapatites, J. Mater. Sci. Mater. Med. 13 (2002) 685–693. doi:10.1023/A:1015793927364.
[218] L. Berzina-Cimdina, N. Borodajenko, Research of Calcium Phosphates Using Fourier Transform Infrared Spectroscopy, (2012). doi:10.5772/36942.
[219] T. Hanawa, M. Ota, Calcium phosphate naturally formed on titanium in electrolyte solution, Biomaterials. 12 (1991) 767–774. doi:10.1016/0142-9612(91)90028-9.
[220] I.V. Sieber, H. Hildebrand, S. Virtanen, P. Schmuki, Investigations on the passivity of iron in borate and phosphate buffers, pH 8.4, Corros. Sci. 48 (2006) 3472–3488. doi:10.1016/j.corsci.2005.12.008.
[221] P. Refait, M. Reffass, J. Landoulsi, R. Sabot, M. Jeannin, Role of phosphate species during the formation and transformation of the Fe(II–III) hydroxycarbonate green rust, Colloids Surf. Physicochem. Eng. Asp. 299 (2007) 29–37. doi:10.1016/j.colsurfa.2006.11.013.
[222] R. Gächter, B. Müller, Why the phosphorus retention of lakes does not necessarily depend on the oxygen supply to their sediment surface, Limnol. Oceanogr. 48 (2003) 929–933. doi:10.4319/lo.2003.48.2.0929.
[223] S. Shrivastava, Medical Device Materials: Proceedings from the Materials & Processes for Medical Devices Conference 2003, 8-10 September 2003, Anaheim, California, ASM International, 2004.
[224] M. Rothe, A. Kleeberg, M. Hupfer, The occurrence, identification and environmental relevance of vivianite in waterlogged soils and aquatic sediments, Earth-Sci. Rev. 158 (2016) 51–64. doi:10.1016/j.earscirev.2016.04.008.
[225] J. Hufenbach, H. Wendrock, F. Kochta, U. Kühn, A. Gebert, Novel biodegradable Fe-Mn-C-S alloy with superior mechanical and corrosion properties, Mater. Lett. 186 (2017) 330–333. doi:10.1016/j.matlet.2016.10.037.
[226] E. Mouzou, C. Paternoster, R. Tolouei, A. Purnama, P. Chevallier, D. Dubé, F. Prima, D. Mantovani, In vitro degradation behavior of Fe–20Mn–1.2C alloy in three different pseudo-physiological solutions, Mater. Sci. Eng. C. 61 (2016) 564–573. doi:10.1016/j.msec.2015.12.092.
[227] A.J. Drelich, S. Zhao, R.J. Guillory, J.W. Drelich, J. Goldman, Long-term surveillance of zinc implant in murine artery: Surprisingly steady biocorrosion rate, Acta Biomater. 58 (2017) 539–549. doi:10.1016/j.actbio.2017.05.045.